NOVA SCHOOL OF SCIENCE & TECHNOLOGY

DEPARTAMENT OF MECHANICAL AND INDUSTRIAL ENGINEERING

LUÍS PEDRO ABELHA EUGÉNIO

BSc in Mechanical Engineering Sciences

GRADIENT-BASED TRUSS TOPOLOGY OPTIMIZATION WITH LOCAL STRESS AND BUCKLING CONSTRAINTS CONSIDERING CHAIN EFFECTS

MASTER IN MECHANICAL ENGINEERING

NOVA University Lisbon

November, 2021

DEPARTAMENT OF MECHANICAL
AND INDUSTRIAL ENGINEERING

GRADIENT-BASED TRUSS TOPOLOGY OPTIMIZATION WITH LOCAL STRESS AND BUCKLING CONSTRAINTS CONSIDERING CHAIN EFFECTS

LUÍS PEDRO ABELHA EUGÉNIO

BSc in Mechanical Engineering Sciences

Adviser: Dr. Pedro Samuel Gonçalves Coelho
Professor, NOVA University Lisbon
Co-advisers: MSc Cláudia Sofia João de Almeida
Researcher, NOVA University Lisbon

Examination Committee:

Chair: Dr. José Manuel Cardoso Xavier,
Professor, FCT-NOVA
Rapporteurs: Dr. João Mário Burguete Botelho Cardoso
Professor, FCT-NOVA
Adviser: Dr. Pedro Samuel Gonçalves Coelho,
Professor, FCT-NOVA

MASTER'S IN MECHANICAL ENGENNERING

NOVA University Lisbon
November, 2021

Gradient-Based Truss Topology Optimization with Local Stress and Buckling Constraints Considering Chain Effects

Dedicated to Guilherme.

ACKNOWLEDGMENTS

I would like to start these acknowledgments by thanking this thesis' advisors, Dr. Pedro Coelho, and MSc Cláudia Almeida, who accompanied and guided my work throughout the last 10 month. Their insights and expertise were paramount to the development of this document and the computer program behind it and were delightful to work with. Their excellent work in previous projects were key for the developments presented in this thesis, and I would like to wish them great success in future projects. I would also like to acknowledge the role that NOVA-FCT had in exposing me to the various subjects in Mechanical Engineering. As well as acknowledge the role the faculty and its teachers had in awakening in me my deepest curiosities for the plethora of topics in Mechanical Engineering, sharing with me their knowledge and time. I would like to extend an especial thanks to Professor Dr. Kristen Svanberg for sharing his MMA and GCMMA notes and codes with us.

My family and friends deserve the largest acknowledgement for supporting me in completing this degree, I would like to thank them directly for standing by me through the process of acquiring an engineering education. I will write the next paragraph in Portuguese, so that all of them can read it.

Eu quero agradecer à minha família e aos meus amigos por me acompanharem no árduo processo de obter uma educação em engenharia mecânica. Todos foram importantes em suportarem-me, mas gostava de começar por agradecer à minha família. Aos meus avós que, apesar de apenas serem dotados de uma educação básica, conseguiram que vários membros das suas famílias adquirissem formação superior. À minha mãe Luísa e ao meu pai António cujo apoio e amor incondicional sinto que nunca serei capaz de retribuir e estou por isso eternamente grato. E por último, quero agradecer diretamente ao meu irmão, "Não consigo articular a importância que tiveste na minha vida, obrigado por estares sempre comigo, Gui." Aos meus amigos que como família são, quero agradecer a tolerância, preocupação e companhia que proporcionaram ao longo destes anos. Nuno, Tiago, Inês, Beatriz, Carolina, Miguel e Tomás. Obrigado a todos!

"The most exciting phrase to hear in science, the one that heralds new discoveries, is not "Eureka" but "That's funny..." (Asimov).

ABSTRACT

In this dissertation, a gradient-based optimization, utilizing both MMA and GCMMA optimization algorithms, is applied to a truss topology optimization problem including local stress and buckling constraints. The problems with these constraints are prone to be affected by the singularity phenomenon where the global optimum is in a degenerated region of the design domain. This can prevent the elimination of bars when their areas tend to zero because the stress/buckling constraints are violated. Through a combination of relaxation techniques, namely ϵ-relaxation, a continuation approach and an adaptation of the constraint's formulation, the singularity phenomenon can be overcome. The known chain effect in truss topology optimization is addressed by implementing a reverse SIMP function that is used to smooth out the "jump" in the buckling length. This buckling length correction is thus performed in the continuum set of the problem design variables which allows the use of gradient-based algorithms.

The developed methodology is firstly tested resorting to a set of problems with analytical solutions. Then the proposed algorithm is applied to a new set of complementary examples increasing the number of bar elements. The results found by the MMA optimization algorithm represent reliable solutions that prove the efficiency of the proposed formulation to deal with buckling constraints. Finally, the GCMMA's results agreed with the MMA results in all but two examples, where it showed some difficulties in escaping from local minimum.

Keywords: Buckling, Stress, Chain Effect, Truss, Topology Optimization, MMA

RESUMO

Nesta dissertação, uma otimização baseada no gradiente, utilizando os algoritmos de otimização MMA e GCMMA, é aplicada a um problema de otimização de topologia de treliças incluindo constrangimentos de tensão e de encurvadura locais. Os problemas com estes constrangimentos são propenso a ser afectados pelo fenômeno da singularidade onde o ótimo global está localizado numa região degenerada do domínio de projeto. Isso pode evitar a eliminação de barras quando as suas áreas tendem para zero porque os constrangimentos de tensão/encurvadura são violados. Através de uma combinação de técnicas de relaxamento, nomeadamente, $\epsilon - relaxation$, uma *continuation approach* e uma adaptação da formulação do constrangimento, o fenômeno da singularidade pode ser ultrapassado. O conhecido efeito de cadeia na otimização da topologia de treliça é abordado pela implementação de uma função SIMP reversa que é usada para suavizar o "salto" no comprimento de encurvadura. Esta correção do comprimento de encurvadura é então realizada no conjunto contínuo das variáveis de projeto do problema, o que permite o uso de algoritmos de otimização baseados no gradiente.

A metodologia desenvolvida é primeiro testada recorrendo a um conjunto de problemas com soluções analíticas. Em seguida, o algoritmo proposto é aplicado a um novo conjunto de exemplos complementares aumentando o número de elementos da barra. Os resultados encontrados pelo algoritmo de otimização MMA representam soluções confiáveis que comprovam a eficiência da formulação proposta para lidar com os constrangimentos de encurvadura. Finalmente, os resultados do GCMMA concordaram com os resultados do MMA em todos os exemplos, exceto dois, onde se verificaram algumas dificuldades em escapar a mínimos locais.

Palavras chave: Encurvadura, Tensão, Efeito da Cadeia, Treliça, Otimização Topológica, MMA

CONTENTS

LIST OF FIGURES

LIST OF TABLES

ACRONYMS

DOF	Degrees of freedom.
FEM	Finite Element Method.
FE	Finite Element.
GA	Genetic Algorithms.
GCMMA	Globally Convergent Method of Moving Asymptotes.
KKT	Karush-Khun-Tucker optimality condition.
MMA	Method of Moving Asymptotes.
MMTO	Multi-Material Topology Optimization.
STO	Structural Topology Optimization.

SYMBOLS

Latin

$\mathbf{A}$	Constraint matrix containing each variable coefficients in constraint functions.
A_{ref}	Area cutoff point of the buckling length assessment function.
A_e	Bar element e's cross-sectional area
$\bar{A}$	Average of the adjacent element's area
a_0	Real valued MMA and GCMMA parameter.
a_i	Real valued MMA and GCMMA parameter for every i constraint.
a_{min}	Lower bound imposed on the bar's cross-sectional area.
$\mathbf{b}$	Column vector with the independent terms of the constraint's functions.
C	Convergence constant.
c_i	Real valued MMA and GCMMA parameter for every i constraint.
d_i	Real valued MMA and GCMMA parameter for every i constraint.
E	Material's Young Modulus
e_k	Error between current point and optimum point at iteration k.
f	Generic objective function.
f^e	Applied load vector.
F_e	Internal force applied to element e.
Q^e	Load variation vector with a FE
g	Generic inequality constraint function.
g^σ	Admissible stress constraint.
g^{buc}	Buckling constraint.
$\mathbf{G}$	Global geometry matrix.
h	Generic equality constraint function.
$\mathbf{I}$	Cross-sectional moment of inertia
I_1, I_2	Continuation approach iteration intervals.
I^{max}	Maximum number of iterations
$\mathbf{K}$	Global stiffness matrix.
$\mathbf{K}^e$	Element e's matrix w.r.t. global reference

$\mathbf{k}^{e}$	Element e's local matrix
k^{ct}	Parameter that relates I_2 to I_1.
$\mathbf{L}$	Column vector of element's length
L_{buc}	Buckling length being considered.
L_e	Element's length
$\mathcal{L}(\mathbf{x}, \boldsymbol{\lambda})$	Optimization problem Lagrangian function.
L_j^k, U_j^k	Lower and Upper asymptote value for variable j at iteration k, respectively.
p	Adapted critical load correcting exponent.
P^{cr}	Critical buckling load.
$\vec{p}$	Optimization step direction.
p_{ij}^k, q_{ij}^k	MMA and GCMMA constraint $i's$ gradient approximating functions w.r.t. to variable j.
$\vec{p}_N$	Newton's method step direction.
N_E	Total number of elements in the ground structure.
N_{adj}	Number of adjacent elements.
n_{cr}	Buckling force bar support parameter.
r_C	Optimization algorithm rate of convergence.
r_i^k	MMA and GCMMA constraint i's correcting function at iteration k.
$\mathbf{T}_e$	Element e's transformation matrix
$\mathbf{u}$	Displacement vector.
x_e	e^{th} Design variable.
$\underline{x}_e$	Lower bound for generic design variable x_e.
$\overline{x}_e$	Upper bound for generic design variable x_e.
$\mathbf{x}$	Design variables vector.
$\mathbf{x}^k$	Vector of design variables at iteration k.
$\mathbf{x}^*$	Optimum point.
x_{ρ_e}	Density design variable associated with element e.
x_{A_e}	Normalized area design variable associated with element e.
y_i	Real valued MMA and GCMMA artificial variable.
X	Domain set of **x.**
$\mathbf{Z}$	Null space matrix of **A.**
z_{MMA}	Real valued MMA and GCMMA artificial variable.

Greek

α_j^k, β_j^k	MMA and GCMMA lower and upper move limits, respectively.
α	Percentage of admissible stress considered in μ calcualtion.
B_e	Coefficient that relates an element's area to its moment of inertia
Γ_{adj}	Set of adjacent elements.
γ_j^k	Parameter used to limit the variation of x_j.
ϵ	Constraint Relaxation Parameter.

θ_e	Element e's angle w.r.t the horizontal reference.
$\boldsymbol{\lambda}$	Adjoint method's vector.
$\boldsymbol{\lambda}_{\mathcal{L}}$	Column vector of Lagrangian multipliers.
μ	Adapted critical load correcting constant
π	The ratio of the circumference of a circle to its diameter.
ρ_M	Material's mass density.
$\rho_i^{k,v}$	GCMMA convexity guarantying parameter for outer iteration k and inner iteration v for constraint function i.
σ_e	Stress applied to element e.
σ_{adm}	Admissible stress value.
σ_{cr}^c	Adapted critical buckling stress of element e.
$\sigma_{buc_e}, \sigma_{cr}^c$	Critical buckling stress of element e
σ_Y	Material yield stress.
ϕ	Area scaling parameter
Ψ	Generic functional representing any constrain or objective function.

1

INTRODUCTION

1.1 Context and Motivation

Structural Optimization is a research field with great potential to aid and even automate the design process of a given structure. It started with simple area optimizations carried out on isostatic trusses to obtain the minimum possible mass. These simple problems have developed throughout the last 120 years into complex algorithms that are able to solve increasingly complex problems. Although notions of structural optimization are centuries old, this field can be considered new because the progress made is tied to both computing power and mathematical formulations. New algorithms and methodologies are proposed as computer technology develops, and vice versa. Currently new powerful computing capability has allowed researchers to implement algorithms developed over twenty years ago to solve complex problems.

This thesis intends to contribute to the current framework in structural topology optimization by dealing with a gradient-based optimization to problems with local buckling and stress constraints, using the ground structure approach.

1.2 Problems and Objectives

This thesis intends to contribute to the current framework by applying a structural topology optimization to truss structures considering both local buckling and local stress constraints. These constraints are computationally expensive and have complications relating to the fact that their physical definitions are tied to the area variable, which is also used as a topology variable. When an algorithm removes a bar it usually does it continuously. As the area decreases towards zero the local buckling and stress constraint tend to be violated, preventing the bar from being removed, which threatens the essence of topology optimizations to generate "black-white" designs.

The buckling constraint is commonly used in global terms, with the stability of the structure being attributed to a single constrained value that account for the global state equilibrium

of the whole structure. Furthermore, to circumvent numerical singularities and the requirement that the constraint functions be convex, gradient algorithms may be abandoned in favor of heuristic algorithms, that are not gradient dependent. However, these algorithms are very time consuming because they require many function evaluations which makes gradient-based methods more desirable due to their efficiency.

This thesis aims to not only present a solution to the singularity problems involving local buckling and stress, but also to formulate and solve a problem that considers the chain effect in a gradient-based optimization. This effect is the alternative interpretation of having unstable nodes in truss layout. These nodes are interpreted as internal nodes of a potential larger bar instead of being viewed as compromising the kinematic stability of the truss. This leads to difficulties in the problem formulation as the constraints must contemplate this effect of chain on bar member which directly impact on the buckling length definition.

In a nutshell, the main two problems addressed in this thesis are the following: (1) the numerical singularity phenomenon related to the buckling constraint and the requirement that it be convex, (2) the inclusion of the chain effect in the optimization problem formulation.

1.3 Approach and Contributions

The developed methodology solves the difficulties presented earlier by employing a combination of techniques that allow a gradient-based optimization to accurately solve a set of design problems. These techniques include a $\epsilon - relaxation$, a continuation approach, and a constraint reformulation. When applied simultaneously, these techniques allow the optimizer to deal with buckling constraints more effectively.

In the end, this thesis' contribution is a gradient-based truss topology optimization with both local buckling and stress constraints including the so-called chain effect.

1.4 Document Organization

Regarding this thesis structure. Chapter 1 presents an introduction to the subject and motivation. In Chapter 2, the state of the art is presented including an overview of the literature used to develop the proposed methodology. Chapter 3 presents a more in-depth study of the problem components, those being the objective function and the constraining functions, and it ends with the optimization problem formulation. Chapter 4 presents the sensitivity analysis of the previous chapter's functions, a key aspect in gradient-based optimization. In Chapter 5, a set of truss problems are solved with the proposed methodology, starting with three examples having an analytical solution. Chapter 6 presents the conclusion and some future works suggestions.

2

STATE OF THE ART

This chapter presents an overview of the bibliography required to fundament the dissertation starting with some historic background, followed by with some information about optimization processes and their requirements, after that some consideration pertaining to sensitivity analysis, and it ends with some of the relaxation techniques employed.

2.1 Historic Background

Structural Optimization has its genesis in the works of Maxwell [37] and Michell [38]. In these pioneering works, Maxwell develops a method for obtaining the stresses of a truss structures while Michell continues Maxwell's works by utilizing the gathered stress information to calculate the minimum amount of material that still allows the truss to support the required loads. Michell's algorithm is an early version of dimensional optimization of a truss for minimum weight. However, it wasn't until the decade of 1950 that these works saw any further development as further mathematical and technological advancements were required.

In the decade of 1950, the development efforts in the field of structural topology optimization were led by the aeronautical industry that was formulating and solving problems related to the complex inner structures of airplane wings. By studying the various formulations used to obtain the complex geometries required, Schmit [49] would recognize common features among the many formulations and that ended up on proposing his own standardized formulation. It was composed of an objective function, a set of constraints that limit the variation of the design variable, and the usage of an algorithm that solves the problem. This problem structure developed by Schmit would become a key ingredient of optimization disciplines, in a broader sense, i.e., beyond the structural optimization field.

Earlier, in the decade of 1940, when studying membrane plane stress cases there was a need to apply differential equations related to the stress in a membranes' continuous domain. Since the respective differential equations are so complex in such structural domains, i.e., it's hard to get their solution analytically, numerical methods are required. A discretized version of the continuous domain is used to solve the differential equations in order to simplify their

use. This means that the design domain is modeled by a set of finite elements with pre-defined shape functions that approximate the "exact" function solution of the problem. This method was latter referred to as the Finite Element Method (FEM) [19]. It became an integral part of computer analysis across diverse engineering domains. Based on the FEM, a technique tailored to truss analysis was later developed, the so-called Ground Structure Approach by Dorn et. al. [20]. This technique consists of a group of nodes connected by bars, and an algorithm that searches them for the optimal connectivity of the bars for a given load and support requirements.

Still in the same decade, during the Second World War when resources were scarce, optimization underwent a major development in the field of Operational Research. The need for the correct and efficient use of the available limited resources at that time was mandatory. This demanded the development of simple algorithms that could be resolved by hand using calculation tables, the now famous *Simplex Algorithms*. However, these algorithms proved to be too simple when modern computers emerged in the early 80's. That opened the way for the development of new optimization algorithms, such as integer programing and related heuristic algorithms that are still present in the current literature. [23]

These developments, just summarized here, culminate in the current rich academic environment of topology optimization.

2.1.1 Types of Structural Optimization

While every optimization is based roughly on the same standard mathematical formulation, the different physical meaning of design variables and functions allows distinguishing three main optimization categories (1) Sizing Optimization, (2) Shape Optimization, (3) Topology Optimization, see [18].

The first structural optimization problems have to do with dimensional optimizations as presented by Dorn et al. [20], where a minimum weight problem is solved with a ground structure approach [15]. This revolutionary new technique provides the framework for much of the literature that comes after it. In a Ground Structure Approach, nodes are firstly distributed over the design domain and then connected by potential bars [53]. Although the ground structure method would prove to be a powerful tool in structural topology optimization, the first applications were on simple sizing problems where the objective function is the structure's weight, and the design variables are the areas of the structure's bar elements.

Later works in the decade of 1970, such as Francavilla et all [22], use the position of the nodes as design variables resulting in shape optimization. Currently this kind of optimization is often used in conjunction with one of the remaining categories of optimizations.

Lastly, topology optimization is developed by the works of Svanberg [55] and Bendsoe [9]. In topology optimization the design variables are typically Boolean and are used to determine whether a given element should be removed from the ground structure to decrease either the mass or the compliance, depending on what the objective function is. Topology optimiza-

tion is often used in conjunction with dimensional optimization without distinguishing between the two using a positive lower bound on the area, a_{min} , see [2]. In case such lower bound is touched, the respective bar is considered as being removed from the truss optimal layout.

Using density-based optimization allows for another key feature of modern topology optimization, often called Multi Material Topology Optimization, MMTO. This can impact favorably on further weight decrease as it allows to have a more efficient use of different material specific weights. Works such as [50] shows mass decreases of more than 39% when comparing with single material solutions and [8] shows significant decreases on all the structures studied.

2.1.2 Formulating an Optimization Problem

An optimization problem is defined by an objective function, $f(\mathbf{x})$ whose variables, $x_1, \dots, x_n \in \mathbf{x}$ are affected by a set of constraints, $g_j(\mathbf{x})$, $h_k(\mathbf{x})$ and are bounded by, $x_e \in [\underline{x}_e; \overline{x}_e]$ (Eq. 2.1).

$$\min_{\mathbf{x}} \quad f(\mathbf{x}) \qquad \text{(Eq. 2.1)}$$

$$\text{s.t.} \quad \begin{cases} g_j(\mathbf{x}) \leq 0 & ; j = 1, \dots, m \\ h_k(\mathbf{x}) = 0 & ; k = 1, \dots, p \\ \underline{x}_e \leq x_e \leq \overline{x}_e & ; e = 1, \dots, n \end{cases}$$

In formulation (Eq. 2.1) the objective function is minimized and there are m less-than-or-equal-to constraints, p equality constraints and n bound constraints. A problem that is stated according to this formulation is said to be in the standard format. Many optimization algorithms, especially the ones that are gradient based, require the problem to be formulated in the standard formulation. The objective function, design variables and constraints can have many different types of meanings resulting in different types of formulations, Table 2.1 shows some of those different types of meanings.

Table 2.1 - Possible types of objective function, design variables and constraints for an optimization problem.

Objective Function	**Project Variables**	**Constraints**
Weight	Dimensions	Displacement
Cost	Node Position	Stress
Compliance	Topology	Natural Frequency
		Critical Buckling Factor or Load
		Reliability

2.2 Optimization Algorithms

With the optimization problem formulated, the next step is to solve it. There are many algorithms that have been developed to solve problems of various degrees of complexity. However, in general, optimization algorithms can be categorized as gradient-based optimization and non-gradient based optimization. The decision about what to use will depend mainly on the characteristics of the design variables. For instances, if these variables are discrete then using a non-gradient based method is the only option. In case continuity and differentiability are ensured, a gradient-based method can be advised, as it is typically computationally cheaper although the sensitivity analysis can still be time-consuming and difficult to implement.

2.2.1 Gradient-Based Optimization

Gradient-Based methods utilize an analysis on the gradient of the objective function on a given point to calculate a step direction, $\vec{p}$, a vector which is then added to the set of variables, **x**, resulting in a new point where the process is repeated. For brevity, algorithms applied to linear problems aren't addressed in this document. The simplest nonlinear optimization problems to solve are unconstrained problems where step calculation does not need to consider the feasibility of the end point. One of the first proposals for an algorithm is given by Isaac Newton where a step is calculated based on the second-degree information of the objective function resulting in the commonly known Newton's Step, $\vec{p}_N$, (Eq. 2.2).

$$\vec{p}_N = -\frac{\nabla f(\mathbf{x})}{\nabla^2 f(\mathbf{x})} \qquad \text{(Eq. 2.2)}$$

This step is then added to the Set of Variables (Eq. 2.3),

$$\mathbf{x}^{k+1} = \mathbf{x}^k + \vec{p}_N \qquad \text{(Eq. 2.3)}$$

Resulting in a new point, from which a new step is determined and added to the new set of variables, resulting in an iterative process that determines the minima and minimum of a given nonlinear function. Further explanation of Newton's Method can be consulted in [24].

Newton's method is used as a benchmark for other optimization algorithms, as it has the best convergence rate (Eq. 2.4) possible. All other gradient based methods can be considered an inefficient version of this method resulting in lower convergence rates, Newton's Method is not widely used since it displays some difficulties that are circumvented by other optimization algorithms.

$$\lim_{k\to\infty} \frac{\|e_{k+1}\|^{r_c}}{\|e_k\|} = C \qquad \text{(Eq. 2.4)}$$

Where e_k is the error at iteration, $\mathrm{e_k} = \mathbf{x}^{\mathrm{k}} - \mathbf{x}^*$, and if $C < \infty$ then the sequence of solutions converges at rate r_C and with convergence constant C. The convergence rate is usually used for comparing algorithms and how they converge, usually $r_C \in [1; 2[$. The quadratic convergence rate of 2 is only achieved by Newton's method when close to the local optimum. However, one of the disadvantages of Newton's Method is that it only works well close enough to the local optimum.

Adding a constraint to a nonlinear problem greatly increases its difficulty requiring a modified version of Newton's Method. It is then necessary to include information about the constraints into the function before the optimization algorithm minimizes it. Let an optimization problem be defined by the formula (Eq. 2.5).

$$\begin{aligned} \min \quad & \mathrm{f}(\mathbf{x}) \\ \text{s.t.} \quad & \mathbf{A}\mathbf{x} = \mathbf{b} \end{aligned} \tag{Eq. 2.5}$$

Where $\mathbf{A}$ is a full rank constraint matrix and $\mathbf{b}$ is a column vector with as many entries as there are constraints, it stores to the constraints' right-hand side. The Lagrange Function associated with this problem is given by (Eq. 2.6).

$$\mathcal{L}(\mathbf{x}, \boldsymbol{\lambda}) = \mathrm{f}(\mathbf{x}) - \boldsymbol{\lambda}_{\mathcal{L}}^{\mathrm{T}}(\mathbf{A}\mathbf{x} - \mathbf{b}) \tag{Eq. 2.6}$$

Where $\boldsymbol{\lambda}_{\mathcal{L}}$ is the column vector of the Langrage multipliers. The Lagrange multipliers define the gradient at the optimum as a linear combination of the derivative of the constraint matrix (Eq. 2.7).

$$\nabla \mathrm{f}(\mathbf{x}^*) = \mathbf{A}^{\mathrm{t}} \cdot \boldsymbol{\lambda}_{\mathcal{L}} \tag{Eq. 2.7}$$

These Lagrange multipliers are known as dual variables while $\mathbf{x}$ are the primal variables. Many problems that solve nonlinear constrained optimization problems use primal-dual algorithms to reach an optimum.

Usually, an optimization will iterate until some stopping conditions are verified. In addition to a maximum number of iterations it would be convenient to use the optimality conditions as stopping criteria. These conditions guarantee that the point being analyzed after some design iterations is a local minimum. In fact, when dealing with gradient-based optimization it is only possible to prove that a given point is a local minimum. To find the global minimum all local minima would need to be analyzed. The conditions that indicate a local minimum presence, for a nonlinear constrained optimization problem, are known as the Karush-Kuhn-Tucker Conditions, henceforth referred to as KKT Conditions. These conditions are applicable to inequality constraints and are either the necessary conditions for optimality if the left-hand side of (Eq. 2.11) is positive semi-definite or sufficient condition if it is positive definitive.

$$\nabla_x \mathcal{L}(\mathbf{x}_*, \boldsymbol{\lambda}_*) = 0 \quad \text{(Eq. 2.8)}$$

$$\boldsymbol{\lambda}_* \geq 0 \quad \text{(Eq. 2.9)}$$

$$\boldsymbol{\lambda}_*^{\mathrm{T}} g(\mathbf{x}_*) = 0 \quad \text{(Eq. 2.10)}$$

$$\mathbf{Z}(\mathbf{x}_*)^{\mathrm{T}} \nabla_{xx}^2 \mathcal{L}(\mathbf{x}_*, \boldsymbol{\lambda}_*) \mathbf{Z}(\mathbf{x}_*) \geq 0 \quad \text{(Eq. 2.11)}$$

Matrix Z is the null space matrix of $\mathbf{A}(\mathbf{x})$. If the KKT Condition are met at a candidate point, (x_*, λ_*) then that point is guaranteed to be a local minimizer of the original function f(x). The KKT conditions can be used to evaluate if the current iteration point is a local minimum.

The optimization algorithm used in both Pratas [46] and Almeida [8] is the Method of Moving Asymptotes, MMA, see [55]. Since this dissertation can be seen as a follow up on these two previous works, the same algorithm will be employed with some modification in its implementation. Furthermore, an improved version of MMA is also employed, the Global Convergent Method of Moving Asymptotes, so-called GCMMA. The difference on utilizing MMA when compared to the Newton Method is the latter's reliance on second order derivative information, that MMA does not require, at the cost of a linear rate of convergence, lower than Newton's Method [54].

2.2.1.1 Method of Moving Asymptotes

The Method of Moving Asymptotes, MMA, is used to solve the problem of the following form,

$$\begin{aligned} \min_{x} \quad & f_0(x) + a_0 z_{MMA} + \sum_{i=1}^{m} \left(c_i y_i + \frac{1}{2} d_i y_i^2 \right) \\ s.t \quad & g_i(x) - a_i z_{MMA} - y_i \leq 0, \quad i = 1, \dots, m \\ & \mathbf{x} \in X, y \geq 0, \; z_i \geq 0 \end{aligned} \quad \text{(Eq. 2.12)}$$

Where, $X = \{\mathbf{x} \in \Re \,|\underline{x}_e \leq x_e \leq \overline{x}_e, e = 1, \dots, n\}$. The objective function f_0 and constraint functions $g_i, g_1, \dots, g_m$ are given, continuously differentiable, real-valued function on X. $a_0, a_i, c_i \; and \; d_i$ are given real numbers which satisfy $a_0 > 0, a_i \geq 0, c_i \geq 0, d_i \geq 0$ and $c_i + d_i > 0$ for all i, as well as $a_i c_i > a_0$ for all i with $a_i > 0$. Lastly the optimization variables are only x_j since y_i and z_{MMA} are artificial variables.

Since one of the limitations of optimization algorithms is that the functions in the problem formulation need to be convex, MMA solves this restriction by using approximating function that are defined by (Eq. 2.13), these functions can be guaranteed to be convex.

$$g_i^k(x) = r_i^k + \sum_{j=1}^{n}\left(\frac{p_{ij}^k}{U_j^k - x_j} + \frac{q_{ij}^k}{x_j - L_j^k}\right) \quad \text{(Eq. 2.13)}$$

Where

$$p_{ij}^k = \begin{cases} \left(U_j^k - x_j^k\right)^2 \frac{\partial g_i}{\partial x_j} & \text{if} \frac{\partial g_i}{\partial x_j} > 0 \\ 0 & \text{if} \frac{\partial g_i}{\partial x_j} \leq 0 \end{cases} \quad \text{(Eq. 2.14)}$$

$$q_{ij}^k = \begin{cases} 0 & \text{if} \frac{\partial g_i}{\partial x_j} \geq 0 \\ -\left(x_j^k - L_j^k\right)^2 \frac{\partial f_i}{\partial x_j} & \text{if} \frac{\partial g_i}{\partial x_j} < 0 \end{cases} \quad \text{(Eq. 2.15)}$$

$$r_i^k = g_i\left(x^k\right) - \sum_{j=1}^{n}\left(\frac{p_{ij}^k}{U_j^k - x_j^k} + \frac{q_{ij}^k}{x_j^k - L_j^k}\right) \quad \text{(Eq. 2.16)}$$

In these approximating functions the values of L_j^k and U_j^k are the moving asymptotes that give name to the method and limit the value of x_j because $L_j^k \leq x_j \leq U_j^k$, these are chosen according to two heuristic rules from [55]:

- If the process tends to oscillate, then it needs to be stabilized. This is accomplished by moving the asymptotes closer to the current iteration point.
- If, instead, the process is monotone and slow, it needs to be relaxed. This is accomplished by moving the asymptotes further away the current iteration point.

Furthermore, choosing a finite value for asymptotes U_j^k and L_j^k guarantees that the resulting approximation is a convex function [55].

Depending on the sign of the original function's first derivative the approximating function will either be defined by p_{ij}^k or q_{ij}^k with r_i^k being a correcting function. The approximating function is a first order approximation of $g(x)$, see (Eq. 2.17).

$$g_i^k\left(x^k\right) = g_i\left(x^k\right) \text{ and } \frac{\partial g_i^k}{\partial x_j} = \frac{\partial g_i}{\partial x_j} \text{ at } x = x^k \quad \text{(Eq. 2.17)}$$

This approximation function is used to solve a primal-dual sub problem whose solution is then used in the next iteration.

$$\min_{x} \quad \sum_{j=1}^{n}\left(\frac{p_{0j}^{k}}{U_j^k - x_j} + \frac{q_{0j}^{k}}{x_j - L_j^k}\right) + r_0^k \tag{Eq. 2.18}$$

$$\text{S.t.} \quad \sum_{j=1}^{n}\left(\frac{p_{ij}^{k}}{U_j^k - x_j} + \frac{q_{ij}^{k}}{x_j - L_j^k}\right) + r_i^k \le g_i \tag{Eq. 2.19}$$

$$\max\{x_j, \alpha_j^k\} \le x_j \le \min\{x_j, \beta_j^k\} \tag{Eq. 2.20}$$

The parameters α_j^k and β_j^k are called move limits and are defined by (Eq. 2.21) and (Eq. 2.22).

$$\alpha_j^k = 0.9L_j + 0.1x_j^k \tag{Eq. 2.21}$$

$$\beta_j^k = 0.9U_j + 0.1x_j^k \tag{Eq. 2.22}$$

These so-called move limits limit the variation in x_j^k avoiding numerical singularities because they are chosen so that $L_j^k < \alpha_j^k < x_j^k < \beta_j^k < U_j^k$. This stabilizes the optimization algorithm by limiting its convergence. The move limits are implemented according to (Eq. 2.23) and (Eq. 2.24) utilizing a constant that controls the interval in which these move limit can vary, k_α.

$$\max\{\underline{x}_j; L_j + k_\alpha(x_j^k - L_j)\} \tag{Eq. 2.23}$$

$$\min\{\overline{x}_j; U_j + k_\alpha(x_j^k - U_j)\} \tag{Eq. 2.24}$$

When implementing the asymptotes, the first two iterations of the sub problem calculate the upper and lower bounds differently (Eq. 2.25) than the following iterations do, (Eq. 2.26) see [56].

$$\begin{cases} l_j^k = x_j^k - 0.5(\overline{x}_j - \underline{x}_j) \\ u_j^k = x_j^k + 0.5(\overline{x}_j - \underline{x}_j) \end{cases} \tag{Eq. 2.25}$$

$$\begin{cases} l_j^k = x_j^k - \gamma_j^k(\overline{x}_j - \underline{x}_j) \\ u_j^k = x_j^k + \gamma_j^k(\overline{x}_j - \underline{x}_j) \end{cases} \tag{Eq. 2.26}$$

This γ_j^k is a parameter used by Svanberg [56] to limit the variation in the value of x_j from one iteration to the next. It was critical to apply a continuation approach to it so that the solution to the buckling constraint would give a reasonable solution. This would restrict the progress of the iteration point so that a more reasonable step direction is chosen, as when this

parameter is low the value of x_j cannot tend towards local minimum within the first few iterations.

2.2.1.2 A Globally Convergent version of MMA

The distinction between the underlying MMA calculations presented and the globally convergent version of the algorithm is in the approximating function for the sub problem. GCMMA is processed in two iterative loops, an 'outer' iteration loop, and an 'inner' iteration loop. The outer iteration is where a new iteration point is picked from, while the inner iteration is where the approximating function are recalculated until they are greater than or equal to the original function.

For this to work, a new iteration k will denote the outer iterations while v will denote the inner iteration with the double index notation (k, v) being used. The optimization will run as indicated in [58]. The approximating function are defined based on (Eq. 2.27).

$$g_i^{k,v}(x) = r_i^{k,v} + \sum_{j=1}^{n}\left(\frac{p_{ij}^{k,v}}{U_j^k - x_j} + \frac{q_{ij}^{k,v}}{x_j - L_j^k}\right) \tag{Eq. 2.27}$$

where

$$p_{ij}^k = \left(U_j^k - x_j^k\right)^2\left(1.001\left(\frac{\partial g}{\partial x_j}\left(x^k\right)\right)^+ + 0.001\left(\frac{\partial g}{\partial x_j}\left(x^k\right)\right)^- + \left(\frac{\rho_i^{k,v}}{\overline{x}_j - \underline{x}_j}\right)\right) \tag{Eq. 2.28}$$

$$q_{ij}^k = \left(x_j^k - L_j^k\right)^2\left(0.001\left(\frac{\partial g}{\partial x_j}\left(x^k\right)\right)^+ + 1.001\left(\frac{\partial g}{\partial x_j}\left(x^k\right)\right)^- + \left(\frac{\rho_i^{k,v}}{\overline{x}_j - \underline{x}_j}\right)\right) \tag{Eq. 2.29}$$

$$r_i^{(k)} = g_i\left(x^k\right) - \sum_{j=1}^{n}\left(\frac{p_{ij}^k}{U_j^k - x_j^k} + \frac{q_{ij}^k}{x_j^k - L_j^k}\right) \tag{Eq. 2.30}$$

The novelty in this new definition is manly the new parameter $\rho_i^{k,v}$ which is updated in each inner iteration, changing the approximations p_{ij}^k and q_{ij}^k such that it they are guaranteed to be convex and conservative with respect to the original function and its gradients.

2.2.2 Non-Gradient Based Optimization

Also known as derivative-free optimization, it is common to find in the literature non gradient based optimization algorithms that use heuristic methods to solve the optimization problem. For example, some authors use Genetic Algorithms (GA) to solve regular Structural Optimization Problems (STO) [41].

Some authors have also applied neural networks to solve structural optimization relying on a machine learning algorithm to overcome some stability difficulties with an interesting proposition of even being able to solve plastic design of steel structures. [7]

In [51] it is argued that non-gradient based optimization on a small-scale problem can (1) have better convergence, (2) deal with discrete designs, (3) it's easy to implement, as it lacks the need for gradients, and (4) it shows potential for parallel computing techniques. However, these methods lose these benefits as the number of variable increases as it is often the case in topology optimization design problem.

2.2.3 Sensitivity Analysis

One critical aspect of gradient-based optimization is associated with determining the various gradients themselves as that process has a significant computational cost. The commonly used Finite Element Method (Eq. 2.31) is usually underlying many optimization problems so its treatment in stress derivatives requires special attention.

$$\mathbf{K}(\mathbf{x})\mathbf{u} = \mathbf{f}(\mathbf{x}) \tag{Eq. 2.31}$$

Equation (Eq. 2.31) represents an equilibrium problem in elasticity problems of solid mechanics. The element stiffnesses matrices are assembled into the global matrix $\mathbf{K}(\mathbf{x})$, a load $\mathrm{f}(\mathbf{x})$ is applied producing the displacement vector $\mathbf{u}$.

Consider the generic functional $\Psi\big(\mathbf{x}, \mathbf{u}(\mathbf{x})\big)$ representing any constrain or objective function in a FE-based design domain. Typically, these are either constraints or objective functions that are defined based on information about both the variable value, x_i, and/or the displacement associated with it, $u(x)$. The stress function is a good example of such functional. It depends on the extension of the bar, which in turn depend on the design variables, see (Eq. 2.32).

$$\sigma_e\big(u(x)\big) = E_e \varepsilon\big(u(x)\big) = E_e \frac{u_e(x)}{L_e} \tag{Eq. 2.32}$$

To calculate the sensibility of $\Psi\big(x, u(x)\big)$ a total derivative is applied based on the chain rule resulting in (Eq. 2.33), see also [46].

$$\frac{d\Psi}{dx}\big(x, u(x)\big) = \frac{\partial \Psi}{\partial x} + \frac{\partial \Psi}{\partial u}\frac{\partial u}{\partial x} \tag{Eq. 2.33}$$

Usually, the first partial derivative (explicit) is easy to resolve since it can be computed directly in its analytical form. However, the second derivative (implicit) can be more complex due to the contribution of $\frac{\partial u}{\partial x}$, see [8]. Differentiating (Eq. 2.31) and solving for $\frac{\partial u}{\partial x}$ results in (Eq. 2.34) which can be reintroduced to equation (Eq. 2.33) resulting in (Eq. 2.35).

$$\frac{\partial u}{\partial x} = K(x)^{-1}\left[\frac{\partial f}{\partial x} - \frac{\partial K(x)}{\partial x}u(x)\right] \quad \text{(Eq. 2.34)}$$

$$\frac{d\Psi}{dx}\big(x, u(x)\big) = \frac{\partial \Psi}{\partial x} + \frac{\partial \Psi}{\partial u}K(x)^{-1}\left[\frac{\partial f}{\partial x} - \frac{\partial K(x)}{\partial x}u(x)\right] \quad \text{(Eq. 2.35)}$$

Computing the inverse of the global stiffness matrix results in added complexity and, therefore, computational cost. So, the problem of solving $\partial u/\partial x$ can be addressed via the Direct Differentiation or the Adjoint Method as summarized below.

2.2.3.1 Direct Differentiation

Here one calculates the derivatives directly from equation (Eq. 2.36) which results in a system of equation with as many equations as there are design variables, see [18].

$$K\frac{du}{dx} = \left[\frac{\partial f}{\partial x_i} - \frac{\partial K(x)}{\partial x}u\right] \quad \text{(Eq. 2.36)}$$

2.2.3.2 Adjoint Method

This method is recommended for topology optimization problems characterized by number of design variables that is higher than the number of constraints defined by function, $\Psi\big(u(x)\big)$, as aforementioned [10]. The adjoint method's formulation is presented below.

$$K\lambda = z\,,\, z_i = \frac{\partial \Psi}{\partial u_i}\,,\, \lambda = \frac{\partial \Psi}{\partial u_i}K^{-1} \quad \text{(Eq. 2.37)}$$

In the adjoint problem's formulation z_i is called the dummy load vector and is given by differentiation of $\Psi\big(x, u(x)\big)$ with respect to the displacements, while $\boldsymbol{\lambda}$ is called the adjoint vector. Applying the adjoint problem methodology to (Eq. 2.33) results in a formulation that will be and used to develop the sensitivity analysis of the stress constraints, (Eq. 2.38).

$$\frac{d\boldsymbol{\Psi}}{dx}\big(x, u(x)\big) = \frac{\partial \boldsymbol{\Psi}}{\partial x} + \boldsymbol{\lambda}^T\frac{d}{dx}(\mathbf{f} - \mathbf{K}\mathbf{u}) \quad \text{(Eq. 2.38)}$$

In Pratas [46] a very thorough and well explained comparison between the two methods is presented that concludes that a direct differentiation method is preferred when de number

of constraints, m, is higher than the number of variables, n. And conversely the adjoint method is preferred when the number of constraints is lower than the number of variables, $m > n$.

Both methods behave identically when the number of constraints is close to the number of variables, $m \cong n$. Initially, it may be obvious that a direct differentiation is preferred since the number of constraints per element is two, resulting in twice as many functions to derive than variables, $m = 2n$, as will be shown by the problem formulation. However, both the stress constraint and the buckling constraint are based on the element's stress which is a functional dependent on the node displacement, (Eq. 2.32). This rearrangement of the sensibility calculus will result in the same number of constraints as there are variables, $m = n$, for which it would be preferred to apply a direct differentiation as it is algorithmically easier to implement. Yet the adjoint method was implemented regardlessly, because the work done in this dissertation was not done in isolation, it was based on previous dissertations and will, hopefully, constitute the basis of future similar works. At the cost of some difficulty in the present other future projects were simplified such as adding multi-material density variables.

Because of this, the adjoint method is preferred. On the other hand, the stress associated with an inactive constraint does not need to be considered, reducing the number of adjoint problems to be considered, and thus justifying using the adjoint problem method when solving for the constraint's derivatives, since the effective number of constraints can be significantly smaller than the number of variables. This is because to minimize the number calculations done within the MMA algorithm only the active constraints are sent to optimizer, an idea inspired by active constraint methods.

2.2.3.3 Sensitivity Formulation Readjustment

This dissertation takes as a basis primarily the work done by Pratas [46] and Almeida [8] in which the adjoint method is applied directly to a constraint, as they consider only an admissible stress constraint of the form shown in (Eq. 2.39).

$$g^{\sigma} = \left(\frac{\sigma_e}{\overline{\sigma}_e}\right)^2 - 1 \leq 0 \qquad \text{(Eq. 2.39)}$$

The sensitivity analysis presented applies the adjoint method directly to this constraint results in formula (Eq. 2.40) since in the context of this problem the load vector is independent from the project variables.

$$\frac{dg^{\sigma}}{dx_e} = \frac{\partial g^{\sigma}}{\partial x_e} - \lambda_e^T \frac{\partial \mathbf{K}}{\partial x_e}\mathbf{u} \qquad \text{(Eq. 2.40)}$$

However, this methodology is only applicable when only one constraint is considered. If another constraint was to be applied another adjoint set of linear equation would have

needed to be solved, greatly increasing the number of calculation necessary and forgoing the benefits of employing the adjoint method.

A significant readjustment to how the constraint sensitivity is calculated was done, since the optimization is a stress-based optimization. As previously mentioned, both the admissible stress constraint and the buckling stress constraint, as well as other mechanical resistance constraints are defined as higher-order function defined based on stress functions. Therefore, a derivative of the stress is always implicitly calculated when calculating constraints sensitivity. That means that determining the derivative of the stress function can be taken as a common step between the different constraints' sensitivities, even if those constraints refer to different mechanical phenomenon.

Let the stress on a given element be defined by (Eq. 2.41), a more detailed explanation of this expression is given in chapter 2.3.

$$\sigma_e\big(u(x)\big) = E_e \begin{Bmatrix} \cos\theta \\ \sin\theta \\ -\cos\theta \\ -\sin\theta \end{Bmatrix} \frac{\mathbf{u}(x)}{\mathbf{L_e}} \qquad \text{(Eq. 2.41)}$$

Applying the adjoint method to this stress definition results in formula (Eq. 2.42).

$$\frac{d\sigma_e}{dx_e} = \frac{\partial\sigma_e}{\partial x_e} - \lambda_e^T \frac{\partial \mathbf{K}}{\partial x_e}\mathbf{u} \qquad \text{(Eq. 2.42)}$$

Calculating the stress sensitivity directly with the adjoint method allows for a simpler implementation of further constraints of mechanical resistance, since the sensitivity of those constraints is now calculated directly apart from the stress derivative which is calculated only once by the adjoint method. This stress sensitivity calculation is explored further in section 4.2.

2.3 Finite Element Method

The FEM was briefly touched upon in the previous section the following is a more insightful demonstration of the method. Courant [19] was one of the first implementations of what would later be known as the Finite Element Method, a term coined by Clough [16] is developed partly as an aid for the development of airplane wings by the Structural Dynamics Unit under the Boeing Airplane Company.

The FEM presents a discretization of a continuous domain by simple subdomains, called finite elements, which allow for the construction of approximating functions. Resulting in powerful features when compared with other discretization methods. [17] The FEM is comprised of three stages (1) Pre-processing, (2) solution and (3) post-processing.

In a pre-processing stage the continuous domain to be studied is represented by a preselected type of element that will approximate it. Several points in space, or nodes, are distributed across the domain and then several elements connect those nodes to each other. Figure

2.1 shows a schematic representation of this process which is often referred to as meshing and is the source for several errors when applying a FEM.

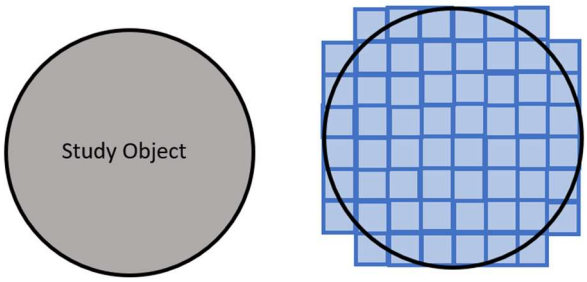

Figure 2.1 - Meshing process (a) original study domain (b) schematics of a meshed domain

After a domain is properly discretized, or meshed, the approximating function need to be derived. The approximating function is usually of the form presented in the second-order differential equation (Eq. 2.43) since it can represent many physical processes.

$$-\frac{d}{dx}\left(a\frac{du}{dx}\right)+cu-f=0 \qquad \text{(Eq. 2.43)}$$

Where u is the dependable variable that satisfies the differential equation, and it is usually dependent on the independent variable x. The other parameters' meaning changes depending on the type of physical settings that are considered therefore the FEM is constant through many applications and the context is what gives these parameters their meaning. The Finite Element method can be applied to a wide variety of problems like solid and structural mechanics, fluid dynamics including viscous or compressible fluids, mechanical vibration problems with coupled vibrations or damped vibration or even the more complex forced vibrations, heat transfer problems and so on. [40]

The topic of solving differential equation is lengthy however when dealing with the FEM an approximation of the exact solution is used resulting in (Eq. 2.44)

$$\mathbf{K}^{e}\mathbf{u}^{e}=\mathbf{f}^{e}+\mathbf{Q}^{e} \qquad \text{(Eq. 2.44)}$$

Where $\mathbf{K}^{e}$ is the coefficient matrix of element e and $\mathbf{f}^{e}+\mathbf{Q}^{e}$ are the load vector, with $\mathbf{f}^{e}$ being constant load and $\mathbf{Q}^{e}$ being the load variation from one node to the next, if applicable, it simply represents a distributed load. In a structural environment the coefficient matrix is known as the stiffness matrix, the load vectors are known as force vectors and u is the displacement suffered in each of the degrees of freedom, DOF.

With the element's approximating function derived the next step is to assemble all the local solutions onto a global problem formulation. This assemblage is done based on the nodes that a given element interfaces with, so an element that connects nodes 1 and 2 will impact the

global matrix in positions associated with the DOF's of nodes number 1 and 2 with a compounding effect from all the other elements affecting those nodes. Figure 2.2 schematizes how the local stiffness matrix are put together into the global stiffness matrix.

(a) (b)

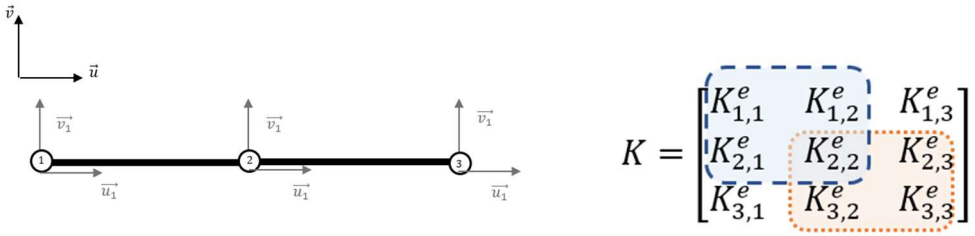

Figure 2.2 - Assembling the global stiffness matrix. (a) 3 Bar structure (b) assembling of stiffness matrix

This concludes the pre-processing stage of the FEM resulting in a matrix equation (Eq. 2.45).

$$\mathbf{Ku} = \mathbf{f} \qquad \text{(Eq. 2.45)}$$

The following stage is the solution stage that solves the previous equation although there are some nuances to the process of solving a matrix equation and there are other types of problem formulations, those won't be addressed in this dissertation.

The last stage is the post-processing stage where the results of the equation are dealt with and interpreted by the user.

2.3.1 Bar, a Finite Element

Truss structures are comprised of unidirectional elements to define its structure so the recommended type of finite element would also be a unidirectional element. Considering that unidirectional structural elements are either a beam element or a bar element and usually the decision of which to employed is based on the type of internal loads that the element is supposed to model. A bar element models a bar, a mechanical element that supports only axial loads and only has two degrees of freedom on its local coordinate system that capture the movement of nodes along the element's axis. As opposed to a beam element that has two nodes on its extremities and two degrees of freedom per node, four in total, referring to the node's rotation and movement in an orthogonal direction, there exists a complex finite element that combines bars and elements named framed element, that captures all the loads supported by each of these two finite elements.

With the added complexity of a beam element, they should only be considered for analysis when strictly necessary since the lower cost of bar elements would allow the analysis of larger and more complex structures. A bar element is comprised of two connected nodes $i\ and\ j$ and is defined by the length between those nodes and the cross-sectional area of the element, it can also have material information for the purposes of structural optimization the Young's Module and the specific density are required since the rigidity of the element and its mass are important for defining the constraint and objective function.

For a bar on its local coordinate system the local stiffness matrix is defined by (Eq. 2.46)

$$\mathbf{k}^{e} = \frac{A_e E}{L_e}\begin{bmatrix} 1 & -1 \\ -1 & 1 \end{bmatrix} \tag{Eq. 2.46}$$

However, since the bars may have different alignments the global coordinate system must be considered, that is done by considering a transformation matrix that converts the coordinates form the local to de global matrix coordinate system, (Eq. 2.47)

$$\mathbf{K}^{e} = \mathbf{T}_e^{T}\mathbf{k}^{e}\mathbf{T}_e, \text{ with } \mathbf{T}_e = \begin{bmatrix} \cos\theta_e & \sin\theta_e & 0 & 0 \\ 0 & 0 & \cos\theta_e & \sin\theta_e \end{bmatrix} \tag{Eq. 2.47}$$

Where θ is the angle of the element w.r.t. with the horizontal axis. In (Eq. 2.48) and (Eq. 2.49) the same process is applied to the load and DOF vectors.

$$[\mathbf{F}^{e}] = [\mathbf{T}_e]\{\mathbf{f}^{e}\} = \begin{bmatrix} f_1^e \cos\theta \\ f_1^e \sin\theta \\ f_2^e \cos\theta \\ f_2^e \sin\theta \end{bmatrix} \tag{Eq. 2.48}$$

$$[\mathbf{U}^{e}] = [\mathbf{T}_e]\{\mathbf{u}^{e}\} = \begin{bmatrix} u_1^e \cos\theta \\ u_1^e \sin\theta \\ u_2^e \cos\theta \\ u_2^e \sin\theta \end{bmatrix} \tag{Eq. 2.49}$$

When applying a finite element analysis to structural topology optimization it is important to note that the force applied in each element is dependent both on the area of that element and on its material properties.

2.4 Buckling Constraints

Buckling is a phenomenon that is prevalent in column mechanical components such as beams and bars under compression where the load that provokes the component's failure may be far inferior to the material's compressive yield. The critical buckling load, P^{cr}, given by Euler's Column Formula (Eq. 2.50) [39], indicates the limiting value for this behavior.

$$P^{cr} = \frac{\pi^2 EI}{(n_{cr}L)^2} \quad \text{(Eq. 2.50)}$$

In this formulation E represents the material Yield Strength, I represent the cross-sectional moment of inertia, $\mathbf{L}$ represents the column's length and lastly n_{cr} is a parameter that accounts for the end conditions of the column and controls the effective buckling length, since the columns used in this work will be articulated at both ends, $n_{cr} = 1$. This formula appears in the various buckling problem formulations. A further rearrangement can be made to this formula since $I = B_e A_e^2$, for a circle cross-section $B_e = 1/4\pi$ (Eq. 2.51) [3]. Defining the moment of inertia this way facilitates having the area as an optimization variable and let's change, when implementing, the shape of the element's cross-sectional area.

$$P^{cr} = \frac{\pi^2 E B_i a_i^2}{\mathbf{L}^2} = \frac{\pi E A_e^2}{4\mathbf{L^2}} \quad \text{(Eq. 2.51)}$$

To get the previous formula to be in accordance with a stress base formulation it is simply necessary to divide the critical load by the elements area to get the elements' critical stress, (Eq. 2.52).

$$\sigma_{cr_i} = \frac{\pi E a_i}{4L^2} \quad \text{(Eq. 2.52)}$$

In topology optimization if only stress and buckling constraints are employed the solution may lead to unstable structure given that there are unsupported hinges within the final solution [64]. Therefore, one of two solutions may be proposed either dealing with the hinge stability, with a Global Buckling Approach, or removing the hinge entirely, interpretating a bar is modelled by more than one element, with a Local Buckling Approach [48].

2.4.1 Global Buckling Approach

For a global approach to structure buckling an additional constraint is used (Eq. 2.53) which is based on an Eigen values problem (Eq. 2.54).

$$\mathbf{K(t)} + \mathbf{G(u,t)} \succcurlyeq \mathbf{0} \quad \text{(Eq. 2.53)}$$

$$\big(\mathbf{K(t)} + \boldsymbol{\lambda}\mathbf{G(u,t)}\big)z = \mathbf{0} \quad \text{(Eq. 2.54)}$$

In which $\mathbf{K(t)}$ and $\mathbf{G(u,t)}$ are global matrices for stiffness and geometry, respectively [12]. The first Eigen value, λ, is often called the critical load factor since it is a multiplicative factor by which the load must be multiplied to cause structural buckling. This constraint can

only consider the rotation of members in relation to each other since Local Buckling does not influence it therefor is used to avoid hinge instability. [29]
Utilizing global stability structures alongside other optimizing routines it is possible to solve large structure problems [62],[45]
Some authors use imperfections in a ground structure so that the alignment between elements isn't perfect motivating support elements to the unsupported hinge. [35],[44]

2.4.2 Local Buckling Approach

This approach is used when the desired result is to have elements of the ground structure merged into longer bars, but it suffers from a phenomenon known as jumping buckling length [3]. A phenomenon that occurs when at a node the only remaining bars with non-zero area are collinear therefor the length to be considered in Euler's Column Formula, the buckling length, has "jumped" from the length of one bar to the length of two.

Since there is a sudden change in the critical buckling load as some areas tend to zero the feasible region of the areas belonging to collinear members is discontinuous. Gradient based optimization cannot deal with discontinuous feasible regions.

Some strategies have been employed to deal with this phenomenon. The optimization of chains when the adjacent element's area is zero leading to removing the discontinuity from the problem [4]. With a given ground structure divided onto its possible chains the length to be evaluated can either be the length of an individual member or the length of the larger chain if the areas associated with the elements supporting a hinge are zero.

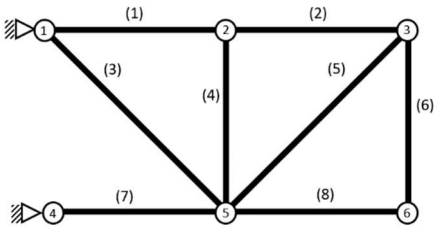

Figure 2.3 - Simple ground structure for chain analysis

In Figure 2.3, each element can be in one of three categories it can be an aligned element, it can be a supporting element, henceforth referred to as adjacent elements, or it can be an unrelated element to the hinge. These categories will create dependencies that will influence the sensitivity as will be shown in following chapters. Considering node 5, the lined elements would be elements (7) and (8), the elements adjacent to that node would be (3), (4) and (5),. Lastly the unrelated elements for node 5 would be (1), (2) and (6), henceforth non-adjacent elements. This distinction into these three categories is important for the computer implementation of this methodology as well as the sensitivity analysis since some properties will have dependency on the adjacent elements.

Other works employ an overlapping larger bar to the ground structure while either using Global Constraints to solve the problem allowing the algorithm to have the alternative between two small bars whose hinge needs support or one longer bar with increased area [25]. Or even by introducing a penalization to the length of each bar discouraging the use of individual member over the usage of the underlying longer bars [47].

Achtziger's work has been used in a large set practical applications in many different problems found in the literature therefore, it will be the preferred method for dealing with the jumping buckling method of this paper. Some works that reference Achztiger's work [21][13],[62]. It is also referred to when dealing with global buckling constraints in conjunction with member buckling because of the treatment of buckling constraint's difficulties even though the jumping buckling length problem is avoided by utilizing the global buckling constraints.

2.5 Epsilon Relaxation

In a stress-based formulation of a topology optimization problem there is a discontinuity that stops the iterative process and is the result of having zero valued areas, since as the area approaches zero the stress approaches infinity. This problem can be circumvented by imposing a minimum value for the area, $\epsilon < A_i$ [27]. Called $\epsilon -$ relaxation it has been shown that it can bridge the gap between sizing and topology optimizations [14]

The structure shown in Figure 2.4 is taken from Guo [26] as well as the member stress that will show what the impact of this $\epsilon -$ relaxation is.

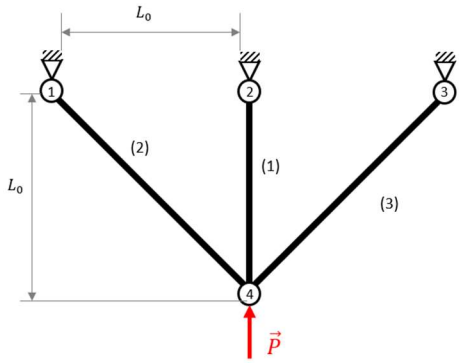

Figure 2.4 - Structure for analysing both the constraint behaviour and the continuation approach from [26]

So that the following calculations are simplified the length shown is attributed as $L_0 = 1$. The stress in the elements shown is given by (Eq. 2.55)and (Eq. 2.56).

$$\sigma_1 = -\frac{2}{2A_1 + \sqrt{2}A_2} \quad \text{(Eq. 2.55)}$$

$$\sigma_2 = \sigma_3 = -\frac{1}{2A_1 + \sqrt{2}A_2} \quad \text{(Eq. 2.56)}$$

Assuming the constraint, g_e^{σ}, shown in (Eq. 2.57) where σ_e is the stress on element e, σ_{adm} is the admissible stress that will be considered the same for every element, and ϵ is the parameter with regards to the $\epsilon-$ relaxation approach. Note that the constraint should be multiplied by the element's area in order to avoid the discontinuity of the stress constraint, instead dealing with internal forces [27].

$$g_i^{\sigma}: A_i\left(\left(\frac{\sigma_i}{\sigma_{adm}}\right)^2 - 1\right) \leq \epsilon \qquad \text{(Eq. 2.57)}$$

Since the stress for elements 2 and 3 are defined by equivalent formulas only g_1^{σ} and g_2^{σ} will be considered.

(a) $\epsilon = 0.000$ (b) $\epsilon = 0.001$

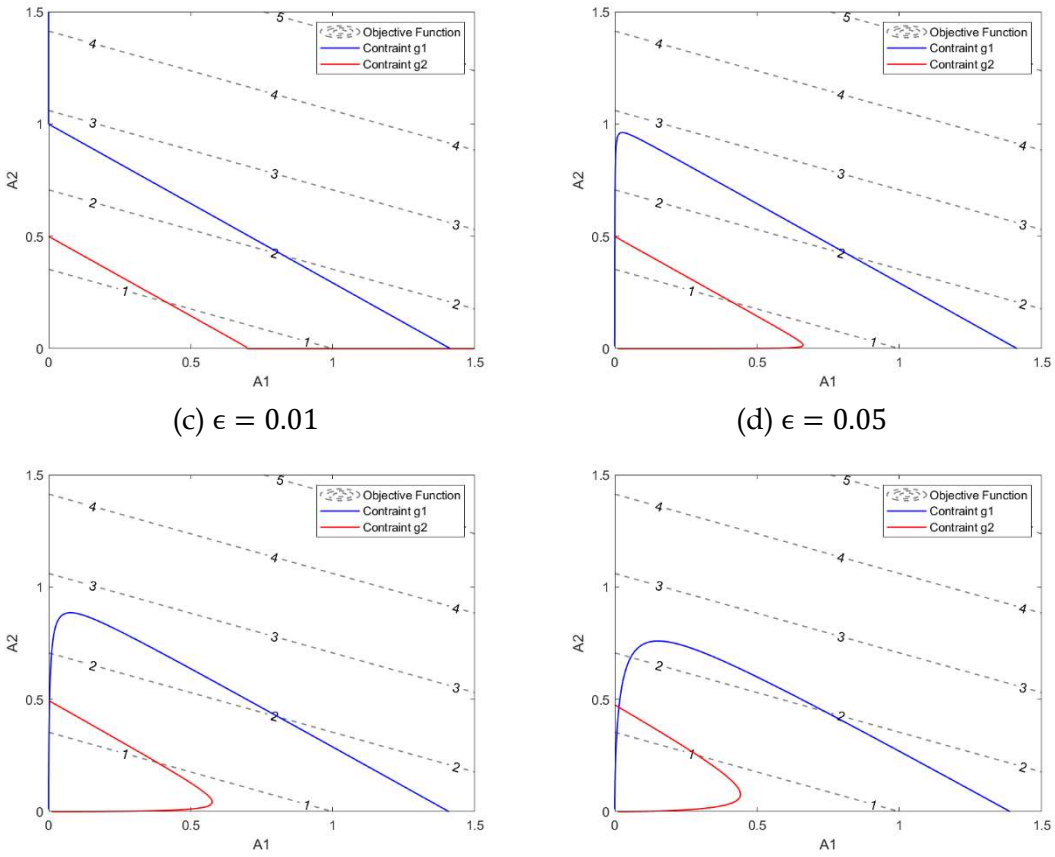

(c) $\epsilon = 0.01$ (d) $\epsilon = 0.05$

Figure 2.5 - ϵ relaxation of the stress constraint with increasing relaxation

Considering the graphs presented in Figure 2.5, it is possible to note that point $(A_1, A_2) = (0,0.5)$ transforms from a discontinuity when $\epsilon = 0$ to a connected area of the admissible region this allows a sizing formulation of an optimization problem to eliminate the necessary bars, merging sizing and topology optimization into the same problem. [14]

2.6 Continuation Approach

Analyzing graphs like the ones presented in Figure 2.5, Guo and Cheng [27] propose that the attractive region of the global optimum increases as ϵ increases. This allows the optimization algorithm to follow a path from an initial relaxed design, where all elements have the same value for their cross-sectional area, until the global optimal point is hopefully reached simply by decreasing ϵ. [15] This approach allows for previously inaccessible sub regions of the admissible region to be accessed by gradient based optimization.

In both Pratas [46] and Almeida [8] the continuation approach is comprised of two distinct stages: a variation stage and a stabilization stage represented by I_1 and I_2 respectively. There is a small initial number of iterations, $\delta_\epsilon I_1$, of I_1 were the parameters are kept constant so that the algorithm has time to adjust to the initial unconstrained problem, according to Pra-

tas [46] $\delta_\epsilon \in [0.05\ 0.20]$. The variation stage I_2 is defined by $\frac{I_1}{k^{ct}}$ with $k^{ct} = 2.5$, finally the number maximum of iteration is given by $I^{max} = I_1 + I_2$. It is important to reference that in Pratas [46] the second interval I_2 is used to restrict the intermediate material constraint g^ϵ as by their notation, this constraint only becomes relevant when dealing with densities has the variables for the optimization problem,

So, starting from a relaxed form, as the iteration progress a linear variation of the relaxing parameter, ϵ, is used to transition onto more restrictive solution, "trapping" the algorithm away from the local minimum with all bars present.

3
PROBLEM FORMULATION AND CONSTRAINT ANALYSIS

3.1 Introduction

In this chapter an analysis of the employed constraints, the nuances of employing them, and some graphical analysis is performed to justify and understand some of the decisions and options that were took when developing the present work and its formulation.

Since the elected type of elements is a bar the only types of loads to be considered are either compression or tension, in both cases they are an axial load with the only difference being the direction the load is applied in. However, the behavior of a bar under these loads differs. While under tension a bar can support almost as much stress as its material tensile yield strength, under compression, and depending on the slenderness of the bar, the same bar may only support fractions of its compressive yield stress, or not even being able to support its own weight. This is due to the buckling phenomena that affects slender mechanical components under compression. A buckling constraint will be developed and implemented in the following chapters so that the stress value of any component under compression is limited to a value lower in value than the critical stress, ensuring that the analysis is performed in the linear stages of the stress curve, simplifying the computation.

When designing any kind of structure, it is important to know what failure criteria will be applied to the material, since it will have implications in the dimensional aspects of the structure. Although there is extensive literature developing algorithms that solve optimization problems with dynamic phenomena such as vibrations [60] or fatigue [36], these will not be included on the current problem formulation. Therefore, the following analysis will only need to consider static effects.

A criterion commonly used is the von Mises stress defined by (Eq. 3.1)

$$\sqrt{\frac{(\sigma_1-\sigma_2)^2+(\sigma_2-\sigma_3)^2+(\sigma_3-\sigma_1)^2}{2}}=\sigma_Y \qquad \text{(Eq. 3.1)}$$

Where, σ_1, σ_2 and σ_3 are the principal stresses and σ_Y is the yield stress for a material determined by a uniaxial tensile test. This definition correlates the state of tension on with a singular scalar parameter that can be correlated directly with the material yield stress. This

von Mises stress-based criteria is also known as maximum distortion strain energy criterion, it is required and regulated by some design norm codes. As it is a bad practice to design components considering that the loads applied to it will develop a stress in the components close to its yield stress, usually a safety coefficient is employed, which is also regulated by norm codes. Resulting in a new limiting stress that will be referred to as admissible stress, σ_{ADM}. In the present work the safety coefficient will be considered one, making the admissible stress equal to the tensile yield stress. This note is important when defining the optimization parameters if a real structure is to be designed.

Elaborating on the energy-based formulation, some earlier works solve the optimization problem of maximizing potential energy [59] which equates to solving a maximum stiffness problem [33]. These works are then referenced to when developing a problem formulation of minimum potential where there are different constraining values for the stress when a component is compressed and when it is tensioned [6].

3.2 Stress Constraint

The previous developments to the current algorithm, performed by Pratas [46] and Almeida [8] only contemplate one single constraint per element, the stress constraint. In their dissertation Pratas [46] explains the three problems of employing a constraint in the form (Eq. 3.2), which are (1) non-linear behavior, (2) local nature and (3) singularity phenomenon.

$$g_i: \left(\frac{\sigma_e}{\sigma_{Adm}}\right)^2 - 1 \leq 0 \qquad \text{(Eq. 3.2)}$$

The nonlinear behavior of the stress constraint can be solved by a mesh convergence analysis, resulting in two types of mesh refinements, *h*-method if the number of elements is increased, or *p*-method if the number of nodes is increased [46]. In a scenario where the test problems are based on defined ground structures changing the mesh layout may be undesirable. So, to deal with nonlinear optimization it is possible to either linearize the constraint or use nonlinear optimization algorithms to solve the problem [28].

The local nature of the stress constraint, comes from the fact that each elements stress needs to be compared to the limiting stress value, resulting in at least as many constraints as there are elements in the ground structure. One of the techniques used to avoid the local nature is aggregation techniques, that deal with a singular overall constraint that results from aggregating the information from every bar [46]. The computational cost of this local nature may turn some examples prohibitively expensive, limiting the size of problem that can be solved. So much so that the efficiency of the programmatic implementation of the algorithm is the key to solve larger and more complex problems. Some authors have applied parallel computing to reduce the time taken to solve such complex problem [31].

The singularity phenomenon is direct consequence of how the stress of an element is calculated since it depends on the element's cross-sectional area. As it approaches zero, in a topology context that should be interpreted as the bar being eliminated, however as the area decreases the element's internal stress tends to infinity. This would mean that the tensile yield criterion is violated and so the elements cross-sectional area needs to be increased, disallowing the topology optimization to continue and reach the true global optimum, since the algorithm gets "trapped" on those local optimums that include bars that should have been removed.

To solve this last problem Pratas [46] presents two different relaxation techniques, the ϵ-relaxation (Eq. **3.3**) and the qp-approach (Eq. 3.4), based on [15],[32].

$$g_i: \left(\left(\frac{\sigma_i(x_{A_i})}{\sigma_{Adm}}\right)^2 - 1\right) x_{A_i} \leq \varepsilon \qquad \text{(Eq. 3.3)}$$

$$g_i: \left(\frac{\sigma_i(x_{\rho_i})}{x_i^q \sigma_{Adm}}\right)^2 - 1 \leq 0 \qquad \text{(Eq. 3.4)}$$

Choosing which of these techniques to apply depend on the type of design variable being used, and since this dissertation's design variable is solely the cross-sectional area, the employed relaxation will be the appropriate $\epsilon -$ relaxation, so the stress constraint will be defined in the form of (3.3). However, the qp-approach will not be removed from the algorithm's implementation, since it is a core component when dealing with density design variables, and it would facilitate the study of this algorithm in a multi-material setting.

3.3 Buckling Constraint

Euler's buckling load defines the maximum load, either stress or force, that a component can support under compressive load, (2.34). To correctly model a truss structure, this phenomenon must be taken into account in the problem formulation since any bar under compression is at risk of buckling. Initially and taking advantage of the fact that buckling only affects elements under compression, a constraint may be formulated understanding that any member's tension stress, σ_i,that is larger than its critical buckling stress, σ_{buc_i}, does not produce buckling [3] (Eq. **3.5**).

$$-\sigma_{buc_e} \leq \sigma_e \qquad \text{(Eq. 3.5)}$$

The above constraint is a concave inequality which cannot be integrated into a convex problem optimization [45]. Poulsen linearizes the constraint trough an iterative process that deals with the derivative of Euler's Buckling. The problem of concave constraints can also be

avoided by dealing with member stress instead of force, but this process introduces discontinuities in the feasible domain. Figure 3.1 shows the feasible regions of a single bar of fixed length with a force applied to its extremities both when studying either the force environment or the stress environment.

(a)

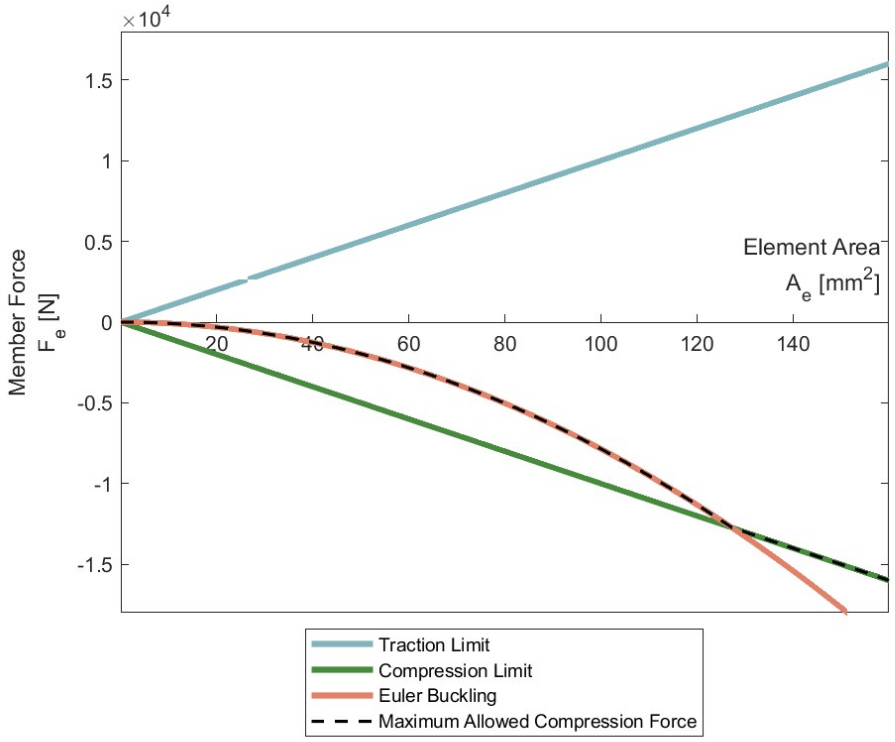

(b)

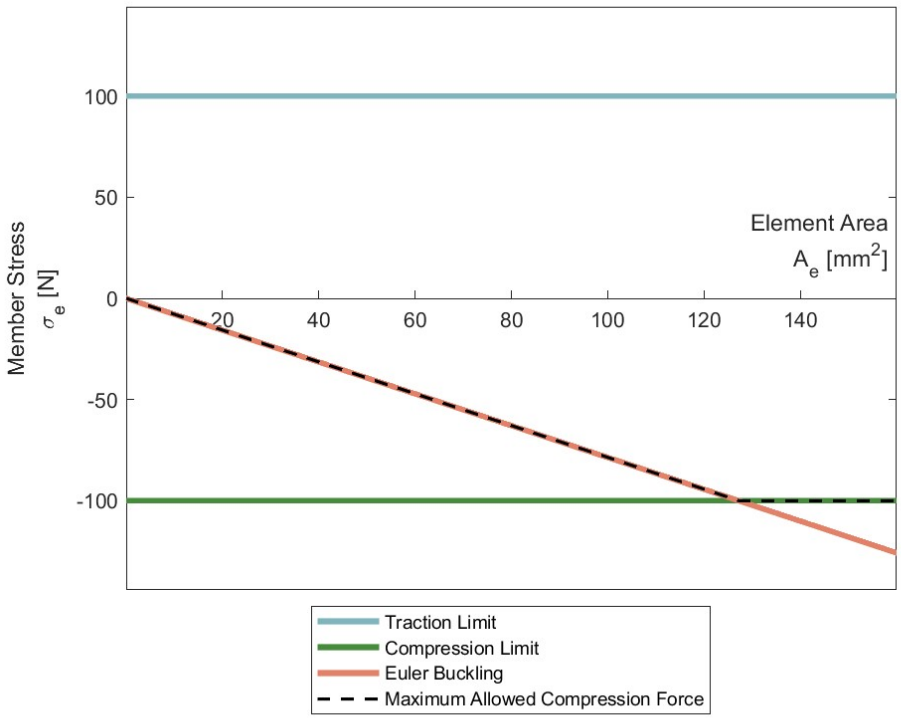

Figure 3.1 - Feasible Region in (a) Force based formulation (b) Stress based formulation

When analyzing the graph presented in Figure 3.1 (a) there are three regions that can be identified. The first region is the elastic case where the generated stress is smaller than the compressive yield stress, this would be the region above the compression limit line. The second region is the plastic case where the generated stress is larger than the compressive yield stress, this would be the region below the compression limit line. Lastly, the third region is the slenderness case which corresponds to the region where the limiting effect is the critical buckling stress instead of the material's compression limit, which would be the region of the graph in between the Euler buckling limit line and the compression limit line [42].

It is interesting to note that the derivative of a force constraint in terms of the design domain, the cross-sectional areas, results in stress information. Linearizing a problem by dealing with the derivative of forces or linearizing by dealing with a stress formulation has the same physical principle behind it. Note also, however, that the 1st order derivatives of a stress function lose physical meaning.

One of the recommendations to correctly apply the optimizing algorithms, both MMA and GCMMA, is that the constraint should have its value comprised in between $0 \leq g_i \leq 100$. For that reason, a normalization of the constraint is applied resulting in the equation shown in (Eq. 3.6)

$$\frac{\sigma_e}{\sigma_{cr}} - 1 \leq 0 \qquad \text{(Eq. 3.6)}$$

However, this transformation isn't as straightforward as shown because of how the element's tension and its critical tension interact as an area tends to zero in value, since both of those parameters depend on the element's area. Consider a given element under a constant force, F_e, such that the stress applied to that element,σ_e, is simply the applied force divided by the element's area, (Eq. 3.7), and its limiting buckling force is given by Euler's Formula, σ_{cr} (Eq. 2.52).

$$\sigma_e = \frac{F_e}{A_e} \qquad \text{(Eq. 3.7)}$$

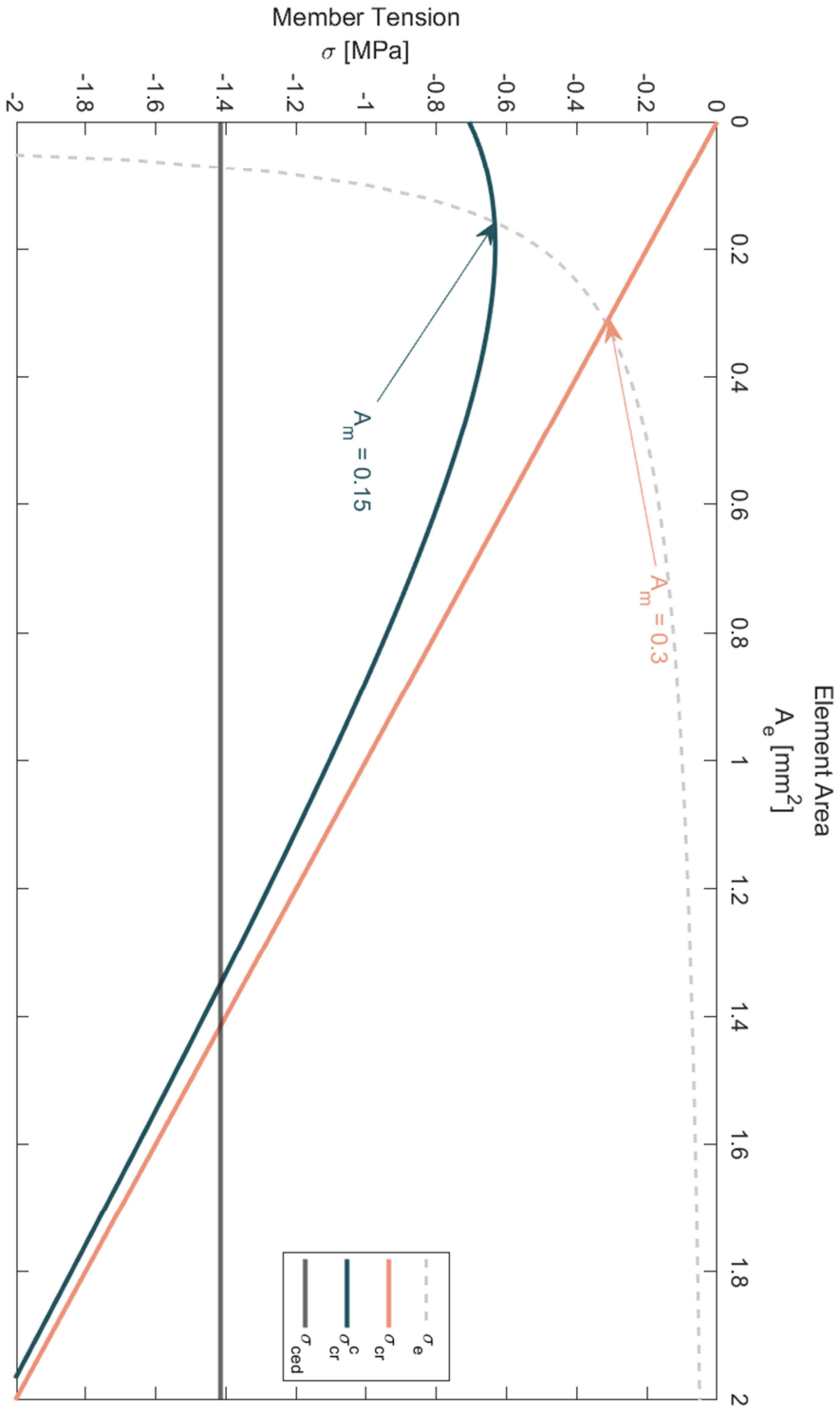

Figure 3.2 - Singularity Plot

As shown in Figure 3.2 as the area tends to zero the stress on that member, σ_e, sharply rises giving rise to a problem when trying to apply a topology optimization algorithm. Similarly, to the stress constraint, the bars won't be eliminated because there is a point at which decreasing the area further would violate the buckling constraint, σ_{cr}. Such a problem necessitates the adaptation of the constraint, by altering the critical stress formula σ_{cr}^{c}, noting that the problem arises from the way this formula behaves as the area tend to an infinitesimal value. Although it is true that a small area would be unstable, it is also true that small enough areas are to be disregarded, when in a topology optimization environment. It should be interpreted that the element is to be eliminated from the final layout, if the area crosses some predetermined threshold, since the area is the topological variable and is of real value. Considering only an initial adaptation of the formula the minimum area allowed by the constraint goes from $A_{min} = 0.3$ to $A_{min} = 0.15$.

The balancing between disregarding small areas and capturing the behavior of small areas without singularity problems can be achieved by adding a new function to the critical stress formula. This function would have little influence in Euler's buckling formula when the function's value is large enough, but it changes the behavior of the function when the area tends to zero and the function itself approaches singularity situations.

The necessary behavior can be observed in a hyperbolic function such as $f(x) = \frac{1}{x}$, adding this kind of function to the critical stress formula would change how the formula behaves for small values of critical load. This is because as the area tends to zero the new added function's value would take over and correct the overall constraint. In Figure 3.2 the line attributed to σ_{cr}^{c} is the product of this adaptation as dictated by formula (Eq. 3.8)

$$\sigma_{cr}^{c}(A_e) = \sigma_{cr}(A_e) + \frac{1}{(A_e + \mu)^p} \qquad \text{(Eq. 3.8)}$$

With

$$\mu = \left(\frac{1}{\alpha \cdot \sigma_{adm}}\right)^{\frac{1}{p}} \qquad \text{(Eq. 3.9)}$$

This new adaptation allows the element's area to approach zero without violating the constraint and as the area increases, the difference between the two formulations tends to zero because $\lim_{A_e \to \infty} \sigma_{cr}^{c} = \sigma_{cr}$. The definition of parameter μ is such that it connects this new added formula to the element's admissible stress, grounding a somewhat abstract concept in physical properties.

It is then important to understand the influence of parameters α and p in the new limiting function since they are independent parameters with great influence in the final constraint. In Figure 3.3, a chart is presented where both parameters are varied such that the new constraint can be plotted in conjunction with the dashed element tension line, σ_e.

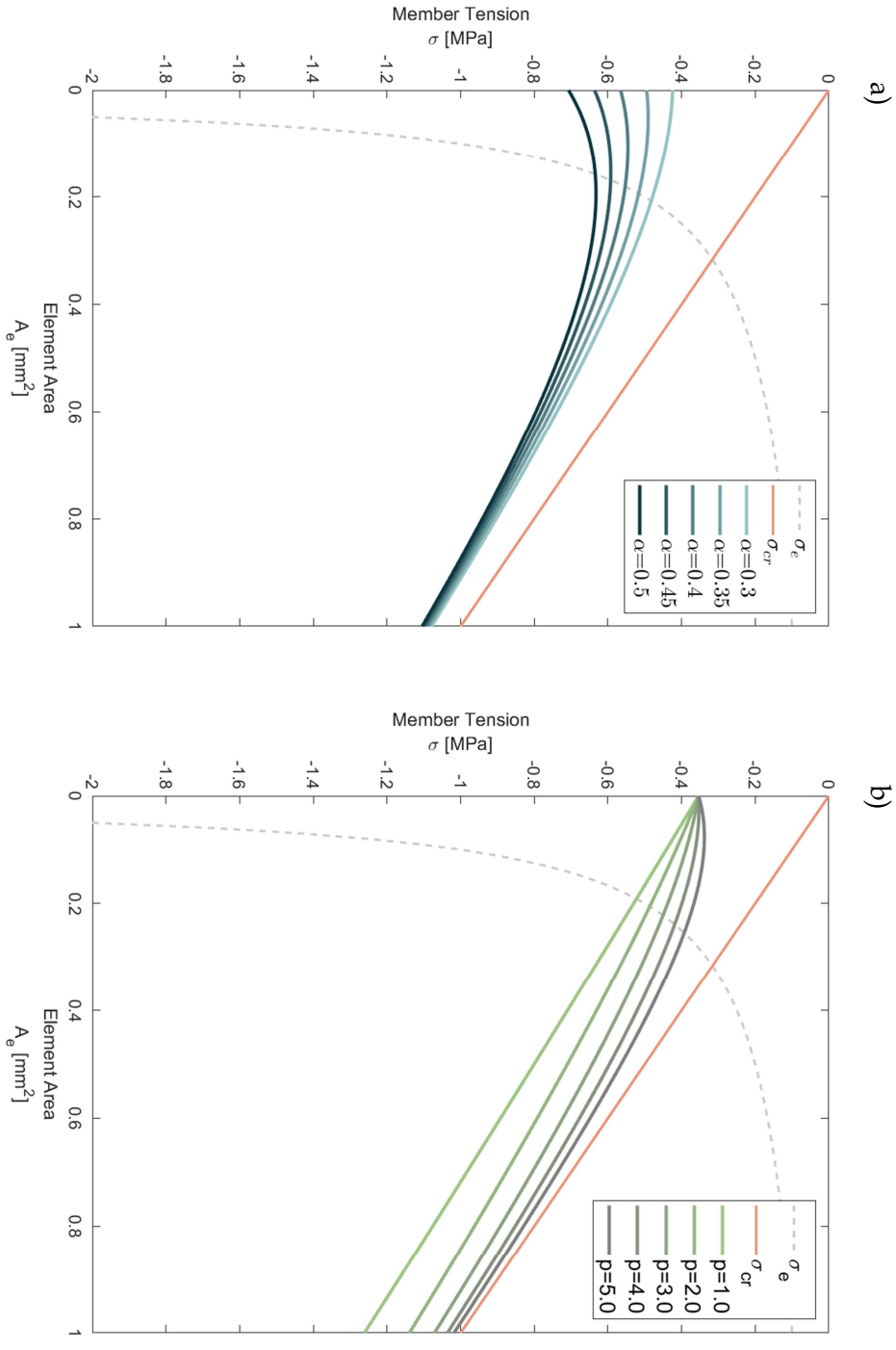

Figure 3.3 - Variation Chart for (a) α with $p = 3$ and (b) p with $\alpha = 0.25$

As seen in Figure 3.3, the larger the value of p is, the closer the new function becomes to the original function while the smaller the value of α, the smaller the different between the functions is. This understanding is important when it comes to defining the behavior of multiple elements and their interaction with each other. However, it is pertinent to note that it is possible to turn this well-behaved function into a concave constraint that might destabilize the optimization algorithm. Note that the intersection point between the element's stress line and the different constraints moves to smaller values of the area, allowing for a more relaxed version of the same problem, since the area variable can take smaller values without violating the modified constraint.

For clarification, the objective of this modification to Euler's buckling formula is to improve the behavior of the overall constraint when small areas are obtained, this results in the partial destruction of the linearization obtained by dealing with a stress-based formulation. The effects of this new adaptation and its importance will hopefully become apparent when analyzing scenarios with more than one element done in 3.3.1.

Another implementation that will facilitate the area of a given member to reach zero is by changing the constraint's formulation so that it vanishes from the problem, changing the number of constraints that are considered in each iteration. This is achieved by rewriting the constraints in the form of $g_i \cdot x_i \leq 0$ [5]. According to Guo, by multiplying the constraint by its area is done, the formulation changes from a stress-based formulation to a force-based formulation [14], this is easily confirmed when considering the stress definition (Eq. **3.7**) and taking considering that the design variable represents the element's cross-sectional area. However, when the constraint is normalized to fit with the optimizing algorithm's requirements it makes the constraint dimensionless, removing all physical meaning. The objective of formulating the local constraints as itself multiplied by the variable they address, then becomes the removal of those constraints [5]. The difficulties associated with including buckling in the constraint do not need to be considered if the constraint is absent, so this reformulation of the constraint improves it's relaxation without sacrificing the meaning of the constraint when dealing with larger areas.

To ensure the value of a constraint defined this way is below one hundred as per the recommendation of the optimizing algorithm, the initial constraint must respect $-1 \leq g_i \leq 1$ because the project variable is defined by $0 \leq x_i \leq 100$. However, this leads to a formulation whose areas cannot be larger than 100, which is inconvenient, so a scaling factor is introduced, ϕ. Applying this scaling factor to the variable, x_{A_i}, so that it captures any element's real area, A_i, results in (Eq. 3.10).

$$A_i = \phi \cdot x_{A_i} \qquad \text{(Eq. 3.10)}$$

The parameter ϕ affects the entire problem formulation, so it is not element dependent, this mean it is a scaling parameter that will affect the entire constraint. The fact that the area

variable is now always bounded by $0 \leq x_i \leq 100$, results in a notion of normalized area variable, x_{A_i}. With the motivation of presenting a cohesive version of the constraint, only the normalized area variable will be multiplied by the constraint, omitting the scaling factor ϕ, since it applies to every element. The disappearing constraint effect is preserved since as x_{A_i} tends to zero so does the overall constraint.

The result of the previous considerations is a constraint that is defined as shown in (Eq. 3.11). This constraint resolves the singularity issues of including the buckling effect into the problem formulation with normalized constraints applicable to MMA and GCMMA by aggregating two attenuating effects, the relaxation of Euler's formula and erasing the constraint as x_{A_i} tends to zero.

$$g_i: \left(\frac{\sigma_e}{\frac{\pi E_e \phi \cdot x_i}{4L^2} + \frac{1}{(x_i + \mu)^p}} - 1 \right) \cdot x_{A_i} - \varepsilon \leq 0 \qquad \text{(Eq. 3.11)}$$

With

$$\mu = \left(\frac{1}{\alpha \cdot \sigma_{adm}} \right)^{\frac{1}{p}} \qquad \text{(Eq. 3.12)}$$

This constraint is not yet the final form the constraint will take as it does nothing to address the jumping buckling length phenomenon, but it is important to first analyze this intermediate form of the constraint to prevent the analysis of the full constraint from being too cumbersome. So, to better understand the importance of this definition, in the following chapter, a two variable problem is created and studied such that a visual representation on a Cartesian graph is possible.

3.3.1 Structural Optimization Problem with Two Variables

Because a graphical representation is usually helpful to understand a complex mathematical problem, a two variable problem is used such that its solution is a known point. Starting from a five-bar ground structure, seen in Figure 3.4, the five potential variables, associated with each of the elements' bars, $x_{A_1} \rightarrow x_{A_5}$ are grouped into one of two auxiliar variables, A_1 and A_2. This grouping is done such that the elements grouped into A_1 are the only elements present on the optimum point of the 5-bar problem. In this case the grouping is done according to (Eq. **3.13**).

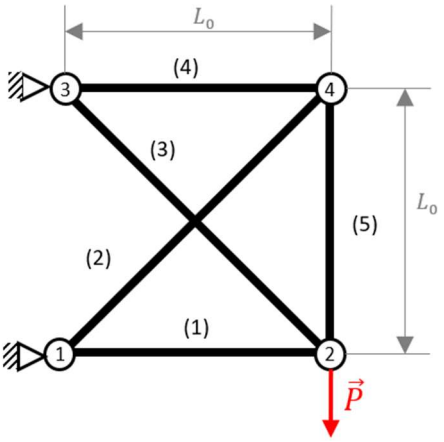

Figure 3.4 - 4 node ground structure

$$\begin{aligned} A_1 &= x_{A_1} = x_{A_3} \\ A_2 &= x_{A_2} = x_{A_4} = x_{A_5} \end{aligned} \qquad \text{(Eq. 3.13)}$$

When analyzing the 5-bar problem it is apparent that only two bars are under compression, bar (1) and bar (2), therefore only two buckling constraints influence the optimal solution. This way a constraint can be associated with each auxiliar variable resulting in a buckling constraint for each variable. This effectively changes the topology optimization problem from a 5-constraint problem into a 2-constraint problem when only buckling constraints are applied.

The value of the optimum auxiliar variables can further be simplified if the adequate physical properties are chosen, Table 3.1. These properties are chosen so that the final optimum design is simply $(A_1, A_2) = (1,0)$, this point will be referenced as point *B* in the following graphs.

Table 3.1 - Simplified material properties

Property	Value
Young Modulus, E_i [Pa]	$\frac{4}{\pi}$
Cell Length, L_0 [m]	1
Applied Force, $\vec{P}$ [N]	1
Admissible Stress, σ_{ADM} [Pa]	$\sqrt{2}$

Applying these parameters to both the definition of stress and critical stress solved both for the element's area, (Eq. 3.14) and (Eq. 3.15) respectively, results in an optimum point that is fully stressed.

$$A_e = \frac{F_e}{\sigma_{adm}} \qquad \text{(Eq. 3.14)}$$

$$A_e = \sqrt{\frac{4L^2}{\pi E} \cdot F_e} \qquad \text{(Eq. 3.15)}$$

With only two buckling constraints it is possible, as mentioned, to plot out the admissible region as a 2D graph, Figure 3.5 shows the graphical representation of a simple application of a buckling constraint, (Eq. **3.16**)). This initial constraint will serve as a baseline from which increasing complexity will be added.

$$g_i : (\sigma_i - \sigma_{crit_i})A_i \leq 0 \qquad \text{(Eq. 3.16)}$$

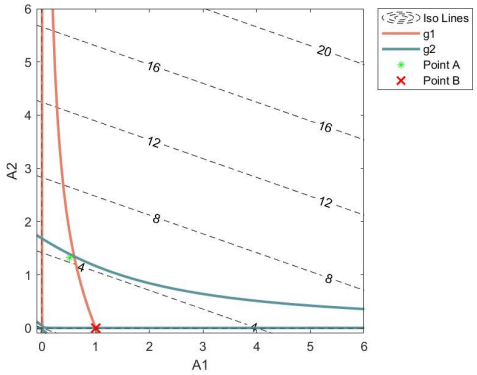

Figure 3.5 - Basic Formulation

The graphical representation of this constraint clearly shows why a gradient based optimization would not deal with this feasible region, since it would tend towards Point A and would have no means of "jumping" the discontinuity onto the true optimum point, Point B. The lines shown have an asymptotic behavior with regards to their respective axis, and so the feasible region is discontinuous. To solve this discontinuity a $\varepsilon - relaxation$ is employed resulting in a formulation that will be referred to as Guo's Formulation, defined by (Eq. **3.17**). The graphical representation of this constraint is shown in Figure 3.6.

$$g_i : (\sigma_i - \sigma_{crit_i})A_i \leq \varepsilon \qquad \text{(Eq. 3.17)}$$

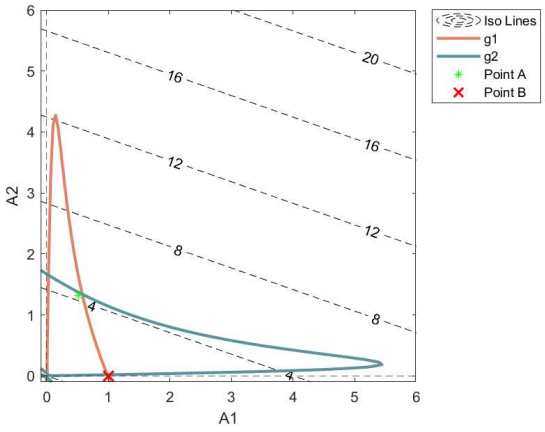

Figure 3.6 - Guo's Formulation

This new constraint initially solves the problems of dealing with a buckling constraint however it is not in accordance with the recommendation for applying the optimizing algorithm [30] and with the works of Pratas [46] and Almeida [8]. Normalizing Guo's Formulation results in (Eq. 3.18) and its graphical representation, Figure 3.7.

$$g_i : \left(\frac{\sigma_i}{\sigma_{crit_i}} - 1\right) A_i \leq \varepsilon \qquad \text{(Eq. 3.18)}$$

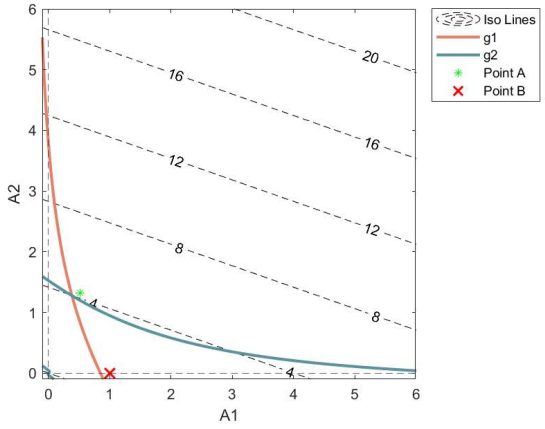

Figure 3.7 - Guo's Formulation Normalized

One realizes that normalizing Guo's Formulation, as per the requirements of MMA algorithm reverts the behavior of the problem, such that an almost asymptotic situation is reappears. It is critical for the optimizing algorithm to recover the buckling constraint's lost behavior. This was achieved by implementing the previously discussed adaptation to Euler For-

mula, (Eq. 3.8), resulting in constraint (Eq. 3.19) equivalent to (Eq. **3.11**) and its graphical representation Figure 3.8. This implementation henceforth be referred to as normalized epsilon relaxation.

$$g_i : \left(\frac{\sigma_i}{\sigma^c_{crit_i}} - 1\right) A_i \leq \varepsilon \qquad \text{(Eq. 3.19)}$$

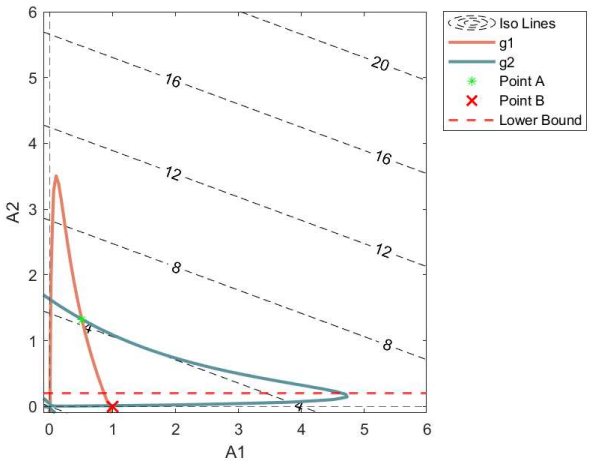

Figure 3.8 - Normalized Epsilon

It is important to note the effect of a lower bound on the optimum point since if the lower bound is high enough it can interfere so much with the admissible region that the optimum is altered, as seen by the red dashed line on the graph. If this line represents a lower bound it will limit the admissible region in such a way that Point B is unattainable, so Point A will be considered the optimum point. This may lead to solution where no bars are eliminated from the final solution therefore defeating the purpose of the topology optimization process.

3.3.2 Jumping Buckling Length

The jumping buckling length is a phenomenon that manifests itself when dealing with buckling constraints on a STO environment because as bars are removed, some nodes may become unsupported. That is to say that only two colinear bars remain attached to the node, in that case the actual buckling length is the sum of both bars' length resulting in an abrupt change of the buckling length to a higher value greatly increasing the minimum allowed area for both bars.

This property creates disjointed admissible areas that make it difficult to apply a gradient based method. It is important to transform this "jump" into a "slope" so that a contiguous region is created. It is possible to overcome this difficulty by defining a problem based on the possible chain within a given ground structure [3]. The basis for this study is a 9 node, 20 bar element ground structure, present in Figure 3.9.

Take for instance node (2), from the five elements connected to it, two are colinear, (1) and (2), and would form a chain. Then if the areas of the other members, the adjacent elements, are set to zero the buckling length to be considered would be the sum of elements (1) and (2) since the node became a hinge.

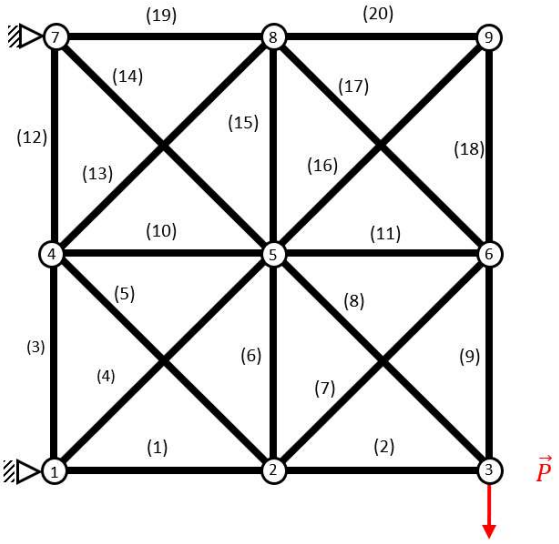

Figure 3.9 - 9 Node Ground Structure

Achtziger would define a constraint using a branched function since there are two scenarios to be considered in the constraint, both an unsupported and a supported node. Therefore, a constraint is defined in the form presented in (Eq. 3.20).

$$g_i : F_i \geq \begin{cases} -\dfrac{\pi E_Y a_i^2}{4L_i^2} & \text{if } C_i(a) = \emptyset \\ -\dfrac{\pi E_Y a_i^2}{4L(c)^2} \ \forall c \in C_i(a) & \text{if } C_i(a) \neq \emptyset \end{cases} \quad \text{(Eq. 3.20)}$$

In which $C_i(a)$ is the set of active chains, c, in a given ground structure, a chain is defined as active if the area of all adjacent elements is zero. This approach of identifying adjacent elements to determine which chains are active is paramount for the methodology employed although as it will be presented some slight modifications were done. The algorithm developed is comprised of two stages, an initial construction of a table that stores the chain information comprising all the chains in the current ground structure, the intermediary nodes associated with each chain and the adjacent elements to each chain. And a second stage performed during the iterative process where the adjacent elements' areas are monitored so that if a node becomes unsupported the correct buckling length is used.

Achtziger's approach proposes that a table of chains is constructed such that as the supporting elements are removed. The leading element of a given chain acquires the properties of the whole chain. In practical terms it removes an intermediary node from the chain in question.

However, this methodology may lead to difficulties if there is a necessity to reintroduce the node into the structure, so some modifications are employed to identify the chains and act accordingly, without removing the underlaying nodes.

The developed algorithm analyses every node on a ground structure and trough the elements connectivity gathers which elements are connected to the node being analyzed. For the 9-node ground structure, the elements' connectivity of the first nine elements, representing only the bottom half of this structure for brevity's sake, is presented in Table 3.2.

Table 3.2 - First 9 element connectivity table for a 9-node ground structure

Element Number	**Node *ii***	**Node *jj***
1	1	2
2	2	3
3	1	4
4	1	5
5	2	4
6	2	5
7	2	6
8	3	5
9	3	6

Since the connectivity table is prerequisite to defining a ground structure it is useful to base the chain effect analysis in this information. When analyzing node (2), to gather the elements connected to it, it is only necessary to check if in the connectivity table an element is defined based on that node. Associating Table 3.2 with Figure 3.9 it is possible to confirm that only the five elements connected to node (2) have their connectivity defined with it.

After determining which elements are connected to the node in question the next step is twofold, determining which elements are collinear, which then means that all the other elements are supporting elements to the chain made from the collinear ones. Taking advantage of the definition of chains being based on collinear elements, it is only necessary to gather the elements' angle with regards to a horizontal reference and matching the ones that are equal.

Table 3.3 - The angle of elements connected to node 2

Element Number	**Angle, θ_i [°]**
1	0
2	0
5	135
6	90
7	45

Table 3.3 shows the angle of each of the elements connect to node 2, as expected only elements (1) and (2) share the same angle, therefor in node 2 there is only one chain comprised of those two elements, while elements (5), (6) and (7) can be defined as adjacent elements. To reiterate, if at any point during the optimization the areas of elements (5), (6) and (7) approach zero, the node should be considered unsupported, and the chain should be considered active, (Eq. **3.21**), with $\Gamma_{adj}(i)$ being the set of adjacent elements to node i.

$$\phi \sum_{j \in \Gamma_{adj}} x_j = 0 \qquad \text{(Eq. 3.21)}$$

Determining that a node is unsupported is a key feature in distinguishing from sequence of elements in which the buckling length is independent from each other, and a sequence of elements that are modelling a larger component. In which case the buckling length should be the sum of the chain's elements buckling length. The buckling length then becomes dependent on the area of the adjacent elements to a particular chain. This dependency has repercussions that will be explored and dealt with in a later sensitivity analysis.

If the area variable is not allowed to reach zero, the requirement for an unsupported hinge cannot be defined as the sum of the adjacent elements' areas being zero. Since, in a computational environment it is rare to encounter a mathematical exact result, due to numerical errors and therefor the areas will only approach zero never actually reaching it. A requirement for an unsupported hinge rather than being defined by (Eq. 3.21), will be defined by (Eq. 3.22).

$$\phi \sum_{j \in \Gamma_{adj}} x_j \leq \varepsilon \qquad \text{(Eq. 3.22)}$$

This approach of defining a low enough value from which a certain variable should be considered zero is a common occurrence when solving problem with a computer analysis. Yet from this formulation a discrepancy becomes apparent, if a chain is supported by only one other element, that element's area may be equal to ϵ, however. if another chain is supported by four elements the area from which the element is considered erased in one fourth of ϵ resulting in an inconsistency when analysing hinges.

With the intention of developing a strategy that encompasses various node dispositions with various possible number of bars connect to any node. A strategy based on the average area, $\bar{A}$, of the elements connected to a node is developed. In this case a node will be considered unsupported if this average value is below a certain cut off point, A_{ref}. The cut off point, or reference area, plays the role of ϵ in equation (Eq. 3.22). The new expression to determine unsupported hinges is represented in (Eq. 3.23).

$$\bar{A} = \frac{\phi}{N_{adj}} \sum_{j \in \Gamma_{adj}} x_j \leq A_{ref} \qquad \text{(Eq. 3.23)}$$

In which, N_{adj} is the number of elements within Γ_{adj}. The usage of the average area is inspired by the way an unsupported node may be defined in a density variable environment, if there is less than one adjacent node it can be identified by the average of the density variables, since these are Boolean variables. If (Eq. 3.24) is verified, then there is less than one adjacent node.

$$\bar{x}_\rho = \frac{1}{N_{adj}} \sum_{j \in \Gamma_{adj}} x_{\rho_j} \leq \frac{1}{N_{adj}} \Leftrightarrow \sum_{j \in \Gamma_{adj}} x_{\rho_j} \leq 1 \quad \text{(Eq. 3.24)}$$

When a chain is identified as active, two different lengths are important for the optimization algorithm the element e's length, L_e, and the length of the chain, element e is part of, the buckling length, L_{buc}. So, if the average area is zero, the length to be considered is the length of the chain, L_{buc}, while if the area is higher than zero then the length to be considered is only the element's length, L_i. By interpolating between these two extremes, it results in (Eq. 3.25).

$$L_{buc} = L_i + \left(1 - \frac{\bar{A}}{A_{ref}}\right) L_j \quad \text{(Eq. 3.25)}$$

This function dominium is only $\bar{A} \in [0; A_{ref}]$ since having a negative buckling length doesn't have any physical significance. So, for values of $\bar{A}$ above the cut-off points the node should be considered fully supported and thus the buckling length should be only the length of the element. For convenience $\beta(\bar{A})$ is introduced, where $\beta(\bar{A}) = \left(1 - \frac{\bar{A}}{A_{ref}}\right)^{p_L}$, with the application of the exponent, p_L, being inspired by a SIMP penalization, as seen in Figure 3.10. This penalization is motivated by the desire to have values of L_{buc} that are either the value of a member's length or the length of the chain and eliminating intermediary values of length. This, in turn, results in the buckling length of a chain of member i and j to be defined by (Eq. 3.26).

$$L_{buc} = L_i + \beta(\bar{A}) L_j \quad \text{(Eq. 3.26)}$$

Where,

$$\beta(\bar{A}) = \begin{cases} \left(1 - \frac{\bar{A}}{A_{ref}}\right)^{p_L} & \text{if } \bar{A} \leq A_{ref} \\ 0 & \text{if } \bar{A} > A_{ref} \end{cases} \quad \text{(Eq. 3.27)}$$

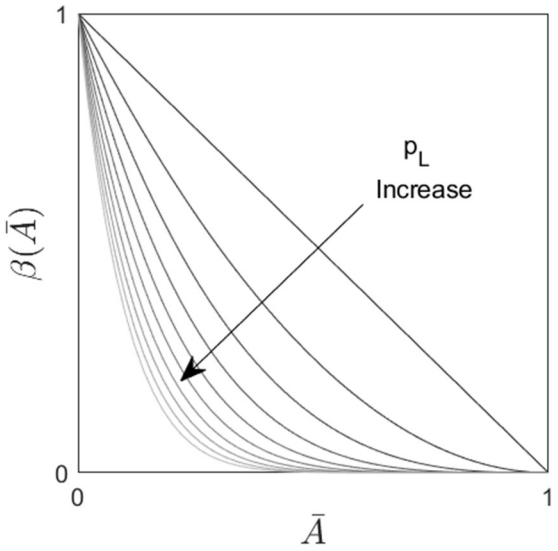

Figure 3.10 - Reverse SIMP behavior of B(A)

Finally, the complete implementation of the buckling constraint for a given element i is given by (Eq. 3.28).

$$g_i^{buc}: \left(\frac{\sigma_e}{\frac{\pi E_e \phi \cdot x_i}{4L_{buc}^2} + \frac{1}{(x_i + \mu)^p}} - 1 \right) \cdot x_i \leq 0 \qquad \text{(Eq. 3.28)}$$

Where,

$$\mu = \left(\frac{1}{\alpha \cdot \sigma_{adm}} \right)^{\frac{1}{p}} \qquad \text{(Eq. 3.29)}$$

$$L_{buc} = L_i + \beta(\bar{A}) \cdot L_j \qquad \text{(Eq. 3.30)}$$

With,

$$\beta(\bar{A}) = \begin{cases} \left(1 - \frac{\bar{A}}{A_{ref}}\right)^{p_L} & if\ \bar{A} \leq A_{ref} \\ 0 & if\ \bar{A} > A_{ref} \end{cases} \qquad \text{(Eq. 3.31)}$$

3.3.3 Analysis of $\boldsymbol{\beta(\bar{A})}$

As indicated by the previous formulation the value of $\beta(\bar{A})$ is very important to control the effect of the Jumping Buckling Length as the steeper the function becomes the more abrupt the change in Buckling length is. To analyze the behavior of this $\beta(\bar{A})$, a similar graphical approach to chapter 3.3.1 is employed. Consider Figure 3.11 taken from [25].

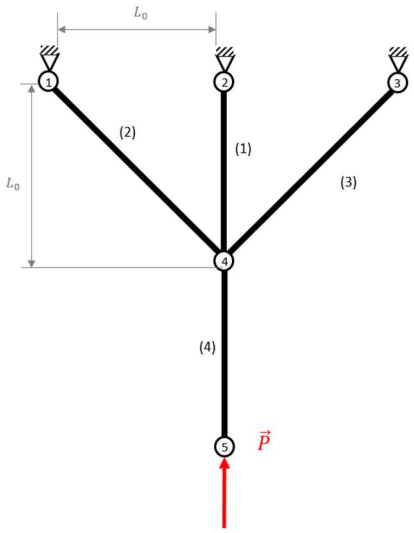

Figure 3.11 - Structure for Jumping Buckling Length Analysis

Has it can be seen in the previous figure, as the area of elements (2) and (3) decreases the stability of node 4 decreases as well resulting in a more pronounced chain between element (1) and (4). Therefor it's important to link the area of elements (2) and (3) with the length of the chain. Applying (3.21), the average area is simply defined by (Eq. 3.32).

$$\overline{A} = \frac{A_2 + A_3}{2} \leq A_{ref} \qquad \text{(Eq. 3.32)}$$

So, if $\overline{A} = 0$ then $L_{buc} = 2L_0$ and, conversely, if $\overline{A} = A_{ref}$ then $L_{buc} = L_0$. By interpolating between the two extremes. a function applicable to the algorithm is obtained, resulting in (3.24).

The simplicity of this example allows for the drawing of a feasible domain in a 2D environment with bars (1) and (4) sharing the same project variable, x_{A_1}, and bars (2) and (3) being associated with another variable, x_{A_2}. The graphs for this example are represented in Figure 3.12 with varying values of both p^L and A_{ref}.

a)

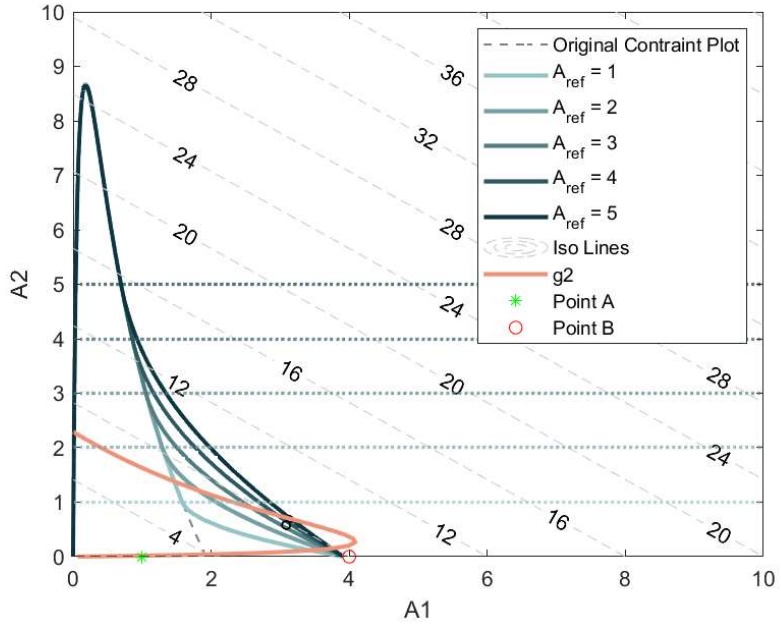

b)

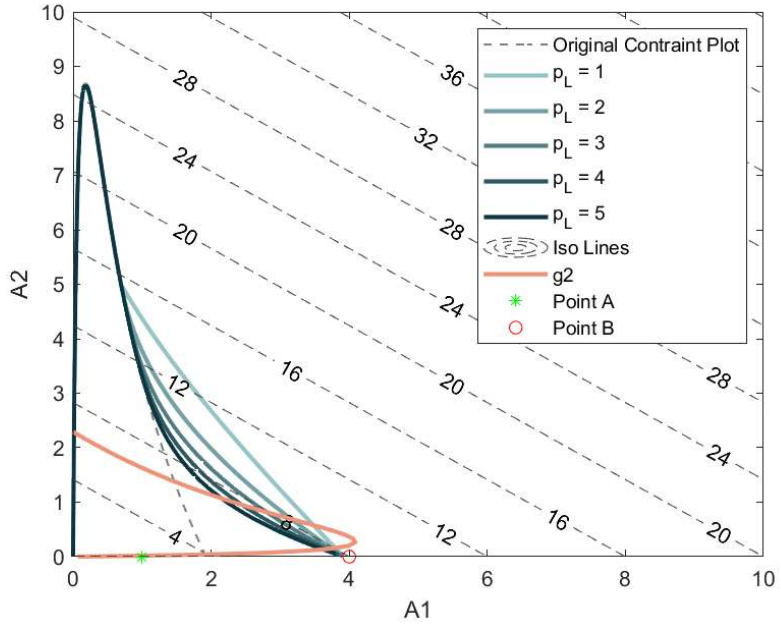

Figure 3.12 - Parameter Analysis of a 4-bar structure varying (a) A_{ref} or (b) p_L

As is in the previous graph the values of A_{ref} and p^L do not affect the value of the optimum area for a topology that doesn't include bars (2) and (3), Point B, these parameters only affect the admissible region. This may make it feasible to include elements (2) and (3) in the final design. In Figure 3.12a, A_{ref} dictates how supported the node is perceived to be. If the cut-off point is set too high the algorithm will have to resist the buckling effect by increasing the area of element (1) and (4). On the other hand, if the cut-off point is set too low it means that any adjacent bar can support the node allowing the algorithm to control the buckling length through function $\beta(\overline{A})$.

When it comes the influence of p_L, at first, it would seem that the better values for a problem solution would be obtained when the value of this exponent is high, according to the reverse SIMP graph presented in Figure 3.10, these high values of p_L would penalize intermediary values of $\beta(\overline{A})$. However, the more accurate behavior is obtained when the value of p_L is relatively low, this would justify an additional constraint to restrict the value of $\beta(\overline{A})$, noting that this function shows a predisposition for utilizing intermediary values of length when p_L is low, similar to how stress based multi material topology optimization choses intermediary material properties.

Analyzing Figure 3.12b, a further justification for the better behavior of low values of p_L can be observed when comparing the point $(A_1, A_2) = (4,0)$ with the intersection of each of the lines for g_1 and g_2 After a certain increase in p_L, the intersection of g_1 and g_2 represents a lower value of the objective function, represented by the isocost lines, this decrease in objective function values is graphically represented by the point being below the isocost line that crosses point $(A_1, A_2) = (4,0)$. The correct solution for this problem would be a solution that doesn't eliminate any bars, reducing the problem to a simple sizing problem.

It is important to note that the simplification preformed to graphical represent the problem can only give a model of how the problem behaviors at a simplified number of variables, if more variables are added the overall complexity increases and encountering the optimum point is not as intuitive as it may seem from this simple graphical demonstration. More applicability would probably be achieved by a 3D graphical representation that would have a more complex local minima setting. However, these were not explored, and the sensibility achieved by understanding well these models allow for a better search of a global minimum from out of the various local minimums.

3.4 Objective Function

The objective function typically is one of two functions, a compliance function (Eq. 3.33) or a volume function which are typically minimized (Eq. 3.34). Some assumptions made for one formulation have correlations to the another, resulting in many authors debating and adapting formulation from one type of problem to the other, when exploring the feasibility of their formulations.

$$f_{obj}(x_A) = \mathbf{f}^T\mathbf{u}(x_A) \quad \text{(Eq. 3.33)}$$

$$f_{obj}(x_A) = \phi\mathbf{L} \cdot \mathbf{x}_A \quad \text{(Eq. 3.34)}$$

A variation of the minimum volume problem that considers the mass density of the material used is a minimum weight problem, these are more adequate when used in a multi material optimization, since varying the material may lead to a lighter solution, even the volume is increased. A minimum weight problem minimizes a formula similar to (Eq. 3.35).

$$f_{obj}(x_A) = \rho_M \phi \mathbf{L} \cdot \mathbf{u}(x_A) \tag{Eq. 3.35}$$

Where ρ_M is the material's mass density and is usually dependent on the variable used for material selection, typically it is a Boolean variable. Although the presented problem is solved in a single material topology optimization environment the objective function used will be the mass function, to maintain the coherence from the preceding works.

3.5 Problem formulation

With all the constraints explained and analyzed and the objective function specified the complete problem formulation is presented below, (Eq. 3.36).

$$\min_{x_{A_e} \in [0;100]} \quad \phi \sum \rho_e L_e x_{A_e} \tag{Eq. 3.36}$$

$$\text{s.t} \quad g^{adm}: \left(\left(\frac{\sigma_e}{\sigma_{adm}} \right)^2 - 1 \right) \cdot x_{A_e} - \epsilon \leq 0 \tag{Eq. 3.37}$$

$$g^{buc}: \left(- \frac{\sigma_e}{\frac{\pi E_e \phi \cdot x_i}{4 L_{buc}^2 (x_{adj})} + \frac{1}{(A_e + \mu)}} - 1 \right) \cdot x_{A_e} - \epsilon \leq 0$$

with

$$\mu = \left(\frac{1}{\alpha \cdot \sigma_{adm}} \right)^{\frac{1}{p}} \tag{Eq. 3.38}$$

$$L_{buc}(x_{adj}) = L_i + \beta(\overline{A}) \cdot L_j \tag{Eq. 3.39}$$

and

$$\beta(\overline{A}) = \begin{cases} \left(1 - \frac{\overline{A}}{A_{ref}} \right)^{p_L} & \text{if } \overline{A} \leq A_{ref} \\ 0 & \text{if } \overline{A} > A_{ref} \end{cases} \tag{Eq. 3.40}$$

$$\overline{A} = \frac{\phi}{N_{adj}} \sum_{j \in \Gamma_{adj}} x_j \leq A_{ref} \tag{Eq. 3.41}$$

4 SENSITIVITY CALCULUS

4.1 Objective Function

The objective function presented in (Eq. 3.36) only depends linearly on the design variables which makes the derivative of this function quite simple to calculate, (Eq. 4.1).

$$\frac{dM(x_A)}{dx_A} = \rho_e L_e \phi \tag{Eq. 4.1}$$

The derivative becomes more elaborated if the material's mass density depends on the design variable, demanding the derivation of the interpolating function. However, the single material nature of the problem greatly simplifies the derivative of the objective function.

If there is an interpolation of the mass density property it would convert the scalar value of the mass density into a function, $\rho_e(x_\rho)$, dependent on the density variable, x_ρ. This interpolation would change the design variable from the element's cross-sectional area into its density variable, a variable that represents the existence or absence of material and is done by a SIMP law [11] defined by (Eq. 4.2). In this equation ρ_e^0 is a low value of material density that simulates the absence of material while also avoiding numerical singularities and ρ_e^1 being the value of the material density for the material phase. A SIMP interpolation of various materials can be used to solve multi material topology optimization problem [52].

$$\rho_e(x_{\rho_e}) = x_{\rho_e}^{p_1}\rho_e^1 + (1 - x_{\rho_e}^{p_1})\rho_e^0 \tag{Eq. 4.2}$$

This function then has influence in the calculation of the derivative and results in (Eq. 4.3), for which the value of x_A is fixed.

$$\frac{dM(x_{\rho_e})}{dx_{\rho_e}} = \frac{\partial \rho_e}{\partial x_{\rho_e}} L_e \phi x_A \tag{Eq. 4.3}$$

In which the derivative of the mass density is given by (Eq. 4.4).

$$\frac{\partial \rho_e}{\partial x_{\rho_e}} = p_1 x_{\rho_e}^{p_1-1}(\rho_e^1 - \rho_e^0) \quad \text{(Eq. 4.4)}$$

This expression has a penalization exponent applied to x_{ρ_e}, p_1, these are used to restrict the density variable to a Boolean behavior, refer to [8].

4.2 Stress Derivative

As discussed earlier on section 2.2.3.2 the applied method for determining the derivative of both constraints is the adjoint method, that will only be applied to the derivative of the stress itself, with both constraints being calculated almost fully by direct differentiation, apart from the value of the stress derivative. In the adjoint method given in equation (Eq. 2.40), the explicit part of this derivative, $\frac{\partial g_e^\sigma}{\partial x_A}$, is null, as the stress definition given in (Eq. 2.41) doesn't directly depend on the cross-sectional area. Note that the stress in each element, e, is defined by the Young Modulus and the extension on that element, $\sigma_e(u) = E_e \varepsilon_e(u)$, and none of these terms are dependent on the area. The result is a simplified version of the adjoint method (Eq. 4.5).

$$\frac{dg_e^\sigma}{dx_A} = -\lambda_e^T \frac{\partial \mathbf{K}}{\partial x_A}\mathbf{u} \quad \text{(Eq. 4.5)}$$

With λ_e being the result of solving an adjunct problem for every element, defined by (Eq. 4.6).

$$\mathbf{K}\lambda_e = \mathbf{z}, \quad \mathbf{z} = \left(\frac{\partial \sigma_e}{\partial u_e}\right)^T \quad \text{(Eq. 4.6)}$$

It is then possible to determine the analytical formula for the fictitious load vector, $\mathbf{z}$, which is dependent on the extension which can be taken as $\varepsilon = \frac{u_e}{L_e}$.

$$z = \left[\frac{\partial}{\partial u_e}(E\varepsilon_e)\right]^T = \left[\frac{E}{L_e}\begin{Bmatrix}\cos\alpha_e \\ \sin\alpha_e \\ -\cos\alpha_e \\ -\sin\alpha_e\end{Bmatrix}\right]^T \quad \text{(Eq. 4.7)}$$

Working back onto the definition of adjoint vector, λ_e, results in (Eq. 4.8)

$$\lambda_e = \mathbf{K}^{-1}\left[\frac{E}{L_e}\begin{Bmatrix}\cos\alpha_e \\ \sin\alpha_e \\ -\cos\alpha_e \\ -\sin\alpha_e\end{Bmatrix}\right]^T \quad \text{(Eq. 4.8)}$$

Lastly, the derivative of the Global Stiffness Matrix, $\frac{\partial K}{\partial x_A}$. For a given bar element in a finite element environment its stiffness matrix is given by (Eq. 4.9).

$$\mathbf{K} = \frac{E_e \phi x_A}{L_e} \begin{bmatrix} 1 & -1 \\ -1 & 1 \end{bmatrix} \quad \text{(Eq. 4.9)}$$

With the derivative as a function of area simply being, (Eq. 4.10).

$$\frac{\partial \mathbf{K}}{\partial x_A} = \frac{E_e \phi}{L_e} \begin{bmatrix} 1 & -1 \\ -1 & 1 \end{bmatrix} \quad \text{(Eq. 4.10)}$$

Which results in the complete formulation of the stress derivative as, (Eq. 4.11).

$$\frac{d\sigma_e(u)}{dx_A} = -\left[\mathbf{K}^{-1} \frac{E_e}{L_e} \begin{Bmatrix} \cos\alpha_e \\ \sin\alpha_e \\ -\cos\alpha_e \\ -\sin\alpha_e \end{Bmatrix} \right]^T \frac{E_e \phi}{L_e} \begin{bmatrix} 1 & -1 \\ -1 & 1 \end{bmatrix} \mathbf{u} \quad \text{(Eq. 4.11)}$$

This definition of the stress derivative is important when it comes to introducing new constraints into the optimization problem since it is possible to calculate the sensitivity of the new constraint in an explicit manner. The derivative of a given generic constraint will be calculated explicitly apart from the value of the stress derivative that will be provided by the adjoint method, not only simplifying the implementation process from a programmer's point of view, but also reducing the computational cost of the algorithm.

It is possible to solve the stress derivative in order to the density variable, laying the groundwork for further implementation of this methodology. Because there will be a need to interpolate the material's Young Modulus, defined by (Eq. 4.12) where E_e^1 and E_e^0 have equivalent meanings to ρ_e^1 and ρ_e^0, respectively. A similar expression to (Eq. 4.4) is used for the derivative of Young Modulus, $\boldsymbol{E}_e(x_{\rho_e})$, seen in (Eq. 4.13).

$$E_e(x_{\rho_e}) = x_{\rho_e}^{p_1} E_e^1 + (1 - x_{\rho_e}^{p_1}) E_e^0 \quad \text{(Eq. 4.12)}$$

$$\frac{\partial E_e(x_{\rho_e})}{\partial x_{\rho_e}} = (E_e^1 - E_e^0) x_{\rho_e}^{p_1 - 1} p_1 \quad \text{(Eq. 4.13)}$$

Applying this definition of Young's Modulus to the definition of the global stiffness matrix and its derivative, (Eq. 4.14) and (Eq. 4.15) respectively. Again, the value of x_A is taken as a constant value.

$$K = \left[x_{\rho_e}^{p_1} E_e^1 + (1 - x_{\rho_e}^{p_1}) E_e^0 \right] \frac{\phi x_A}{L_e} \begin{bmatrix} 1 & -1 \\ -1 & 1 \end{bmatrix} \quad \text{(Eq. 4.14)}$$

$$\frac{\partial K}{\partial x_{\rho_e}} = \left[(E_e^1 - E_e^0)x_{\rho_e}^{p_1-1}p_1\right]\frac{\phi x_A}{L_e}\begin{bmatrix}1 & -1\\ -1 & 1\end{bmatrix} \quad \text{(Eq. 4.15)}$$

Different from the adjoint stress derivation with regards to the normalized area, when dealing with a derivative in order of the density variable the explicit part of the adjoint method is not null and is defined by (Eq. 4.16).

$$\frac{\partial \sigma(x_\rho, u)}{\partial x_\rho} = \frac{\partial E_e(x_{\rho_e})}{\partial x_{\rho_e}}\varepsilon(u) \quad \text{(Eq. 4.16)}$$

The complete expression for the stress derivative, is presented in (Eq. 4.17).

$$\frac{\partial \sigma(x_\rho, \mathbf{u})}{\partial x_\rho} = \frac{\partial E_e(x_{\rho_e})}{\partial x_{\rho_e}}\varepsilon(\mathbf{u}) - \left[\mathbf{K}^{-1}\frac{E}{L_e}\begin{Bmatrix}\cos\alpha_e\\ \sin\alpha_e\\ -\cos\alpha_e\\ -\sin\alpha_e\end{Bmatrix}\right]^{-1}\frac{\partial \mathbf{K}}{\partial x_{\rho_e}}\mathbf{u} \quad \text{(Eq. 4.17)}$$

This stress information for both the derivative with regards to the area and density variables is then allocated in a matrix according to Figure 4.1, where N_E represents the total number of element in the ground structure.

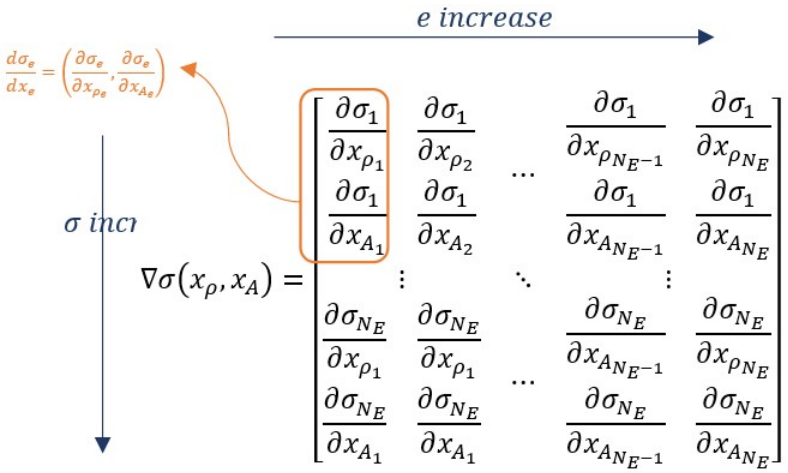

Figure 4.1 - Derivatives alocation onto matrix

It is worth noting that the size of the array of gradient is strongly related to the number of materials per element and therefore each stress must be derived for each material phase plus the area. When only one material in present in the optimization, the stress constraint is derived with regards to two different variables, the element's area and its material density. This may seem superfluous but is done to lay the basis for future projects based on the work done in this dissertation.

4.3 Stress Constraint

With the simplification of getting the stress derivatives as an independent process the constraint is derived quite simply. Firstly, remembering the stress constraint, g_e^σ, shown in (Eq. 4.18),

$$g_e^\sigma : x_A\left[\left(\frac{\sigma_e}{\sigma_{adm}}\right)^2 - 1\right] - \epsilon \leq 0 \qquad \text{(Eq. 4.18)}$$

where σ_e represents the stress in the element e, σ_{adm} represents the admissible stress, x_A is the element area and lastly ϵ is the $\epsilon - relaxation$ parameter.

The derivative associated with this constraint, $\frac{dg_e^{adm}}{dx}$, variable x is a generic variable that can later be interpreted as either a normalized area variable or a density variable, comes naturally as (Eq. 4.19),

$$\frac{dg_e^\sigma}{dx} = \left[\left(\frac{\sigma_e}{\sigma_{adm}}\right)^2 - 1\right]\frac{dx_A}{dx} + 2x_A\left(\frac{\sigma_e}{\sigma_{adm}}\right)\left[\frac{\frac{d\sigma_e}{dx}\sigma_{adm} - \frac{d\sigma_{adm}}{dx}\sigma_e}{\sigma_{adm}^2}\right] \qquad \text{(Eq. 4.19)}$$

when differentiating with respects to the area variable the derivative of the admissible stress is null. However, it is important when differentiating with respects to the density variable, the reverse happens. The normalized area derivative, $\frac{dx_A}{dx}$, is 1 when dealing with area variables and is 0 when dealing with density variables. An advantage of differentiating w.r.t. the area variable is that the admissible stress is constant, simplifying the calculating when comparing with density-based differentiation.

As it is evident by this formulation, all the values were already defined except the admissible stress derivative, whose value is given by expression (4.20). Since the admissible stress is a material property similar to the mass density and Young's Modulus, an equivalent expression is obtained for its derivative.

$$\frac{d\sigma_{adm}}{dx_\rho} = x_\rho^{p_1-1}\left(\sigma_{adm}^0 - \sigma_{adm}^1\right)p_1 \qquad \text{(Eq. 4.20)}$$

4.4 Buckling Constraint

The buckling constraint is a more complex constraint and so it will require some careful analysis, because a lot of functions are concatenated into other functions and there are complex dependencies, the derivatives will share the same level of concatenation. The complete form of the buckling constraint is shown in (Eq. 3.28), however, this formulation is cumbersome and difficult to deal with, so a simpler version is presented in (Eq. 4.21)

$$g_e^{buc} : x_A\left(-\frac{\sigma_e}{\sigma_c^C}-1\right)-\epsilon \leq 0 \quad \text{(Eq. 4.21)}$$

This simplified version allows for the simple application of derivation rules resulting in (Eq. 4.22), here $\frac{dx_A}{dx}$ has the same behaviour has in the admissible stress constraint (Eq. 4.19).

$$\frac{dg_e^{buc}}{dx}=\left(-\frac{\sigma_e}{\sigma_c^C}-1\right)\frac{dx_A}{dx}-x_A\left(\frac{\frac{d\sigma_e}{dx}\sigma_c^C-\frac{d\sigma_c^C}{dx}\sigma_e}{{\sigma_c^C}^2}\right) \quad \text{(Eq. 4.22)}$$

σ_c^C is defined by (Eq. 4.23). The derivate of this function is presented in (Eq. 4.24).

$$\sigma_c^C=\frac{\pi E(x_\rho)x_A\phi}{4L_{buc}(x)^2}+\frac{1}{[x_A+\mu]^p} \quad \text{(Eq. 4.23)}$$

$$\frac{d\sigma_c^C}{dx_{A_1}}=\frac{\phi\pi E(x_\rho)}{4L_{buc}(x_A)^2}\left(\frac{\partial x_A}{\partial x_A}-\frac{2x_A}{L_{buc}(x_A)}\frac{\partial L_{buc}(x_A)}{\partial x_A}\right)-p(x_A+\mu)^{-p-1}\frac{\partial x_A}{\partial x_A} \quad \text{(Eq. 4.24)}$$

When dealing with the buckling constraint, especially when including the chain effect, it is important to understand the interaction between this derivative and the 3 classifications attributed to an element mentioned in section 2.4.2, as the presented formulation is applicable to each of those three cases. When constraint is derived w.r.t to the area of the element it refers to, the term $\frac{\partial x_A}{\partial x_A}$ is equal to 1, and so the terms attached to it are present in the final value, while the term $\frac{\partial L(x_A)}{\partial x_A}$ is null and so it does not influence that final value. The inverse happens if a constraint is derived w.r.t. the adjacent area's variables, since $\frac{\partial L(x_A)}{\partial x_A}\neq 0$ while $\frac{\partial x_A}{\partial x_A}=1$. Additionally, if a constraint is derived w.r.t. any unrelated member's variables the value of $\frac{\partial \sigma_c^C}{\partial x_A}$ is simply null.

Going back to (4.22), if the deriving variable is the density variable, the value of $\frac{\partial x_A}{\partial x_\rho}$ is zero and it cancels a term from the expression, simplifying it, (Eq. 4.25).

$$\frac{dg_e^{buc}}{dx}=-x_A\left(\frac{\frac{d\sigma_e}{dx_\rho}\sigma_c^C-\frac{d\sigma_c^C}{dx_\rho}\sigma_e}{{\sigma_c^C}^2}\right) \quad \text{(Eq. 4.25)}$$

Again, the challenge comes from determining the value of the $\frac{d\sigma_c^C}{dx_\rho}$ since there is a dependency from both the Young's Modulus, $E(x_\rho)$, and the buckling length, $L(x_\rho)$, this situation

is similar to the problem with the normalized area as a design variable, considering (Eq. 4.24), the derivative is of the same form but with x_A substituted by $E(x_\rho)$, resulting in (Eq. 4.26).

$$\frac{d\sigma_c^C}{dx_A} = \frac{\phi\pi x_A}{4L(x_\rho)^2}\left(\frac{\partial E(x_\rho)}{\partial x_\rho} - \frac{2E(x_\rho)}{L(x_\rho)}\frac{\partial L(x_\rho)}{\partial x_\rho}\right) \quad \text{(Eq. 4.26)}$$

The additional function added to the basic Euler formula is primarily done to solve a singularity problem when the area tends to zero, but this singularity problem does not exist when dealing with a density variable, so it is considered constant when differentiating, there may be a need for a different relaxing formula when in a density variable setting.

Expression (Eq. 4.26) can have one of three values depending again on which elements are being considered, if it is the element the constraint refers to $\frac{\partial L(x_\rho)}{\partial x_\rho}$ is null and therefore its accompanying terms are cancelled. If the element is adjacent to the element the constraint refers to, the derivative $\frac{\partial E(x_\rho)}{\partial x_\rho}$ is null since elements cannot influence other element's material properties directly. Lastly, if the derivative is relative to non-related elements the value of $\frac{\partial \sigma_c^C}{\partial x_\rho}$ is null, since they do not affect neither the element's Young Modulus nor its buckling length. When storing the value of $\frac{\partial \sigma_c^C}{x_\rho}$ onto a matrix it is noted that only the diagonal positions and those associated with positions related with adjacent elements are non-zero. This is a direct result of the construction of the constraint. This remark is useful when implementing this complex formula in an algorithm as it can be used to validate that the software is correctly implemented.

5 RESULTS

5.1 Chapter Summary

The objective of this chapter is to show the developed problem formulation applied to a set of examples. The solutions to three of these examples were solved analytically, to give some perspective of how the solution compares to known problems. Apart from two of the examples presented, the 5-bar and 20-bar examples, all other were picked from Almeida [8]. Initially when the buckling constraint was applied to this set of problems, there was a large discrepancy between the values for the areas of elements limited by buckling constraint and those limited by the admissible stress constraint. This discrepancy would have made it difficult to represent in any meaningful way areas limited by buckling and limited by admissible stress in the same graphical. To bring these values closer together, the material used was changed from steel to aluminum, as well as the parameters that define the example, i.e., the length of the elements in the ground structure, were also changed to better suit both constraints.

The analytical solution to those first three problems can then be compared with the solution provided by the algorithm, serving as a benchmark for all the other examples. Although useful to solve the structure analytical in an earlier stage to then compare the solutions obtain, it may lead to some bias in the results, as solutions with lower mass can appear but with different topologies.

After the comparison between the analytical solutions and the topology optimization solutions, the algorithm is extended to the other problems, showing some of the solution's information regarding constraint values, which bars are most requested for each constraint, as well as the value of the objective function and KKT conditions, through the optimization process.

Since the optimization considers only one material phase, the material will be the same for all examples shown. The material chosen was an aluminum 1050-H14, the properties relevant to optimization are shown in Table 5.1, the full material sheet can be consulted at [1].

Table 5.1 - Aluminium 1050-H14 Material Properties

Property	Value
Young Modulus, $\mathbf{E_i}$	69.0 GPa
Admissible Stress, $\boldsymbol{\sigma_{ADM}}$	103 MPa
Mass Density, $\boldsymbol{\rho}$	2705 kg/m^3

5.2 Analytical Results

The three problems that were elected to benchmark the solutions obtained by the optimization algorithm were the 5-bar ground structure, presented earlier in section 3.3.1, but with more realistic parameters, the 10-bar ground structure, the simplest structure studied in [8], and the 36-bar ground structure, a problem whose solution clearly demonstrates chain effect situations.

These problems share a common feature, all their solutions are isostatic trusses, enabling the resolution of internal load with simple node analysis. This allows the characterization of what the minimum areas are for both the admissible stress and the buckling critical load because the internal stress in each element is only dependent on the external applied load. A simple division between the internal force of an element and its limiting stress results in the minimum area.

A comparison between the results obtained from the next chapters analysis, MMA algorithm optimization and GCMMA algorithm for the example of 5-bar, 10-bar and 36-bar ground structures are presented in Table 5.2, and Table 5.4, respectively.

Table 5.2 - Comparison between the analytical results, MMA and GCMA for 5-bar Ground Structure

Element	Analytical Value	MMA Value	GCMMA Value
1	107.392	107.385	107.385
2	0.000	0.004	0.004
3	137.302	138.807	138.807
4	0.000	0.004	0.004
5	0.000	0.004	0.004

Table 5.3 - Comparison between the analytical results, MMA and GCMA for 10-bar Ground Structure

Element	Analytical Value	MMA Value	GCMMA Value
1	194.175	194.6051	194.6051
2	0.000	0.1601	0.1601
3	200.475	200.6912	200.6912
4	141.757	141.9279	141.9279
5	0.000	0.7424	0.7424
6	0.000	0.2011	0.2011
7	137.302	138.8674	138.8674
8	238.406	238.949	238.949
9	137.302	137.0462	137.0462
10	0.000	10.1518	10.1518

Table 5.4 - Comparison between the analytical results, MMA and GCMA for 36-bar Ground Structure

Element	Analytical Value	MMA Value	GCMMA Value
1	0.000	0.010	0.010
2	550.218	775.521	775.521
3	0.000	7.118	7.116
4	82.381	82.337	82.337
5	349.515	349.529	349.529
6	0.000	0.010	0.010
7	930.039	664.228	658.582
8	349.751	349.719	349.719
9	0.000	0.010	0.010
10	349.515	349.496	349.496
11	0.000	414.575	418.766
12	930.039	664.214	658.545
13	0.000	0.010	7.030
14	82.381	111.744	82.338
15	233.010	233.003	233.023
16	0.000	0.500	0.010
17	720.405	616.133	610.169
18	349.751	349.733	349.718
19	0.000	0.010	0.010
20	233.010	232.996	232.991
21	0.000	188.478	193.531
22	720.405	616.120	610.114
23	0.000	0.010	6.831
24	82.381	101.286	82.340
25	116.505	116.498	116.517
26	0.000	0.565	0.010
27	415.926	414.432	414.346
28	349.751	349.728	349.717
29	0.000	0.010	0.010
30	116.505	116.489	116.485
31	0.000	0.010	0.010
32	415.926	414.379	414.276
33	0.000	4.343	4.631
34	82.381	82.359	82.357
35	0.000	0.010	0.010
36	0.000	0.010	0.010

5.2.1 5-Bar Ground Structure

The 5-bar ground structure was already presented in Figure 3.4, the previously mentioned parameter change, to present a more realistic structure, is presented in Table 5.5.

Table 5.5 – 5-bar ground structure properties

Property	Value
Cell Length, $\boldsymbol{L_0}$	$250\ mm$
Applied Force, $\vec{\boldsymbol{P}}$	$10\ kN$

The solution obtained by the algorithm for this problem, without the buckling constraint included, is the 2-bar solution presented in Figure 5.1.

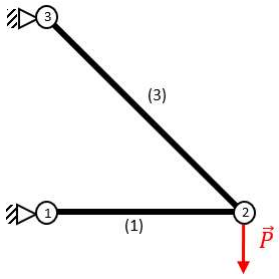

Figure 5.1 - Topology Solution to the optimization of the 5-bar Ground Structure

Because this truss is isostatic the internal forces are easy to determine and therefore the minimum area according to the stress constraint, a_{min}^{adm}, and the buckling constraint, a_{min}^{buc}, can be also calculated and the results are presented in Table 5.6.

Table 5.6 - Values of the Analysis of the 5-bar Ground Structure Optimum Solution

Element	Relation with the applied load	Value of internal force [N]	Minimum area w.r.t. stress, a_{min}^{adm}, [mm^2]	Minimum area w.r.t. buckling, a_{min}^{buc}, [mm^2]
(1)	$-P$	-1×10^4	97.087	107.392
(3)	$\sqrt{2}\,P$	1.414×10^4	137.302	-

Changing the parameters enables having a minimum area that is in the same order of magnitude as the other stress limited areas. It is expected that an optimization algorithm when solving this problem will first be limited by the larger of the two minimum areas, a_{min}^{buc} in the case of element (1). Element (2) is under tension so the buckling constraint does not apply to it. The results presented in Table 5.6 will be compared to the solution of the optimizing algorithm.

5.2.2 10-Bar Ground Structure

The 10-bar ground structure is presented in Figure 5.2, and the ground structure parameters employed are different than the ones used in the previous example.

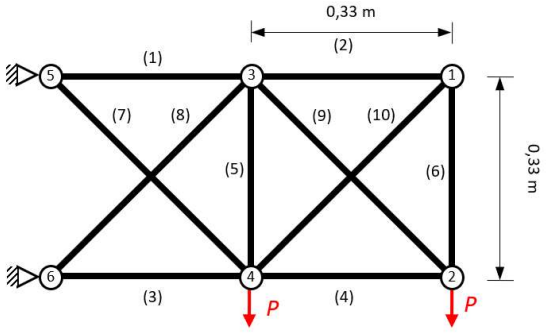

P [kN]	10

Figure 5.2 - 10-Bar Ground Structure

The solution obtained by the algorithm for this problem, without the buckling constraint included, is the 6-bar solution presented in Figure 5.3.

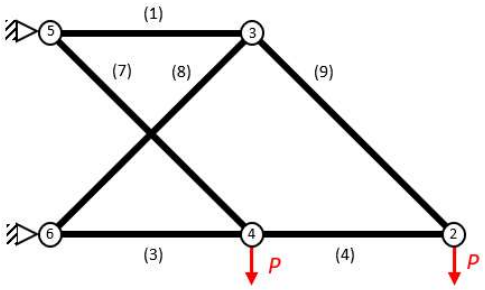

Figure 5.3 - Topology Solution to the optimization of the 10-bar Ground Structure

Because this truss is isostatic the internal forces are easy to determine and therefore the minimum area according to the stress constraint, a_{min}^{adm}, and the buckling constraint, a_{min}^{buc}, can be also calculated and the results are presented in Table 5.7.

Table 5.7 - Values of the Analysis of the 10-bar Ground Structure Optimum Solution

Element	Relation with the applied load	Value of Internal Force [N]	Minimum area w.r.t. stress, a_{min}^{adm}, $[mm^2]$	Minimum area w.r.t. buckling, a_{min}^{buc}, $[mm^2]$
(1)	$2P$	2×10^4	194.175	-
(3)	$-2\ P$	-2×10^4	194.175	200.475
(4)	$-P$	-1×10^4	97.087	141.757
(7)	$\sqrt{2}P$	1.414×10^4	137.303	-
(8)	$-\sqrt{2}P$	-1.414×10^4	137.303	238.406
(9)	$\sqrt{2}P$	1.414×10^4	137.303	-

The results presented in Table 5.6 will be compared to the solution of the optimizing algorithm. The same considerations taken for the previous example can be applied here, where three of the bars are under compression and their a_{min}^{buc} is larger than a_{min}^{adm}, presenting new limits when compared to the non-buckling optimization.

5.2.3 36-Bar Ground Structure

The 10-bar ground structure is presented in Figure 5.4, and the ground structure parameters employed are different than the ones used in the previous example.

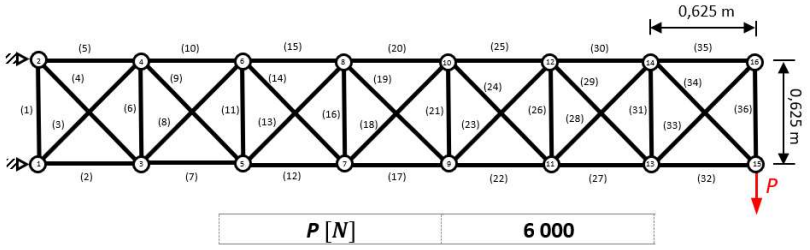

Figure 5.4 - 36-Bar Ground Structure

The solution obtained by the algorithm for this problem, without the buckling constraint included, is the 19-bar solution presented in Figure 5.5.

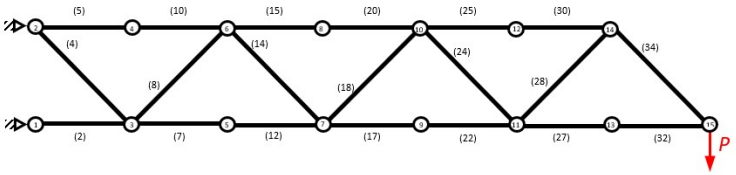

Figure 5.5 - Topology Solution to the optimization of the 36-bar Ground Structure

Because this truss is isostatic the internal forces are easy to determine and therefore the minimum area according to the stress constraint, a_{min}^{adm}, and the buckling constraint, a_{min}^{buc}, can be also calculated and the results are presented in Table 5.8.

Since the solution presented was taken from an optimization without consideration for the stability of the structure the are multiple unsupported nodes, an additional column is added to the result tables that will indicate what would the correct minimum area be if the element's correct buckling length was being assessed, a_{min}^{ce}.

Table 5.8- Values of the Analysis of the 36-bar Ground Structure Optimum Solution

Element	**Relation with the applied load**	**Value of Internal Force $[kN]$**	**Minimum area w.r.t. stress, a_{min}^{adm}, $[mm^2]$**	**Minimum area w.r.t. buckling, a_{min}^{buc}, $[mm^2]$**	**Minimum area w.r.t. buckling with correct L_{buc}, a_{min}^{ce}, $[mm^2]$**
(2)	$-7P$	-42.00	407.767	550.218	-
(4)	$\sqrt{2}\,P$	8.485	82.381	-	-
(5)	$6P$	36.00	349.515	-	-
(7)	$-5P$	-30.00	291.262	465.019	930.039
(8)	$-\sqrt{2}P$	-8.485	82.381	349.751	-
(10)	$6P$	36.00	349.515	-	-
(12)	$-5P$	-30.00	291.262	465.019	930.039
(14)	$\sqrt{2}\,P$	8.485	82.381	-	-
(15)	$4P$	24.00	233.010	-	-
(17)	$-3P$	-18.00	174.757	360.203	720.405
(18)	$-\sqrt{2}P$	-8.485	82.381	349.751	-
(20)	$4P$	24.00	233.010	-	-
(22)	$-3P$	-18.00	174.757	360.203	720.405
(24)	$\sqrt{2}\,P$	8.485	82.381	-	-
(25)	$2P$	12.00	116.505	-	-
(27)	$-P$	-6.000	58.252	207.963	415.926
(28)	$-\sqrt{2}P$	-8.485	82.381	349.751	-
(30)	$2P$	12.00	116.505	-	-
(32)	$-P$	-42.00	58.252	207.963	415.926
(34)	$\sqrt{2}\,P$	8.485	82.381	-	-

The same considerations taken for the previous example can be applied here. However, the significant increase of the minimum area observed in the values of a_{min}^{ce} would indicate that perhaps the topology of the solution is not appropriate when including buckling constraints to the formulation. The effects of this correct assessment of the buckling length will be

firstly shown in the solution obtained by the algorithm and then discussed in the final section of this chapter.

5.3 Complementary Structures

More examples are solved by the algorithm to show how the solutions obtained by it with the added buckling constraint would compare with some of the structures solved in Pratas [46] and Almeida [8].

5.3.1 20-Bar Ground Structure

The 20-Bar Ground Structure's problem was presented in Figure 3.9. The values for the horizontal and vertical element's length and the applied load are presented in Figure 5.6.

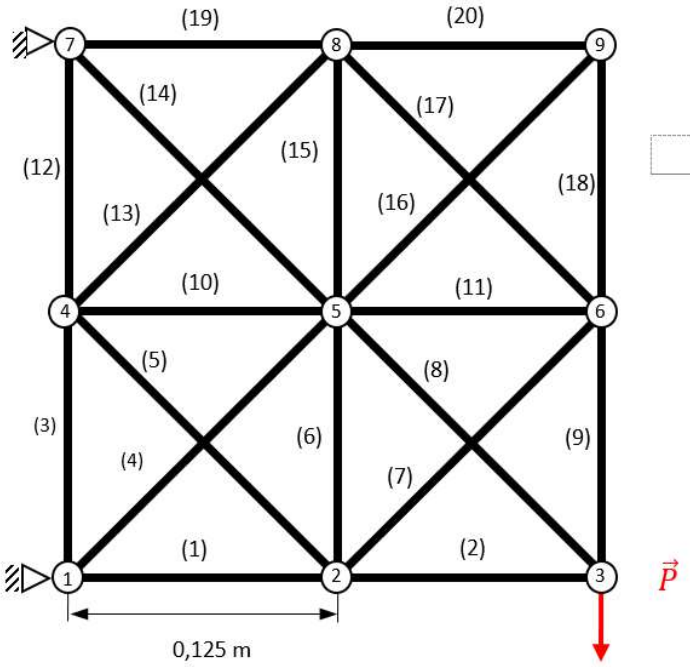

$P\ [kN]$	10

Figure 5.6 - 20-Bar Ground Structure

This example is relevant to demonstrate how the optimization would deal with chain effect, because this is more complex version of the 5-bar ground structure problem, where bars (1) and (2) would equate to bar (1) of the 5-bar examples and bars (8) and (14) would equate to bar (3) of the 5-bar example.

5.3.2 L Bracket

The structure of the L Bracket example is presented in Figure 5.7 as well as the values of the cell length and the applied load.

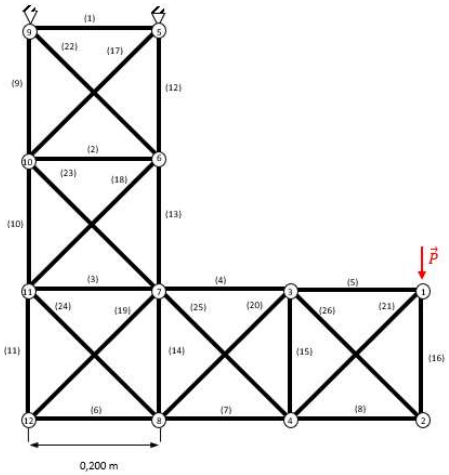

$P\ [N]$	7500

Figure 5.7 - L-Bracket Ground Structure

5.3.3 110-Bar Ground Structure

The 110-bar ground structure is presented in Figure 5.8. Since this structure presents a symmetry along the vertical axis, the number of variables can be significantly reduced from 110 to only 56, a more manageable amount.

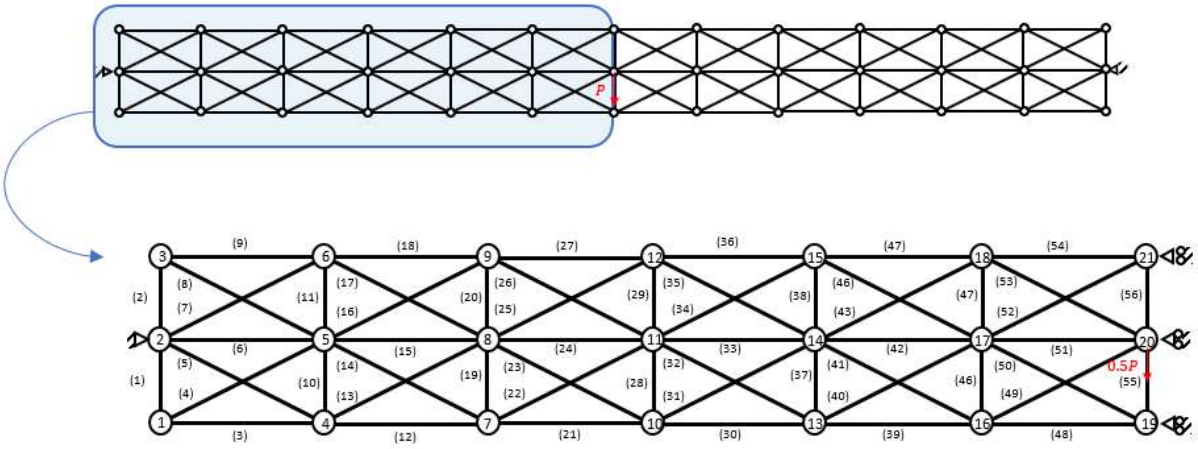

P $[N]$	5 000

Figure 5.8 - 110-Bar Ground Structure

5.3.4 21-Bar Ground Structure

The 21-Bar Ground Structure is presented in Figure 5.9 as well as its defining parameters. Similarly, to what was done with the 110-Bar ground structure, the 21-Bar problem can be simplified and have the number of variables reduced from 21 down to 11.

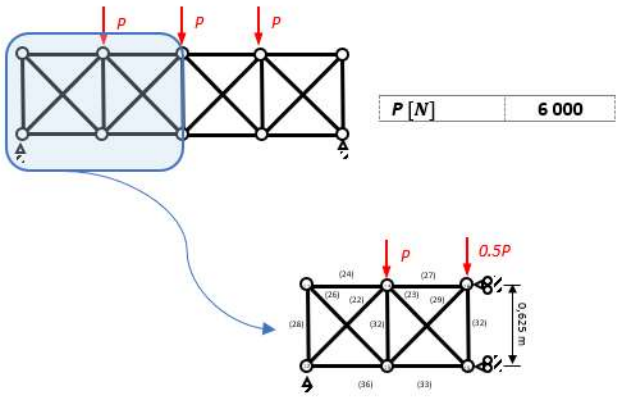

Figure 5.9 - 21-Bar Ground Structure

5.4 Optimization Results

The following subsections will present information about the solutions obtain from the optimization process when applied to the previous examples. Starting with a comparison between the algorithm's behaviour to both a problem formulation with and without buckling constraint, comparing for both the MMA algorithm and the GCMMA algorithm. The first analysis is a strictly visual one, comparing the thickness of the different lines as well as the topologies that result from the optimizations.

A more in-depth demonstration of the results follows these comparisons for each of the ground structures, with the objective of better showing the effects and phenomena regarding the buckling effect constraint. The significant parameters for these optimizations are presented in Table 5.9.

Table 5.9 - Problem's Optimization Parameters

Parameter	5-Bars	10-Bars	36-Bars	20-Bars	21-Bars	L-Bracket	110-Bars
Size of $\boldsymbol{I_1}$	150		210	250	105	300	210
Scaling Factor, $\boldsymbol{\phi}$	4	5	10	3.2	5	5	2
Length Penalization Exponent, $\boldsymbol{p^L}$	1		2	1			
Cut of point w.r.t. total area, $\%\boldsymbol{A_{ref}}$	0.1		0.4	0.4	0.15	0.25	0.5
Tolerance for KKT Conditions, $\boldsymbol{kkt_{tol}}$	1×10^{-3}						

The continuation approach employed varied between the same values for all examples with the difference between examples being the rate at which the variation was done. This rate is controlled by the total number of iterations performed, since the variations intervals are dictated by a percentage of the parameter I_1. A generic representation of this continuation approach is presented in Figure 5.10. The parameters whose values were affected by this continuation approach are the parameter controlling the $\epsilon - relaxation$, ϵ, the parameters associated with the new buckling constraint, α and p, and finally an internal MMA parameter associated with the maximum allowed variation of the variables from one iteration to the next, γ. It was key for the optimization to apply a continuation approach to obtain any usable results, as all other solution would converge to a local minimum.

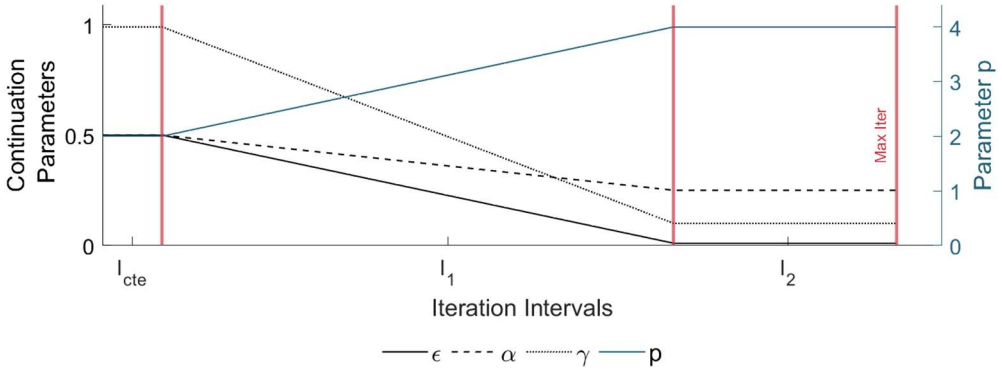

Figure 5.10 - Continuation Approach for the Relevant Parameters

5.4.1 MMA Results

The solutions found by the algorithm, using the MMA optimizer, to the three analytical examples are presented in Table 5.10, where a comparison between the problem with and without the buckling constraint is performed.

Table 5.10 – Comparison between topologies of the solutions with and without the Buckling Constraint (MMA) of the analytical examples

Example	Without buckling	With buckling
5-Bars	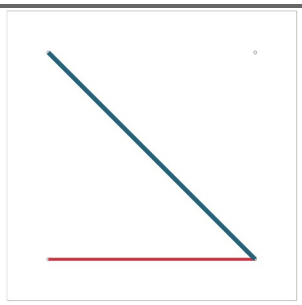	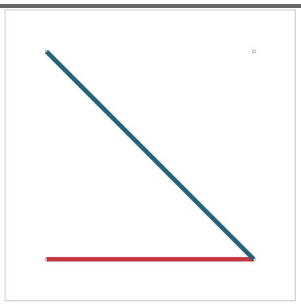
10-Bars	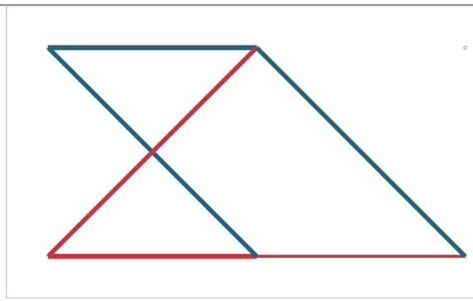	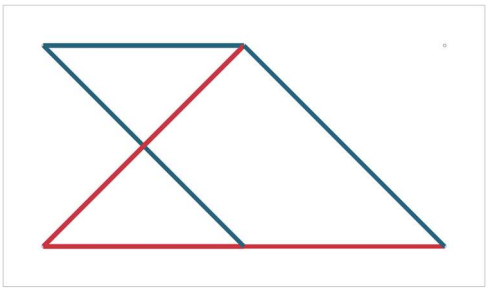
36-Bars	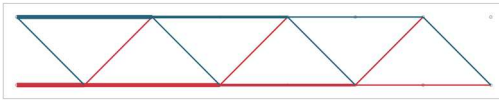	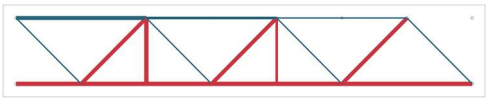

The solutions to the complementary problems are presented in Table 5.11, with the MMA optimizer. These more complex problems present a difference in either the topology or the thickness of the lines, as the ideal structure changes as the buckling constraint is introduced.

Table 5.11 – Comparison between topologies of the solutions with and without the Buckling Constraint (MMA) of the complementary examples

Example	Without buckling	With buckling
20-Bars	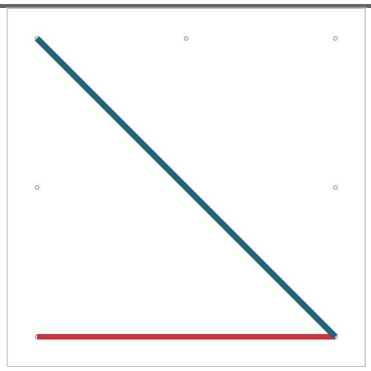	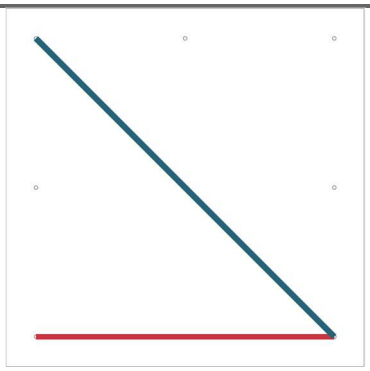
21-Bars	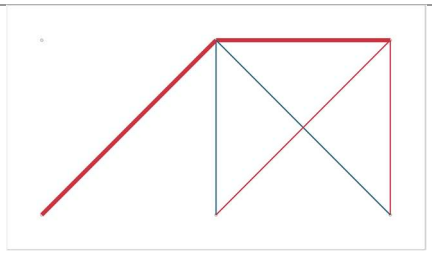	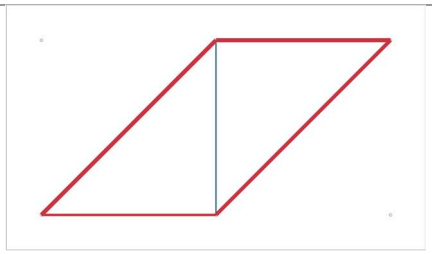
L-Bracket	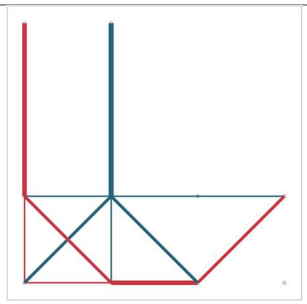	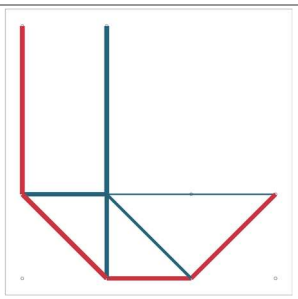
110-bars	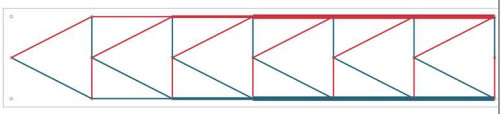	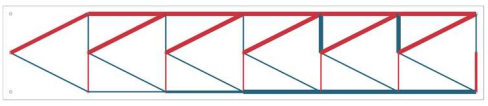

The graphical representations shown in Table 5.10 and Table 5.11, as well as all the following topology representations, have a colored scheme to represent which bars are under tension, in blue, and which are under compression, in red. In addition to the color scheme, on future graphs the buckling length will be included just below each bar, showing what length is being considered for that bar's buckling constraint.

Regarding the analytical examples, the first two problems, shown in Table 5.10, the 5-bar and the 10-bar, do not show any significant change in the structure's topology when comparing a problem solved with and without the buckling constraint. The third example, the 36-bar problem, nonetheless does clearly show two distinct topologies for each formulation, this was to be expected and will be further discussed in this chapter's last section.

In all problems shown, the impact of the buckling constrain can be observed even when the topology is the same, as bars under compression suffer a significant increase in their cross-sectional area when buckling is introduced, represented by a thicker line.

It is possible to compare the objective function between the two formulation and check that, as expected, there is a significant increase in the mass of the structure when including buckling. This is because with the examples chosen the admissible yield stress of a bar under compression in higher in value then the critical stress of those bars, justifying an increase in the element's cross-sectional area. Table 5.12 shows the comparison between the two formulations, worth noting that is possible to change the parameters of the examples so that no bar is restricted by buckling, although that would be counterproductive.

Table 5.12 - Mass Comparison between the formulation with and without the buckling constraint for the MMA Algorithm

Truss	Mass w/o buckling constraint	Mass w/ buckling constraint	Mass Ratio
5-Bars	0.2002	0.2088	104.30%
10-Bars	0.9691	1.1638	120.09%
36-Bars	6.3072	13.9867	221.76%
20-Bars	0.2002	0.2073	103.55%
21-Bars	0.6507	0.7166	110.13%
L Bracket	1.0412	1.1798	113.31%
110-Bars	0.6328	1.0537	166.51%

5.4.2 GCMMA Results

In this chapter a different algorithm will be implemented. It was noted that the MMA algorithm is very problem dependent in the definition of the key parameters. With the intention of alleviating the preliminary work of find the correct parameters, which entails running the algorithm many times with different parameters each time, GCMMA was applied to the same problems. This will provide a benchmark of several examples to compare with MMA. The same problems presented earlier are solved, in this chapter, using the GCMMA optimizer, these results are presented in Table 5.13, for the analytically solved problems, and in

Table 5.14, for the complementary structures. Some of the topologies differ from the previous topologies, the implications of which will be discussed further on in the final section of this chapter.

Table 5.13 – Comparison between Topology Solution with and without the Buckling Constraint (GCMMA)

Example	Without buckling	With buckling
5-Bars	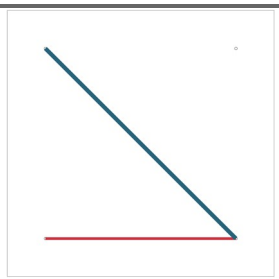	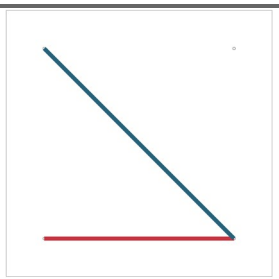
10-Bars	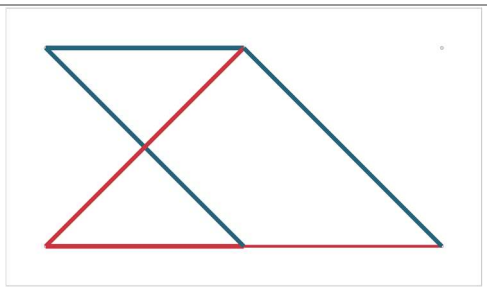	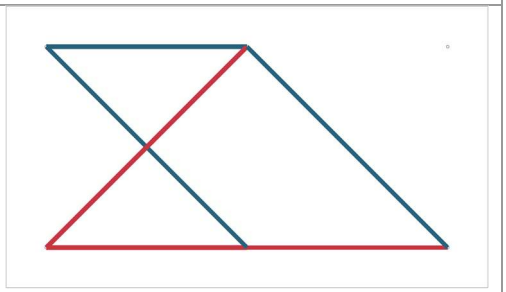
36-Bars	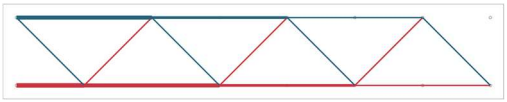	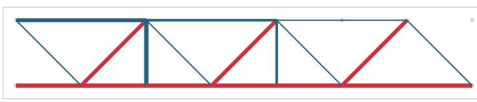

With some of the more complex structures it was not possible to reach a reasonable solution, as the structure's complexity "trapped" the algorithm in some undesired local minimum, a proposition to why this is can be found that the end of this chapter, in the result's discussion.

Table 5.14 – Comparison between topologies of the solutions with and without the Buckling Constraint (MMA) of the complementary examples

Example	Without buckling	With buckling
20-Bars	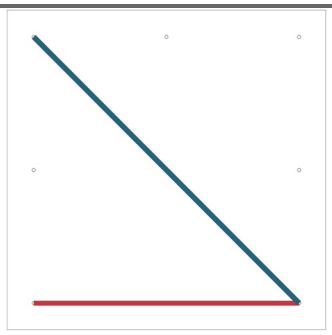	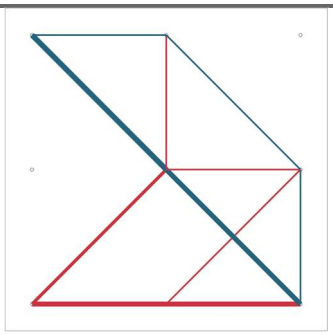
21-Bars	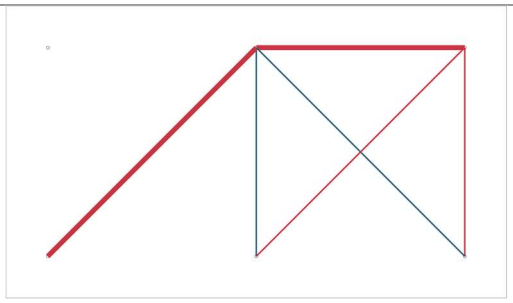	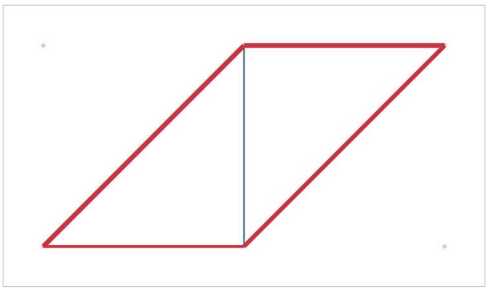
L-Bracket	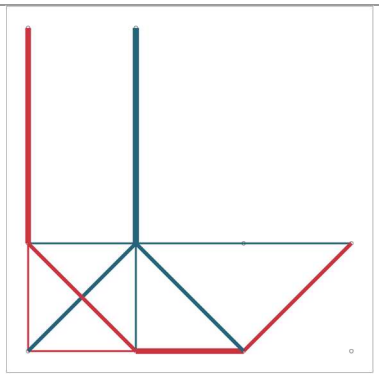	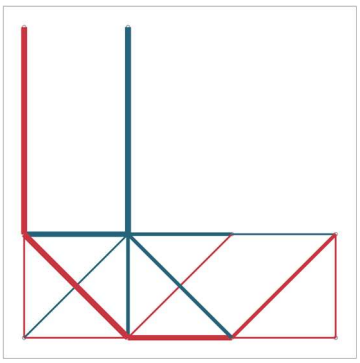
110-bars	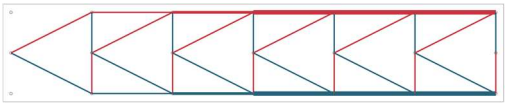	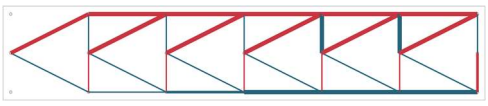

A comparison between the formulation applying the GCMMA algorithm with and without the buckling constraint, similar to the one presented for the MMA algorithm, is presented in Table 5.15.

Table 5.15 - Mass Comparison between the formulation with and without the buckling constraint

Truss	Mass w/o buckling constraint	Mass w/ buckling constraint	Mass Ratio
5-Bars	0.1994	0.2088	104.71%
10-Bars	0.9659	1.1608	120.18%
36-Bars	6.3074	13.8031	218.84%
20-Bars	0.2001	0.2662	133.03%
21-Bars	0.6476	0.7255	112.03%
L Bracket	1.0367	1.2834	123.80%
110-Bars	0.6328	1.0523	166.29%

A further comparison between the two algorithms is required, it is presented in Table 5.16.

Table 5.16 - Mass Comparison between the formulation with and without the buckling constraint

Truss	MMA Optimization	GCMMA Optimization	Mass Ratio
5-Bars	0.2088	0.2088	100.00%
10-Bars	1.1638	1.1608	99.74%
36-Bars	13.987	13.8031	98.69%
20-Bars	0.2073	0.2662	128.41%
21-Bars	0.7166	0.7255	101.24%
L Bracket	1.1798	1.2834	108.78%
110-Bars	1.0537	1.0523	99.87%

As Table 5.16 shows, there are examples where the MMA algorithm's solution agrees with the solution from GCMMA, and there are others where the solution given by MMA is significantly lighter than the one given by GCMMA, while the opposite does not happen.

To better characterize the optimization's solutions a more detailed set of information is presented, in the following subsections.

5.4.3 5-Bars Ground Structure

The information regarding the solution of the 5-Bar ground structure optimization problem is presented in Table 5.17. In this table, three graphical representations of the topology are presented. The first refers to the elements stress state with the same color scheme as before, and the addition of the buckling length information in text just below each element. The second shows how the existing element's stress compares to the elements critical stress, showing where in the topology this critical stress has the most impact as a limiting factor. The third representation, shows a similar relationship between the element's stress and the material's yield stress, showing which bars are critical w.r.t. the admissible stress constraint.

Table 5.17 - Solution Breakdown of the optimization algorithm for the 5-Bar Ground Structure

	Topology	Buckling Constraint	Stress Constraint
Graphical Representation	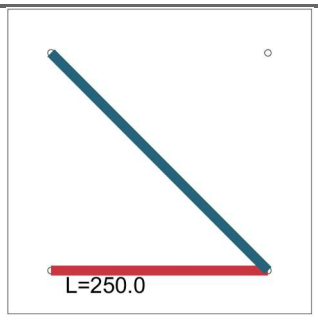	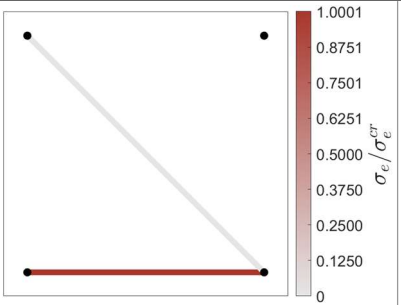	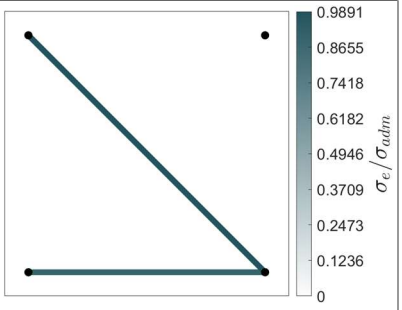
Value per element	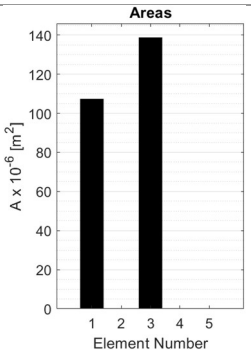	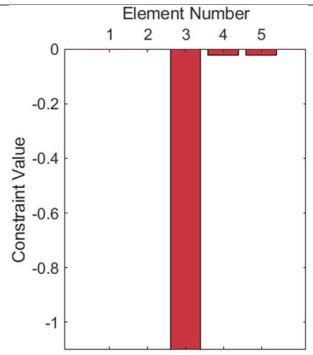	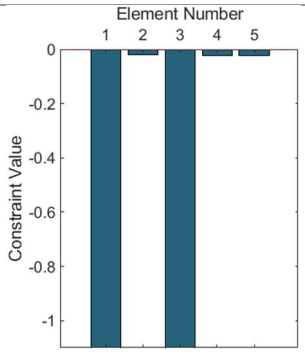

In Figure 5.11, the progression of the objective function and the KKT conditions through the iterations for this example is presented.

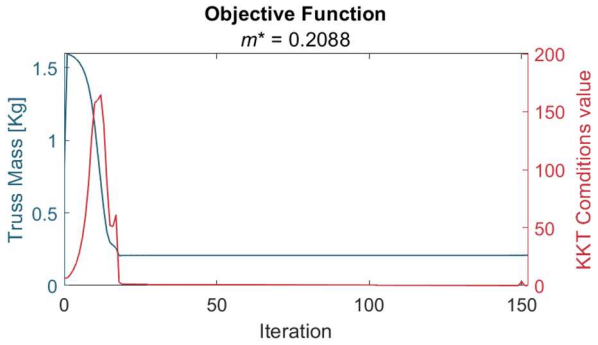

Figure 5.11 - Objective Function Plot for 5-Bar Problem

The graphs presented in Figure 5.12 show the direct relation between the elements stress, σ_e, and both the critical stress value, taken from Euler's Formula, σ_e^{cr}, and the yield stress value, given by the material's properties, σ_{adm}. A discussion of these values and their relationship with the constraints is presented in the final section of this chapter.

(a) (b)

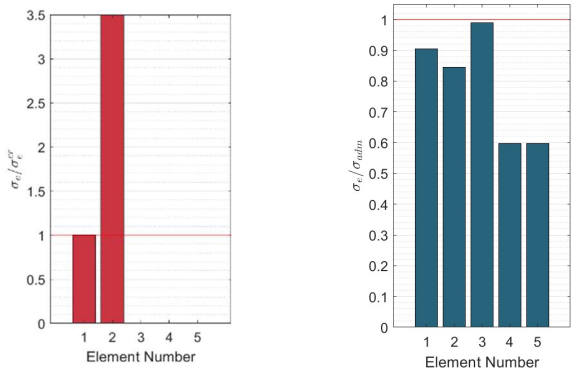

Figure 5.12 - Direct Comparison between member stress and limiting factors for the 5-Bar Ground Structure, (a) $\frac{\sigma_e}{\sigma_e^{cr}}$ (b) $\frac{\sigma_e}{\sigma_{adm}}$

5.4.4 10-Bars Ground Structure

In Table 5.18 shows a set of graphs and plots similar to those presented in the previous section but regarding the 10-Bar ground structure optimization problem.

Table 5.18- Solution Breakdown of the optimization algorithm for the 10-Bar Ground Structure

	Topology	**Buckling Constraint**	**Stress Constraint**
Graphical Representation	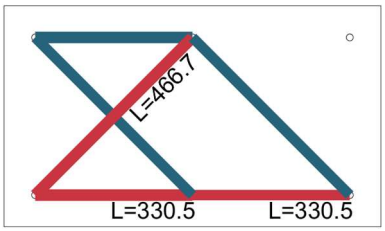	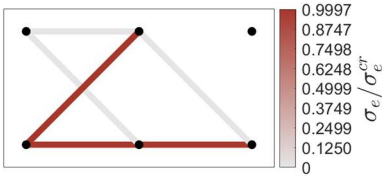	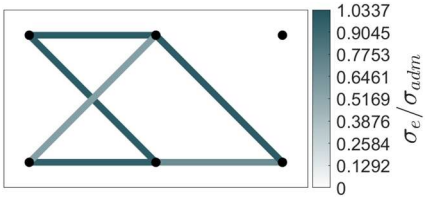
Value per element	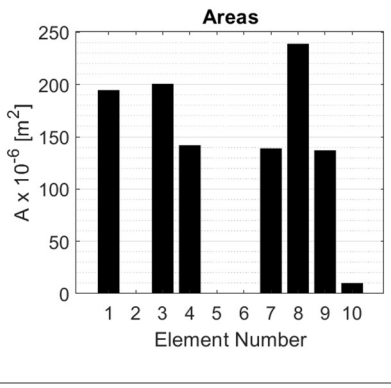	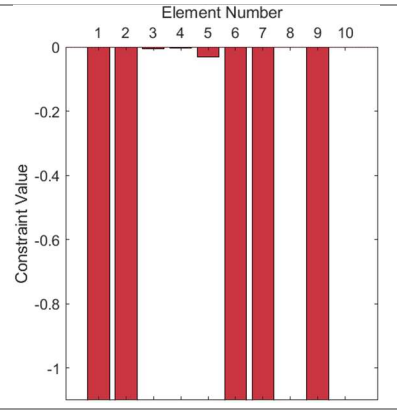	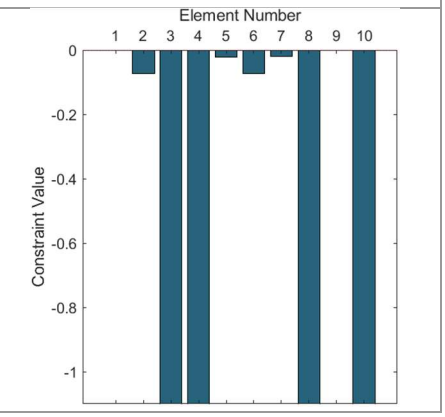

In Figure 5.13, the progression of the objective function and the KKT conditions through the iterations for this example is presented.

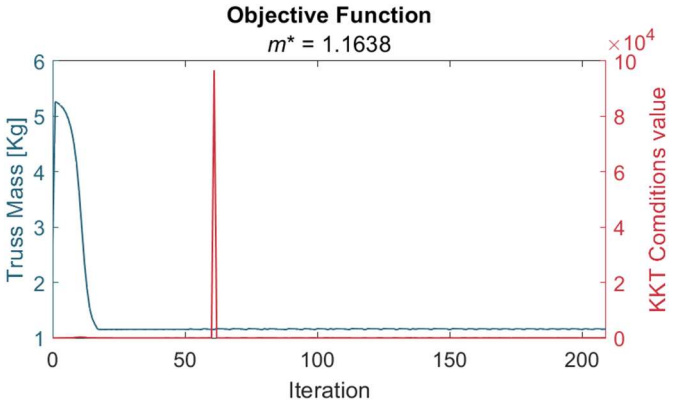

Figure 5.13 - Objective Function Plot for 10-Bar Problem

A graph representing the relation between all the elements' stress and their respective limiting factor is presented in Figure 5.14, similarly to the previous section but regarding the 10-Bar ground structure problem, these results will be discussed in the final section of this chapter.

(a) (b)

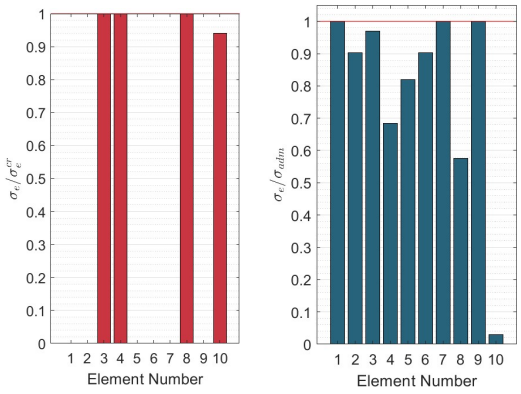

Figure 5.14 - Direct Comparison between member stress and limiting factors for the 10-Bar Ground Structure, (a) $\frac{\sigma_e}{\sigma_e^{cr}}$ (b) $\frac{\sigma_e}{\sigma_{adm}}$

5.4.5 36-Bars Ground Structure

Table 5.19 shows a set of topology graphs similar to part of those previously presented in the last section but regarding the 36-Bar ground structure optimization problem.

Table 5.20 presents the rest of the information regarding this problem.

Table 5.19 - Topology Representations Relating to mass distribution, buckling constraint and stress constraint for 36-Bar Problem

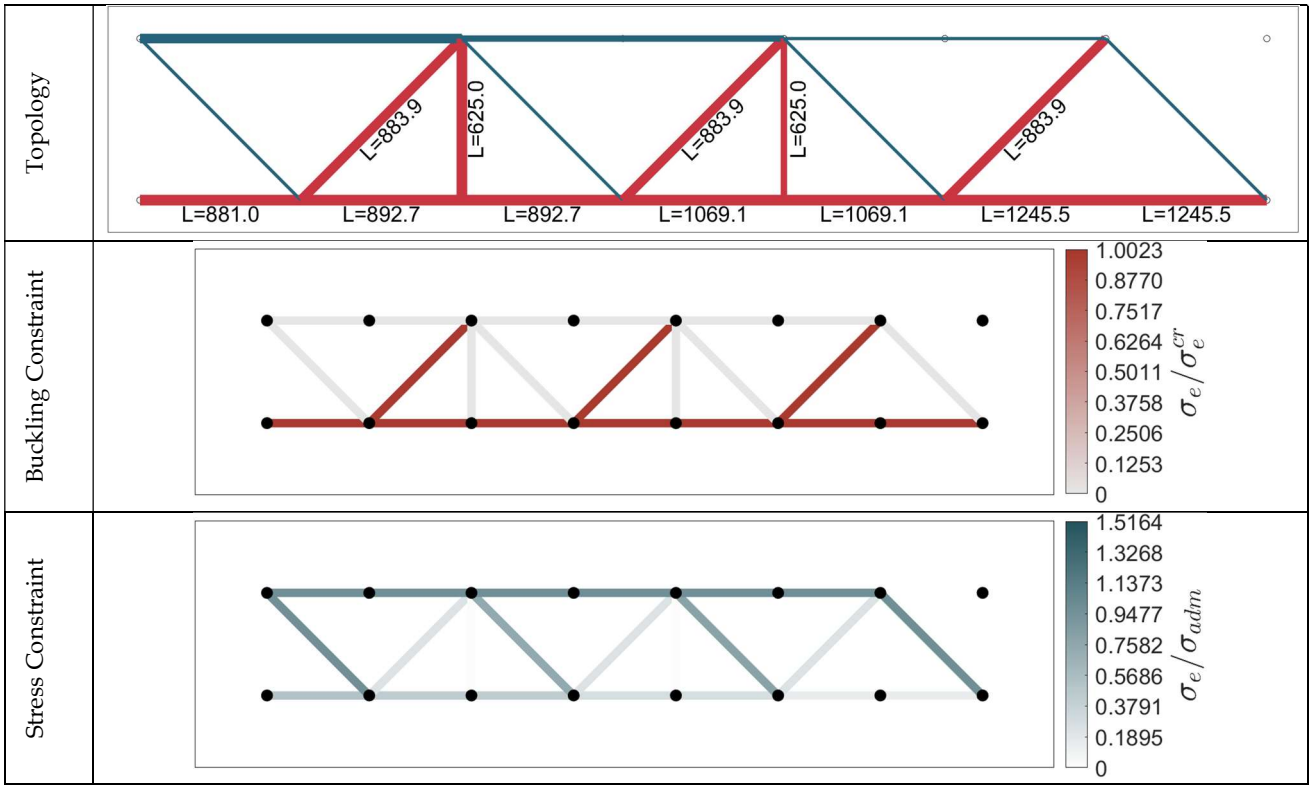

Table 5.20- Solution Breakdown of the optimization algorithm for the 36-Bar Ground Structure, Topology, Bucklin Constraint, and Stress Constraint's Values

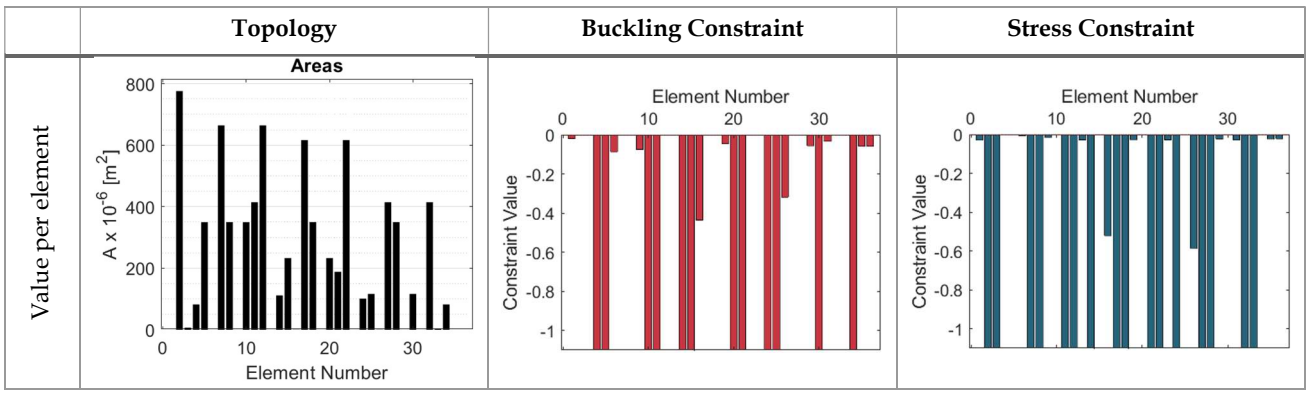

In Figure 5.15, the progression of the objective function and the KKT conditions through the iterations for this example is presented.

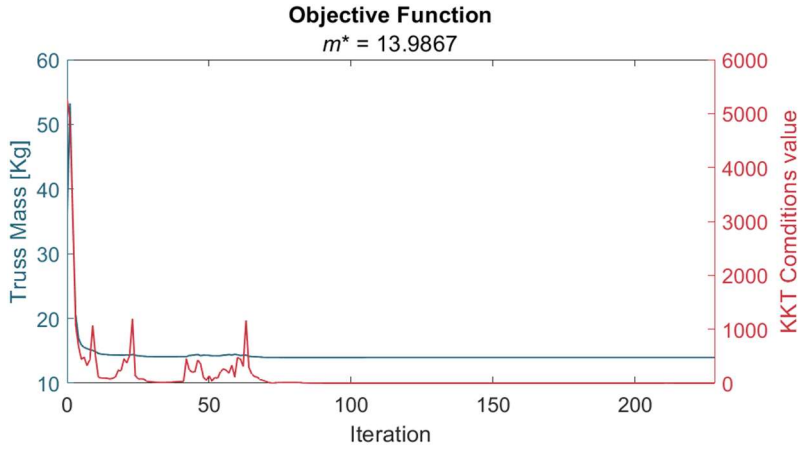

Figure 5.15 - Objective Function Plot for 36-Bar Problem

A graph representing the relation between all the elements' stress and their respective limiting factor is presented in Figure 5.16, similarly to the previous section but regarding the 10-Bar ground structure problem, these results will be discussed in the final section of this chapter.

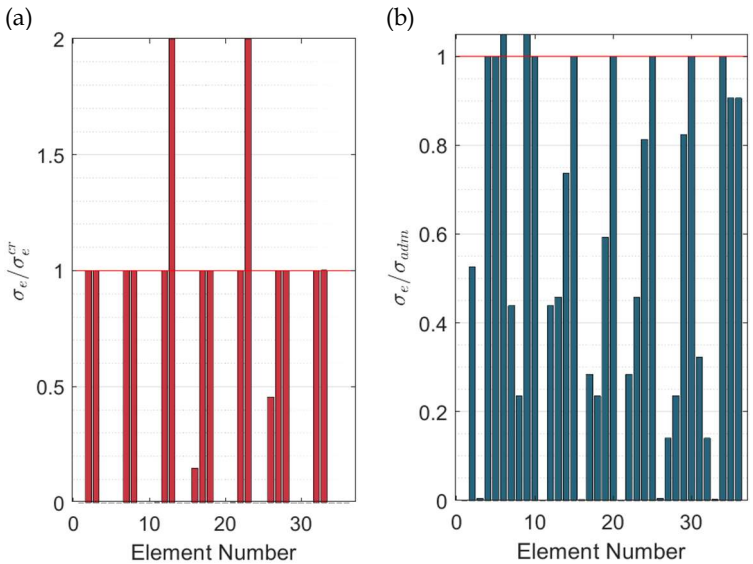

Figure 5.16 - Direct Comparison between member stress and limiting factors for the 36-Bar Ground Structure, (a) $\frac{\sigma_e}{\sigma_e^{cr}}$ (b) $\frac{\sigma_e}{\sigma_{adm}}$

5.4.6 20-Bars Ground Structure

In Table 5.21 shows a set of graphs and plots similar to those presented in previous sections but regarding the 20-Bar ground structure optimization problem solved with MMA algorithm.

Table 5.21 - Solution Breakdown of the optimization algorithm for the 20-Bar Problem, solved with MMA

	Topology	Buckling Constraint	Stress Constraint
Graphical Representation	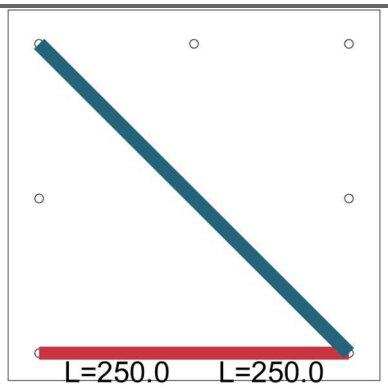	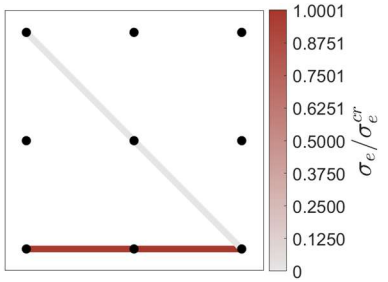	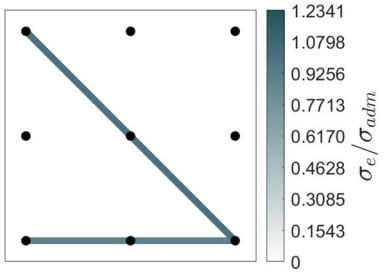
Value per element	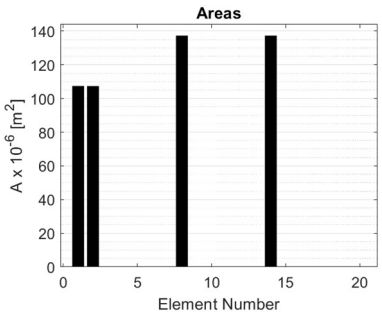	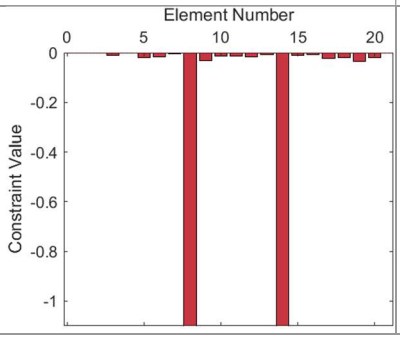	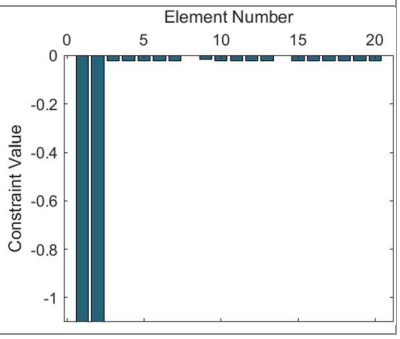

In Figure 5.17, the progression of the objective function and the KKT conditions through the iterations for this example, with the MMA algorithm, is presented.

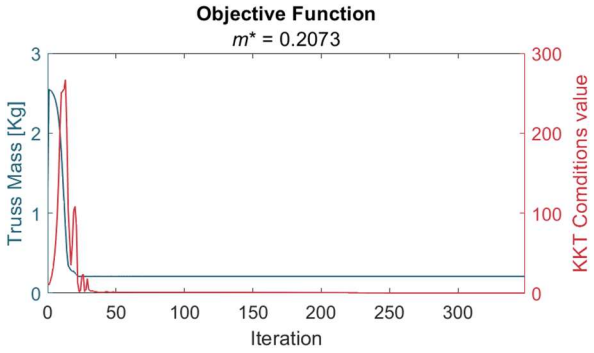

Figure 5.17 - Objective Function Plot for 20-Bar Problem

A graph representing the relation between all the elements' stress and their respective limiting factor is presented in Figure 5.18, similarly to previous sections but regarding the 20-Bar ground structure problem solved with MMA, these results will also be discussed in the final section of this chapter.

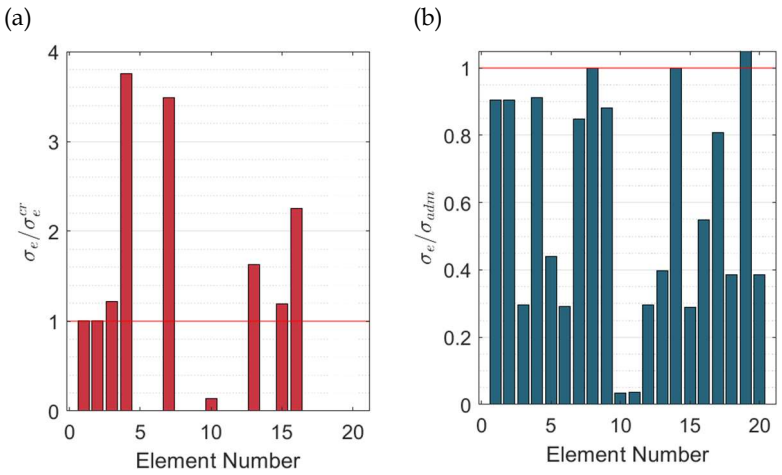

Figure 5.18 - Direct Comparison between member stress and limiting factors for the 20-Bar Ground Structure, (a) $\frac{\sigma_e}{\sigma_e^{cr}}$ (b) $\frac{\sigma_e}{\sigma_{adm}}$

Since in this example there is a difference between the two algorithm's solution, the same results presented for the MMA algorithm are now presented for the GCMMA algorithm. Table 5.22 shows a set of graphs and plots similar to those presented in previous sections but regarding the 20-Bar ground structure optimization problem solved with GCMMA algorithm.

Table 5.22 - Solution Breakdown of the optimization algorithm for the 20-Bar Problem, solved with GCMMA

	Topology	Buckling Constraint	Stress Constraint
Graphical Representation	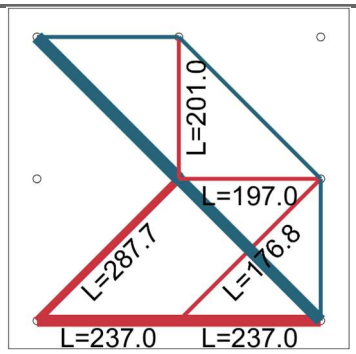	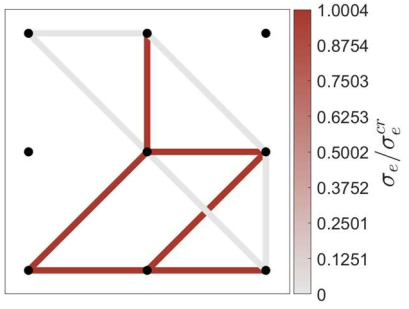	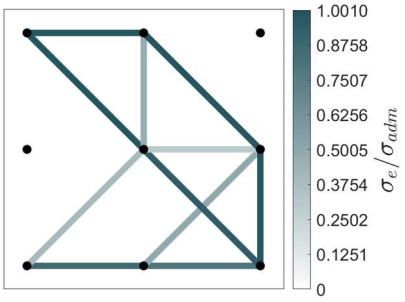
Value per element	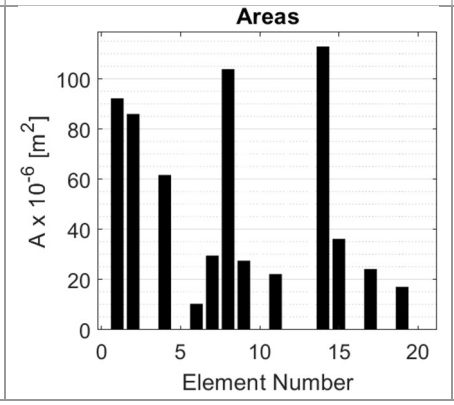	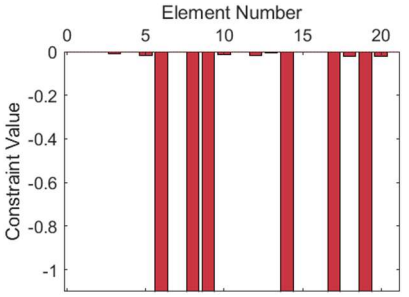	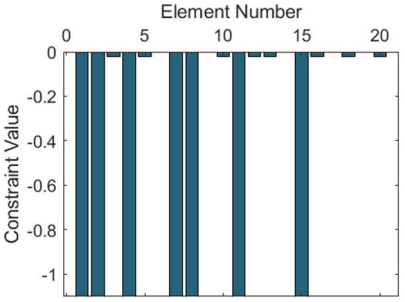

In Figure 5.19, the progression of the objective function and the KKT conditions through the iterations for this example, with the GCMMA algorithm, is presented.

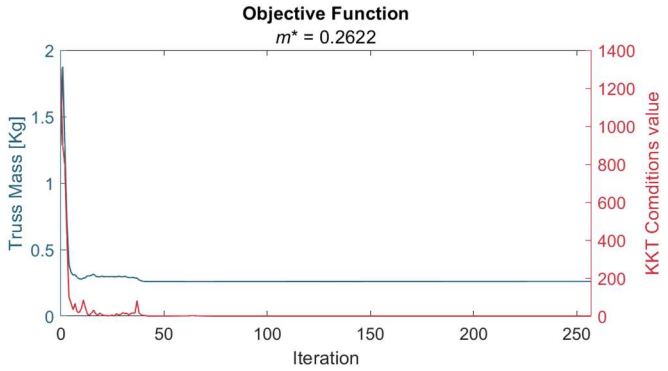

Figure 5.19 - Objective Function Plot for 21-Bar Problem

A graph representing the relation between all the elements' stress and their respective limiting factor is presented in Figure 5.20, similarly to previous sections but regarding the 20-Bar ground structure problem solved with GCMMA, these results will also be discussed in the final section of this chapter.

(a) (b)

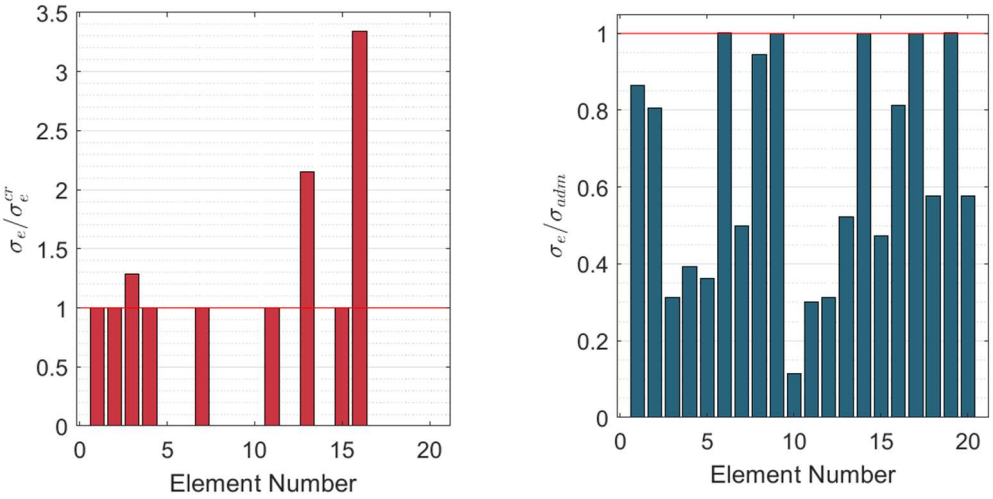

Figure 5.20 - Direct Comparison between member stress and limiting factors for the 20-Bar Ground Structure, (a) $\frac{\sigma_e}{\sigma_e^{cr}}$ (b) $\frac{\sigma_e}{\sigma_{adm}}$

5.4.7 21-Bars Ground Structure

Table 5.23 shows a set of graphs and plots similar to those presented in previous sections but regarding the 21-Bar ground structure optimization problem solved with GCMMA algorithm.

Table 5.23 - Solution Breakdown of the optimization algorithm for the 21-Bar Problem

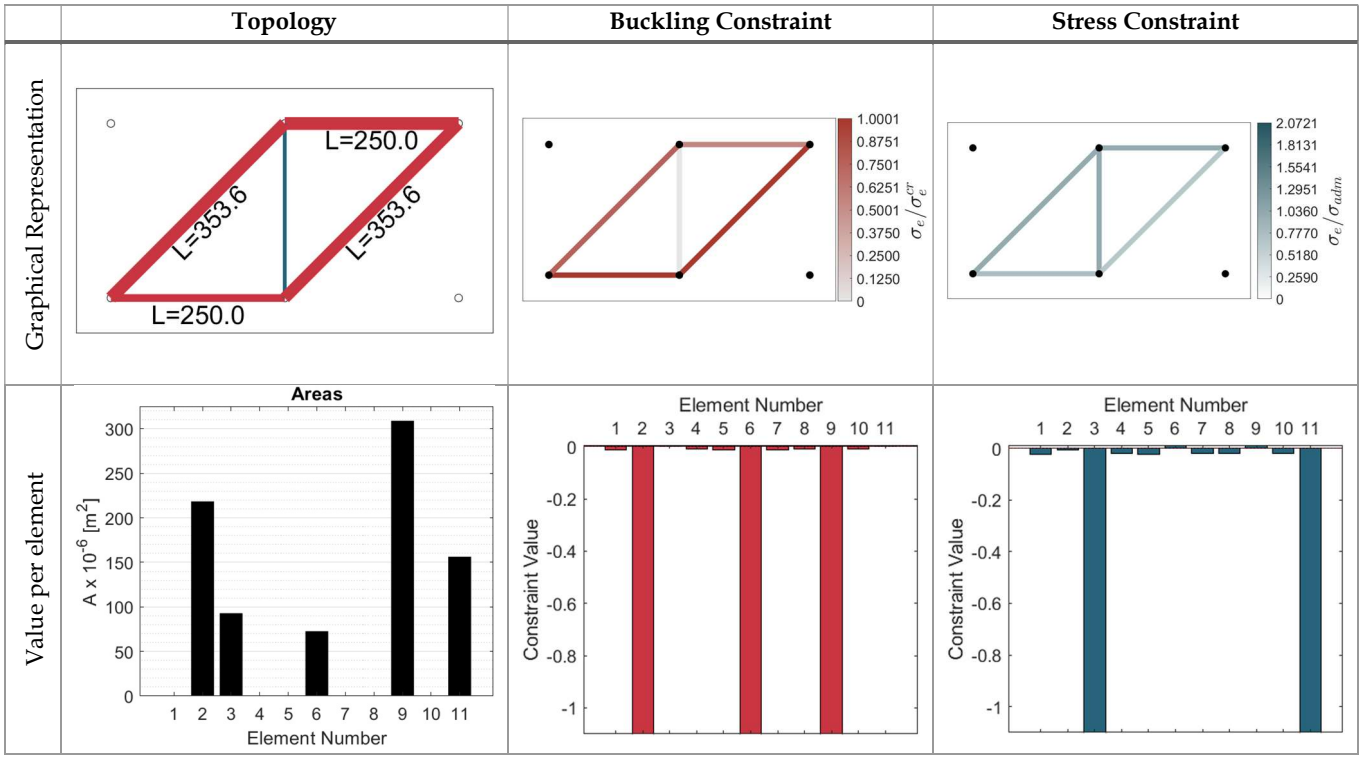

In Figure 5.21, the progression of the objective function and the KKT conditions through the iterations for this example is presented.

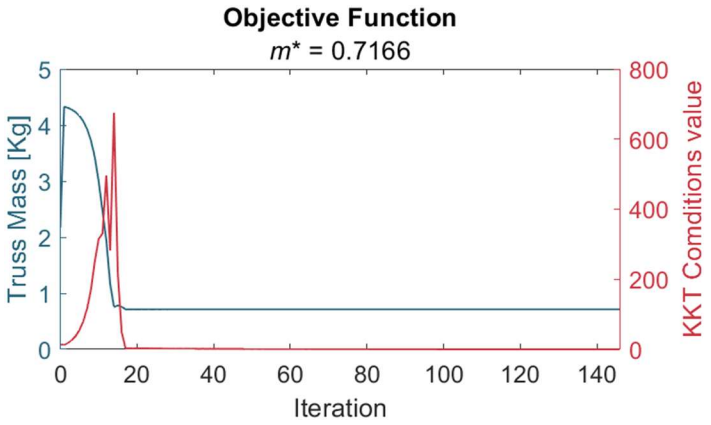

Figure 5.21 - Objective Function Plot for 21-Bar Problem

A graph representing the relation between all the elements' stress and their respective limiting factor is presented in Figure 5.22, similarly to previous sections but regarding the 21-Bar ground structure problem. these results will also be discussed in the final section of this chapter.

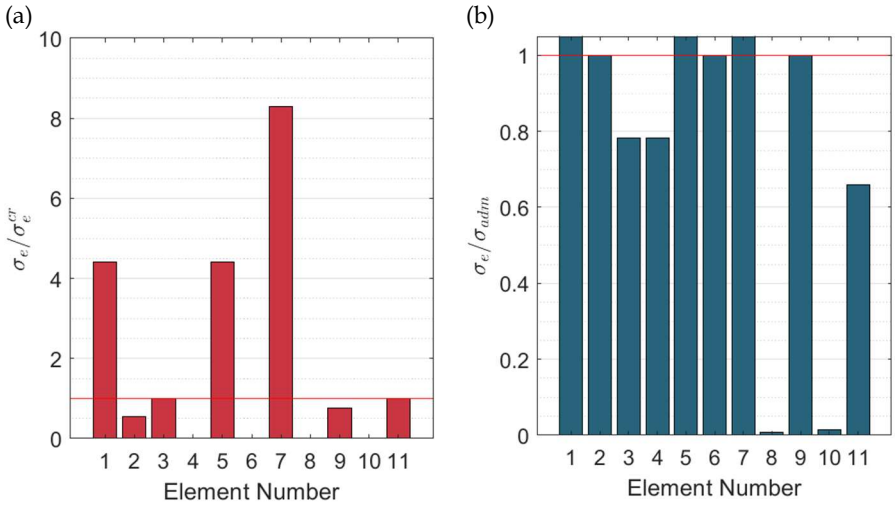

Figure 5.22 - Direct Comparison between member stress and limiting factors for the 21-Bar Ground Structure, (a) $\frac{\sigma_e}{\sigma_e^{cr}}$ (b) $\frac{\sigma_e}{\sigma_{adm}}$

5.4.8 L Bracket Ground Structure

Table 5.24 shows a set of graphs and plots similar to those presented in previous sections but regarding the 21-Bar ground structure optimization problem solved with MMA algorithm.

Table 5.24 - Topology Graphs Relating to mass distribution, buckling constraint and stress constraint for L-Graph Problem

	Topology	Buckling Constraint	Stress Constraint
Graphical Representation	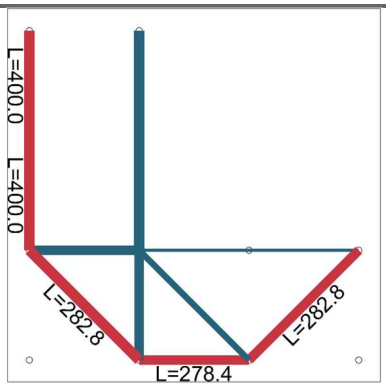	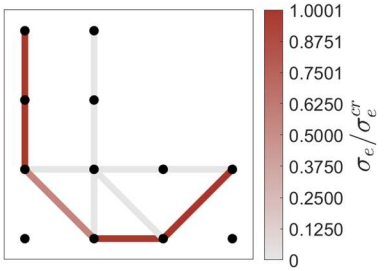	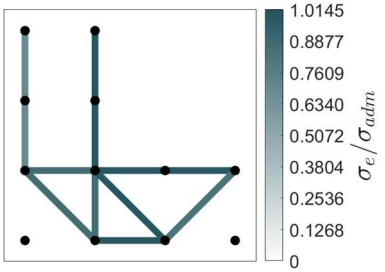
Value per element	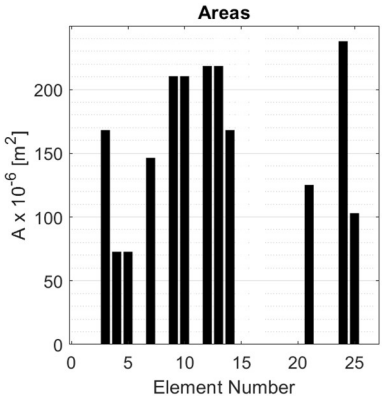	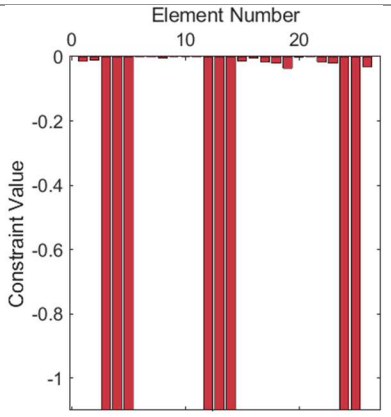	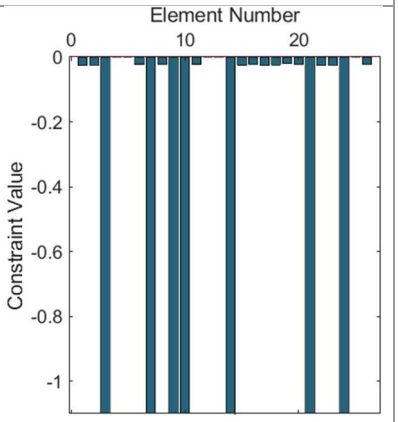

Figure 5.23, the progression of the objective function and the KKT conditions through the iterations for this example, with the MMA algorithm, is presented.

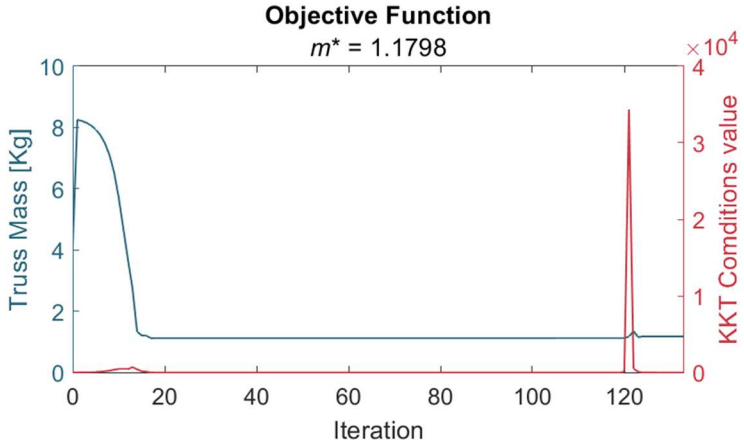

Figure 5.23 - Objective Function Plot for L-Bracket Problem

A graph representing the relation between all the elements' stress and their respective limiting factor is presented in Figure 5.24.

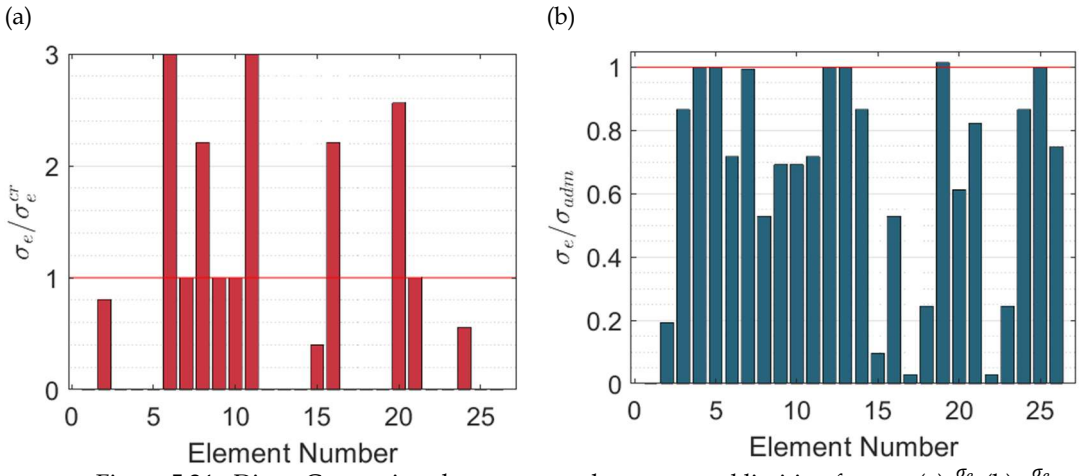

Figure 5.24 - Direct Comparison between member stress and limiting factors, (a) $\frac{\sigma_e}{\sigma_e^{cr}}$ (b) $\frac{\sigma_e}{\sigma_{adm}}$

Since in this example there is a difference between the two algorithm's solution, the same results presented for the MMA algorithm are now presented for the GCMMA algorithm. Table 5.25 shows a set of graphs and plots similar to those presented in previous sections but regarding the L-Bracket ground structure optimization problem solved with GCMMA algorithm.

Table 5.25 - Topology Graphs Relating to mass distribution, buckling constraint and stress constraint for L-Bracket Problem using GCMMA algorithm

	Topology	**Buckling Constraint**	**Stress Constraint**
Graphical Representation	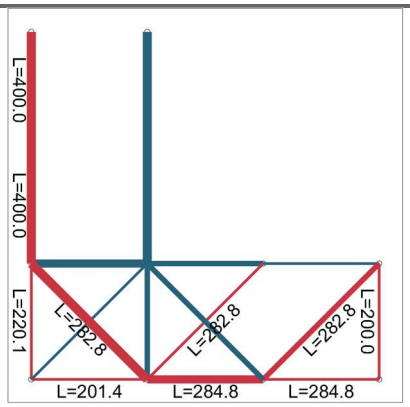	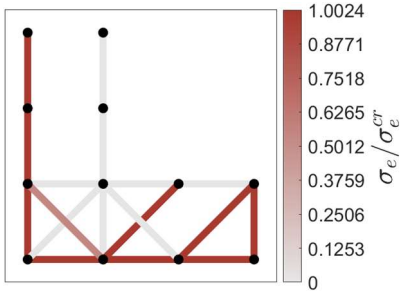	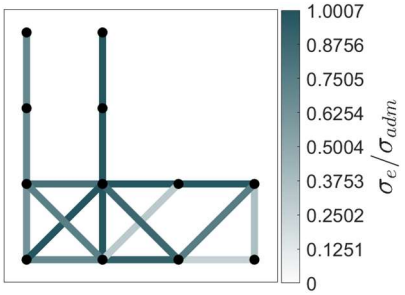
Value per element	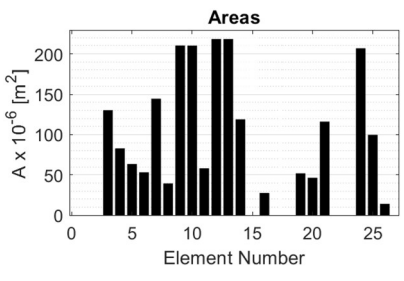	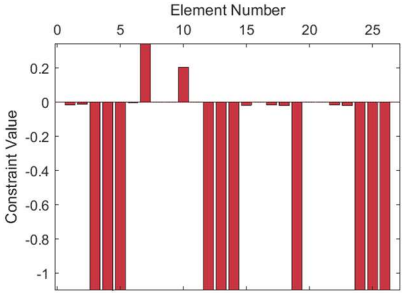	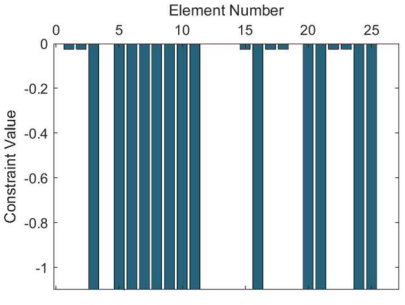

In Figure 5.25, the progression of the objective function and the KKT conditions through the iterations for this example, with the GCMMA algorithm, is presented.

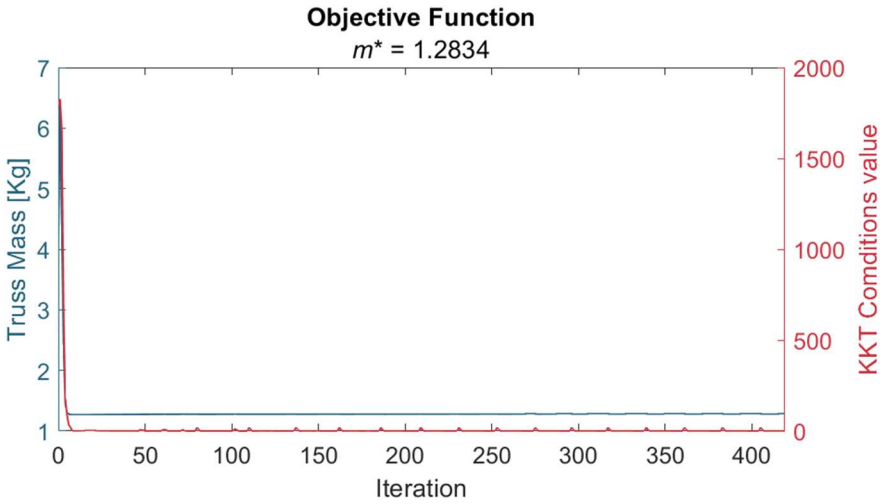

Figure 5.25 - Objective Function Plot for 21-Bar Problem

A graph representing the relation between all the elements' stress and their respective limiting factor is presented in Figure 5.26.

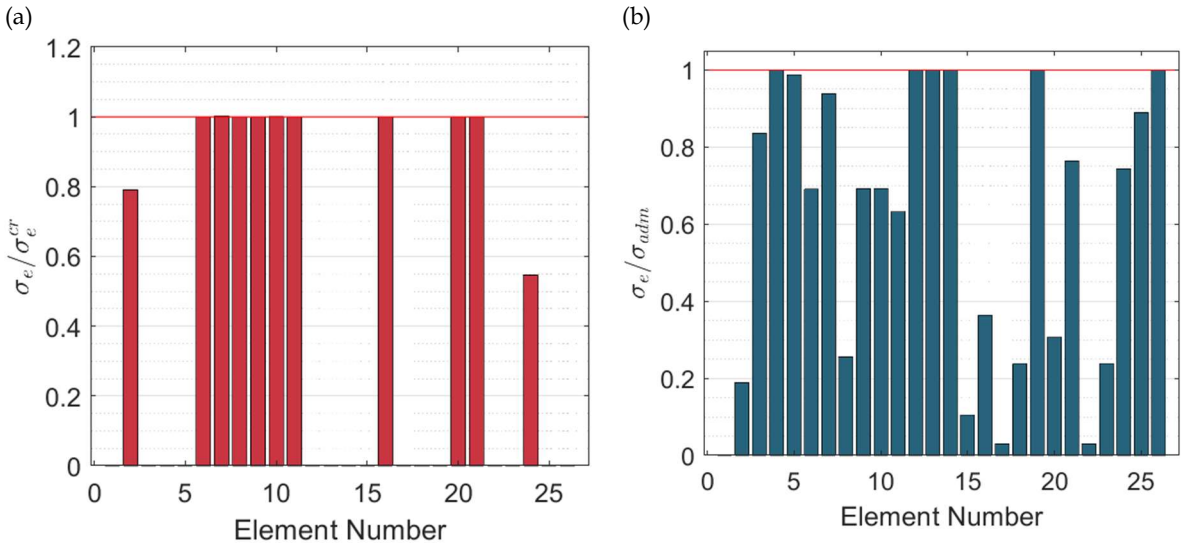

Figure 5.26 - Direct Comparison between member stress and limiting factors for the L-Bracket Ground Structure, (a) $\frac{\sigma_e}{\sigma_e^{cr}}$ (b) $\frac{\sigma_e}{\sigma_{adm}}$

5.4.9 110-Bars Ground Structure

Table 5.26 shows a set of topology graphs similar to part of those previously presented in the last section but regarding the 36-Bar ground structure optimization problem. Table 5.27 presents the rest of the information regarding this problem.

Table 5.26 - Topology Graphs Relating to mass distribution, buckling constraint and stress constraint for 36-Bar Problem

	Graphical Representation
Topology	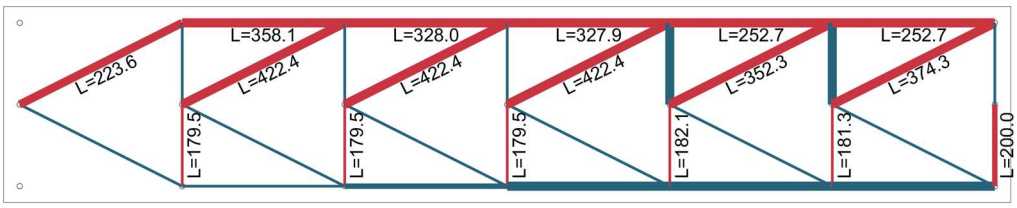
Buckling Constraint	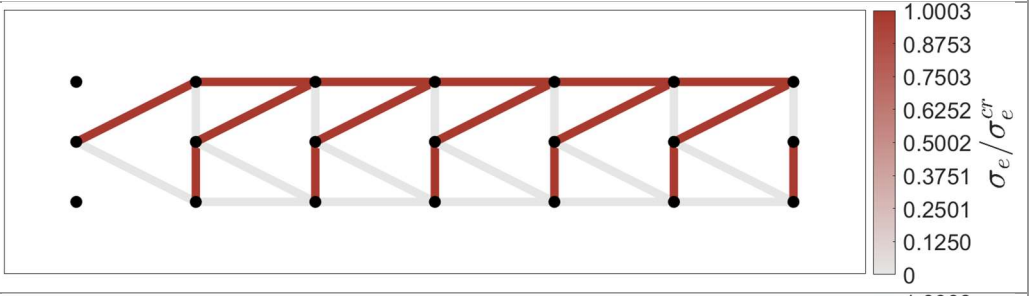
Stress Constraint	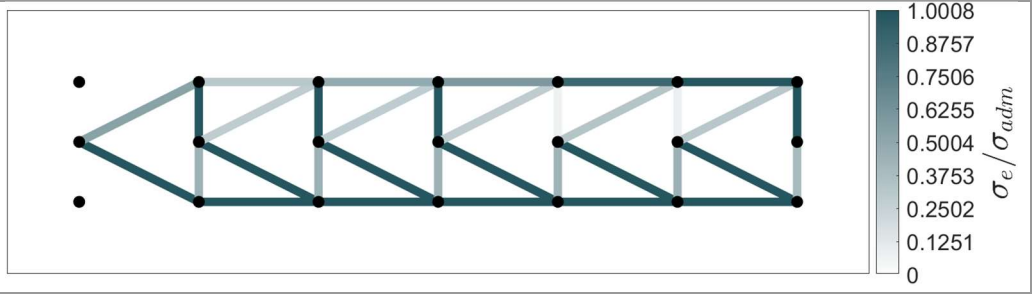

Table 5.27- Solution Breakdown of the optimization algorithm for the 36-Bar Ground Structure

	Topology	Buckling Constraint	Stress Constraint
Value per element	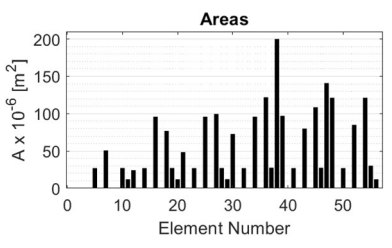	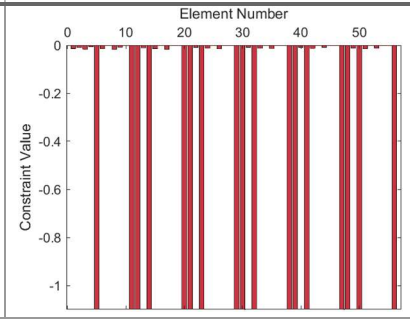	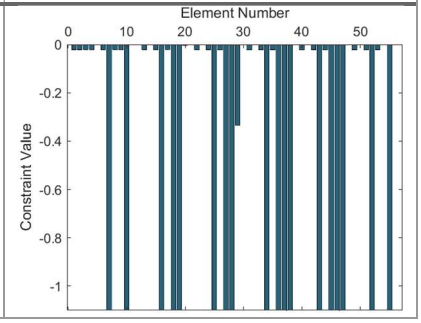

In Figure 5.27, the progression of the objective function and the KKT conditions through the iterations for this example is presented.

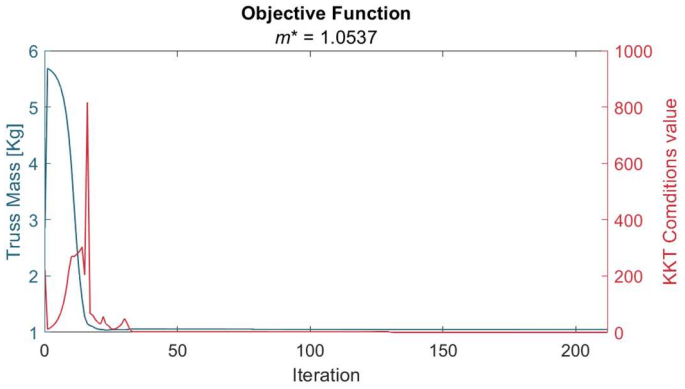

Figure 5.27 - Objective Function Plot for 110-Bar Problem

A graph representing the relationship between the stress of each element and the respective limiting factor is presented in Figure 5.28.

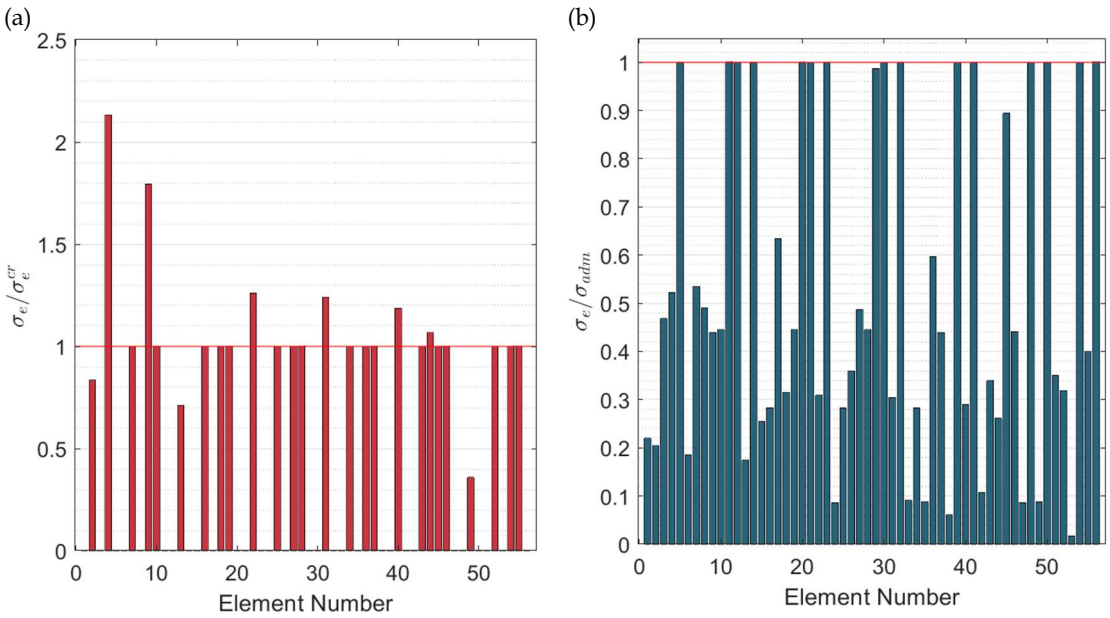

Figure 5.28 - Direct Comparison between member stress and the limiting factors for the 110-Bar Ground Structure, (a) $\frac{\sigma_e}{\sigma_e^{cr}}$ (b) $\frac{\sigma_e}{\sigma_{adm}}$

5.5 Results Discussion

The algorithm proposed in this thesis aims to solve problems with buckling constraints in a gradient-based setting. The results of the 5-bar and 10-bar problems give merit to the proposed algorithm, as the solution found is close in value to the analytical solution found for these trusses. Although the parameters that define these trusses were carefully chosen so that any bar under compression would first trigger the buckling constraint instead of the stress constraint, the solution found can be considered a global optimum as any other topology would imply a solution with more mass. An interesting behavior occurs in the 36-bar ground structure problem, because the inclusion of the chain effect in this structure, very large cross-sectional areas are required to deal with the "jump" in buckling lengths and forces. So, a set of vertical elements are added to some of the unstable nodes.

The noteworthy aspect of these vertical elements is that on the one hand they are null-load elements and on the other not every unstable node requires them. The algorithm can clearly reach a solution where some unstable nodes under compression are left without these vertical bars in the 36-bar topology, Table 5.19. The interpretation here being that these two "unstable" elements under compression model a larger bar, with its length being the sum of these element's lengths. In this node, since the areas of the attached to the unstable node are relatively small, the increase in cross-sectional are due to the larger buckling length does not justify the added mass of a vertical stabilizing bar.

With some confidence in the results obtained, as the algorithm is performing as intended, the methodology is then extended onto other problems, whose solutions were not obtained a priori, with mixed results. It is therefore important to discuss how the parameters used in the problems were obtained. By running multiple sets of optimizations of the same but with varying parameters using the notions obtained from chapter 3.3, the best solution is then selected and shown in this thesis. All the examples shown go through this process so that the solutions presented are as close as possible to the global minimum. Although most of the results for the complementary problems are satisfactory, the solutions for the 20-Bar and L-Bracket ground structures using GCMMA represent only a local minimum, easily proven by the objective function's value obtained through the MMA optimizer being better than the one for the GCMMA algorithm. No matter what parameters where chosen the solution to these problems would always converge to the local minima shown, further experimentation of GCMMA showed some insensitivity to the continuation approach, quickly converging, as seen in the objective function and KKT-Conditions Graphs. The results for all other structure were comparable better as can be checked in the mass comparison in graph Table 5.16. The implementation of GCMMA was done primarily to turn the formulation problem independent and give better stability in the convergence of these results, as with some parameters many of the problems shown wouldn't reach completion, as numerical errors would terminate the optimization. To this effect the inclusion of the optimizer can be considered a success apart from the two examples discussed.

It is unclear if the GCMMA algorithm can be described as "better" or "worse" than the MMA algorithm, as it would require further investigation into the inner works of these algorithms. In sum, GCMMA is much more independent from the continuation approach or initial parameters, while being more prone to local minimum in some situations, especially when those same parameters are used to circumvent local minimum when utilizing MMA.

One manifestation of the relaxation approach employed to the buckling constraint can be seen in figures like Figure 5.22, where the stress of each bar is directly compared with the either its critical load or the material yield stress. Shown in these graphs is a gross violation of the critical load proving that the relaxation was employed with great success, as this violation only occurs in the elements that were eliminated from the topology while the elements still present have their stress in fact correctly limited. In these small bars that are to be eliminated the element's stress does in fact violate the critical load, as this bars quickly become unstable even under their own weight, but the algorithm eliminated them and so their critical does not apply to the relevant constraints.

These graphs also reveal that the admissible stress constraint functions mostly without needing any relaxation, although it is applied for coherency. This result is interesting in that the admissible stress should need to be relaxed, however, it appears that the force associated with an element being eliminated decreases enough through the optimization as to always respect the admissible stress.

6 CONCLUSION AND FUTURE WORKS

6.1 Conclusion

This dissertation's main objective was to develop an algorithm that includes local buckling constraint in a structural topology optimization problem, consequently having to deal with considerations for the chain effect phenomenon. Thus, making a humble contribution to the development of more realistic structural topology optimization algorithms.

Starting with a historic contextualization and a bibliographic review it was noted that the scientific area of topology optimization has seen several re-emerging periods coinciding with computational breakthroughs and methodology improvements, this thesis benefits from some of the latest developments in this area. The expanding body of literature that serves as a basis for this thesis is built upon key developments that were addressed and their technics briefly presented. A special look was taken into the used algorithms, MMA and GCMMA. Because these algorithms are gradient based, they require a formulation that is convex and continuous, justifying adaptations to the functions used so that they are coherent with the optimizing algorithm's requirements. Since the differentiation of the various functions is a key feature in gradient-based optimization, a necessary restructuring of the calculations was presented to obtain the constraint's sensitivity more efficiently and to allow easier implementation of new constraints.

The buckling constraint was then presented and analyzed with a small comparison between a global and local approach. The desired local approach would need a relaxation of the problem which was obtain with three aspects. First, a $\epsilon - relaxation$ was used, secondly, a continuation approach was need because of the algorithm, and lastly, a reformulation of the basic constraint was employed.

The next chapter presented an analysis of this algorithm's more important parts, those being the objective function and the constraints used. Starting with the stress constraint, to circumvent the difficulties associated with an admissible stress constraint, a relaxation technique known as $\epsilon - relaxation$ was required, as well as multiplying the stress constraint by the element's area, allowing constraints associated with small cross-sectional areas to be removed from the active set of constraints. This would address the drawbacks of having an admissible stress constraint, which are also presented and discussed in this section. Further onto this chapter, the buckling constraint is presented with a step-by-step analysis of the final com-

plex constraint that starts with an analysis of the load environment in a single member, identifying the different stress domains present in a loaded element. Then a new limiting formula is presented, with the justification of altering the behavior of Euler's formula when dealing with small area, avoiding numerical singularities while not disturbing the performance of Euler's formula in elements that are present in the optimization. Since when trying to solve for the topology optimization with dimensional optimization included, an element's area is both the topological variable and the dimensional variable. Requiring that when an element's area is reduced beyond some point, they are considered removed from the final topology.

The adaptation to Euler's formula presents the required behavior to process the buckling of a given element when it is present in the topology while allowing the algorithm to remove it when necessary. This formula's behavior is directly governed by two parameters, and a follow up analysis of these parameters was presented in graphical form, to gather some sensitivity of the effects that varying them will have in the overall optimization. This analysis facilitated the following process of running multiple optimizations of the same problem with different problems, since there was a notion of how to change the parameter to escape local minima. With the understanding of how the constraint performs for a single element a two variable problem is formulated so that a 2D graphical analyses of a usually unrepresentable problem is performed. This problem is then used to understand why and how the constraint needs to be formulated the way it is, given the requirements of the optimizers, resulting in an admissible region that is a continuous relaxed domain better suited for the optimization.

Afterwards and still constructing the buckling constraint, the jumping buckling length problem is addressed, presenting a viable methodology to deal with it. This methodology requires the classification of the members of the ground structure and their association based on the nodes they are connected to. Resulting in a table that associates chains of elements with their respective supporting elements. A current limitation of this methodology is the inability to deal with chains of more than two elements. A similar 2D analysis is present for the effects of the chain effect on the buckling constraint, resulting in the appropriate quantification of the parameters that rule the buckling length, of which there are two. With this study complete, the buckling constraint is fully defined and there is a more in-depth understanding of the four governing parameters. Lastly, in this third chapter the objective is briefly presented and then the complete problem formulation is shown ready to be differentiated.

The next chapter, chapter four refers to the function's sensitivity analysis. As this optimization requires the gradient information of the constraints and the objective function, an entire chapter is dedicated to differentiating these formulas. The sensitivity calculus w.r.t. to the constraints was readjusted from the works of Pratas [46] and Almeida [8], in their works the adjoint method would be applied to the admissible stress constraint. Although it makes no significant difference applying the adjoint method to the constraint or the stress information inside it when dealing with only one constraint, when dealing with more than that a redundancy would appear as the same derivatives would repeatedly be calculated. A more efficient application of the adjoint method when dealing with multiple constraints is to apply

it once to the element's stress, then having both the admissible stress and the buckling constraint be differentiated somewhat directly. It is in this chapter that the complexity of the buckling constraint becomes apparent and shows its impact in the differentiation of the constraint as higher order function with complex dependencies lead to complex derivatives.

With the problem defined, the next chapter presents the results for a series of examples that allow for the demonstration of the features of this algorithm. From this selection three example are elected to be solved analytically in order to determine how the formulation behaves when in a more complex formulation than the simpler two variable problems presented in earlier chapters. These analytical solutions can then be compared with the optimization results, given that the optimal solution is known. The algorithm solves the analytical problems with great accuracy and the results for the other examples can logically be considered correct, especially given that many perturbations were experimented with, and the solutions presented are those with the lowest mass. A general comparison between the solutions of both optimizers, MMA and GCMMA, is presented with both agreeing on all the examples, except two. The 20-bar ground structure, and the L-Bracket ground structure problems seem to trap the GCMMA optimizer in local minima, as it tends towards a local minimum. When this same problem happened with the MMA algorithm, a relaxation of some of the parameters would allow the optimization to escape those local minimums, but GCMMA seems to be more independent from the continuation approach employed, as it quickly converges to a solution, regardless of the parameters used.

6.2 Future Works

This dissertation presents the ground works for some further works in topology optimization with local buckling constraints manly the inclusion of density-based optimization onto this formulation, since some of the derivatives were presented with the added differentiation w.r.t the density variable, to facilitate this incorporation process in future projects. Including density-based optimization onto this formulation would possibly allow many improvements to this algorithm.

Firstly, the incorporation of multi-material analysis, which has been shown to greatly decrease the final weight of a structure, an interesting discussion might address which parameter would the algorithm prefer to change. Maybe in some scenarios the material would be preferably changed, as the material's Young Modulus influences Euler's buckling, allowing for a linear influence in the overall constrain. While in other scenarios adding more bars to stabilize nodes, therefore decreasing the effective buckling length of an element, would be preferred because the buckling length has a quadratic influence in Euler's Formula. The result of this optimization would lead to very dynamic solutions and further approximate an algorithm with real world applicability in terms of structural design.

Including density-based optimization onto the formulation would also allow the optimizer to change its topology variable from area to density and allow the area to work within a given interval, separating the topology optimization from the dimensional optimization.

This interval would allow a designer to selected from within a list a given sizes and allow the algorithm to choose, for instances the best profile to select from a list of normalized profiles, approximating the continuous solution given by the dimensional optimization to the discrete values of those normalized profiles. This would further approximate the current algorithm to the actual design process of structures, although maybe in that case a non-gradient optimization would probably better suit this application, the gradient-based optimization may have some unexpected benefits.

Another area of improvement could be considered the optimization of the cross-sectional profile that in this thesis is simply a circle. Because when dealing with axial loads the cross-sectional profile would not influence the admissible stress constraint, as the stress is only dependent on cross-sectional area's value and not its shape, this would impact the buckling constraint. Since, when dealing with Euler's formula the second moment of inertia is used which is dependent on the area's shape, adding a new variable to the optimization which determines what the best profile for a given element is. Possibly a simpler version of this cross-sectional shape optimization would be applicable to a three-dimensional scenario, optimizing then what the best orientation is for a given truss.

Lastly, it is worth noting that the computational cost of this formulation greatly increases when adding problems with such complex constraint as is the buckling constraint. A study of the efficiency of the computing process would allow not only shorter times in obtaining a optimization's solution but also would enable dealing with more complex structures, with order of magnitude more elements. The most immediate improvement to the algorithm's performance would be multi-thread parallel computing, although some other improvement may also be available.

BIBLIOGRAPHY

[1] «MatWeb: Material Property Data». Available in: https://tinyurl.com/3c2tkz88

[2] Achtziger, M., (2007) On simultaneous optimization of truss geometry and topology. Struct Multidisc Optim (2007) 33:285–304. DOI: 10.1007/s00158-006-0092-0

[3] Achtziger, W. (1999). Local stability of trusses in the context of topology optimization Part I: Exact Modeling. Structural Optimization 17, pp. 235-246. DOI: 10.1007/s001580050056

[4] Achtziger, W. (1999). Local stability of trusses in the context of topology optimization Part II: A numerical approach. Structural Optimization 17, pp. 235-246. DOI: 10.1007/s001580050056

[5] Achtziger, W. Optimization with Variable Sets of Constraints and an Application to Truss Design. Computational Optimization and Applications 15, 69–96 (2000). https://doi.org/10.1023/A:1008775015126

[6] Achtziger, W. Truss topology optimization including bar properties different for tension and compression. Structural Optimization 12, 63–74 (1996). https://doi.org/10.1007/BF01270445

[7] Adeli, H., Park, H.S., A NEURAL DYNAMICS MODEL FOR STRUCTURAL OPTIMIZATION-THEORY, Computers & Structures Vol. 57. No. 3. pp. 383-390. 1995. DOI: 10.1016/0045-7949(95)00048-L

[8] Almeida, C. (2020). Projeto de estruturas reticuladas leves e resistentes utilizando variáveis de área e de seleção de material. Faculdade de Ciências e Tecnologias, Universidade NOVA de Lisboa.

[9] Bendsoe, M. K. (1988). Generating optimal topologies in structural design using a homogenization method. Computer Methods in Applied Mechanics and Engineering, 71(2), pp. 197-224. https://doi.org/10.1016/0045-7825(88)90086-2

[10] Bendsoe, M. P., Sigmund, O., Topology Optimization, Theory, Methods, and Applications. Springer-Verlag Berlin Heidelberg 2003 and 2004 (2nd Ed.).

[11] Bendsøe, M.P. Optimal shape design as a material distribution problem. Structural Optimization 1, 193–202 (1989). https://doi.org/10.1007/BF01650949

[12] Ben-Tal, A., Jarre, F., Kočvara, M. et al. Optimal Design of Trusses Under a Nonconvex Global Buckling Constraint. Optimization and Engineering 1, 189–213 (2000). https://doi.org/10.1023/A:1010091831812

[13] Carvalho, J.P.G., Lemonge, A.C.C., Carvalho, É.C.R. et al. Truss optimization with multiple frequency constraints and automatic member grouping. Struct Multidisc Optim 57, 547–577 (2018). https://doi.org/10.1007/s00158-017-1761-x

[14] Cheng, G.D., Guo, X. ε -relaxed approach in structural topology optimization. Structural Optimization 13, 258–266 (1997). https://doi.org/10.1007/BF01197454

[15] Cheng, G.D., Guo, X., (1997) ε -relaxed approach in structural topology optimization. Structural Optimization, Springer-Verlag.

[16] Clough, R. (1960). The finite element method in plane stress analysis. Proc. 2nd A.S.C.E. Conf. on Electronic.

[17] Coelho, P. (2019). Métodos Computacionais em Engenharia Mecânica. Fundamentals of the Finite Element Method. DEPARTAMENTO DE ENG. MECÂNICA E INDUSTRIAL FCT/UNL.

[18] Coelho, P. (2019/2020). Tópicos Avançados em Mecânica Estrutural (1.1 ed.). DEPARTAMENTO DE ENG. MECÂNICA E INDUSTRIAL FCT/UNL.

[19] Courant, R. (1943). Variational Methods for the Solution of Problems of Equilibrium and Vibrations. Bulletin of the American Mathematical Society, 49, pp. 1-23.

[20] Dorn, W., Gomory, R., & Greenberg, H. (1964). Automatic design of optimzal structures. J. Mech, pp. 25-52.

[21] Ferrari, F., Sigmund, O. Towards solving large-scale topology optimization problems with buckling constraints at the cost of linear analyses (2020) Computer Methods in Applied Mechanics and Engineering, 363, art. no. 112911. https://doi.org/10.1016/j.cma.2020.112911

[22] Francavilla, A., Ramakrishnan, C. V., & Zienkiewicz, O. C. (1975). Optimization of shape to minimize stress concentration. Journal of Strain Analysis, 10(2), 63–70. https://doi.org/10.1243/03093247V102063

[23] Fred Glover, Future paths for integer programming and links to artificial intelligence, Computers & Operations Research, Volume 13, Issue 5, 1986, Pages 533-549, https://doi.org/10.1016/0305-0548(86)90048-1

[24] Griva, I., Nash, S.G., Sofer, A., Linear and Nonlinear Optimization. (2nd Ed.) Society for Industrial and Applied Mathematics, Philadelphia.

[25] Guo, X., Cheng, G. & Olhoff, N. Optimum design of truss topology under buckling constraints. Struct Multidisc Optim 30, 169–180 (2005). https://doi.org/10.1007/s00158-004-0511-z

[26] Guo, X., Cheng, G. & Yamazaki, K. A new approach for the solution of singular optima in truss topology optimization with stress and local buckling constraints. Struct Multidisc Optim 22, 364–373 (2001). https://doi.org/10.1007/s00158-001-0156-0

[27] Guo, Xu, Cheng, Gengdong New approach for the solution of singular optimum in structural topology optimization (1997) Acta Mechanica Sinica/Lixue Xuebao, 13 (2), pp. 171-178.

[28] Hodge, P. G., Jr., and Belytschko, T. (December 1, 1968). "Numerical Methods for the Limit Analysis of Plates." ASME. J. Appl. Mech. December 1968; 35(4): 796–802. https://doi.org/10.1115/1.3601308

[29] Kocvara, M. (2002). On the modelling and solving of the truss design problem. Struct Multidisc Optim 23, pp. 189-203. doi:10.1007/s00158-002-0177-3

[30] Krister Svanberg (2007) MMA and GCMMA, versions September 2007, Optimization and Systems Theory, KTH, Stockholm, Sweden.

[31] Liang Xia, Piotr Breitkopf, Concurrent topology optimization design of material and structure within FE2 nonlinear multiscale analysis framework, Computer Methods in Applied Mechanics and Engineering, Volume 278,2014, Pages 524-542, https://doi.org/10.1016/j.cma.2014.05.022.

[32] M. Bruggi e P. Venini, «A mixed FEM approach to stress-constrained topology optimization», Int. J. Numer. Methods Eng., vol. 73, n. 12, pp. 1693–1714, Mar. 2008.

[33] M. P. Rossow, J. E. Taylor (1973). A Finite Element Method for the Optimal Design of Variable Thickness Sheets. AIAA Journal, 11(11), 1566–1569. https://doi.org/10.2514/3.50631

[34] Ma, Z.D., Kikuchi, N. & Hagiwara, I. Structural Topology and shape optimization for a frequency response problem. Computational Mechanics 13, 157–174 (1993). https://doi.org/10.1007/BF00370133

[35] Madah, H., Amir, O. (2017) Truss optimization with buckling considerations using geometrically nonlinear beam modelling. Computers & Structures.

[36] Mattheck, C., Baumgartner, A., Walther, F. Optimization procedures by use of the finite element method (1994) American Society of Mechanical Engineers, Petroleum Division (Publication) PD, 64 (4), pp. 27-32.

[37] Maxwell, J. C. (1870). I.—On Reciprocal Figures, Frames, and Diagrams of Forces. Transactions of the Royal Society of Edinburgh, 26, p. 40. doi:10.1017/S0080456800026351

[38] Michell, A. (1904). LVIII. The limits of economy of material in frame-structures. Philosophical Magazine, 8(47), pp. 589-597. doi:10.1080/14786440409463229

[39] Moura Branco, C. (2011). Mecânica dos Materiais (5ª ed.). Fundação Calouste Gulbenkian.

[40] Norrie, Douglas H., Vries, G. The Finite Element Method. Fundamentals and Applications. Academic Press, New York, and London (1973).

[41] O. E. Canyurt & P. Hajela (2007) A SAND approach based on cellular computation models for analysis and optimization, Engineering Optimization, 39:4, 381-396, DOI:10.1080/03052150601146255

[42] Oberndorfer, J.M., Achtziger, W. & Hörnlein, H.R.E.M. Two approaches for truss topology optimization: a comparison for practical use. Structural Optimization 11, 137–144 (1996). https://doi.org/10.1007/BF01197027

[43] Oberndorfer, J.M., Achtziger, W., Hörnlein, H.R.E.M. (1996) Two approaches for truss topology optimization: A comparison for practical use. Structural Optimization, 11 (3-4), pp. 137-144. https://doi.org/10.1007/BF01197027

[44] Pedersen, N., Nielsen, A. Optimization of practical trusses with constraints on eigenfrequencies, displacements, stresses, and buckling. Struct Multidisc Optim 25, 436–445 (2003). https://doi.org/10.1007/s00158-003-0294-7

[45] Poulsen, P.N., Olesen, J.F. & Baandrup, M. Truss optimization applying finite element limit analysis including global and local stability. Struct Multidisc Optim 62, 41–54 (2020). DOI: 10.1007/s00158-019-02468-4

[46] Pratas, T. (2019). Otimização topológica multimaterial de estruturas reticuladas com constrangimentos de tensão. Faculdade de Ciências e Tecnologias, Universidade NOVA de Lisboa.

[47] Qi Cai, Linwei He, Yimin Xie, Ruoqiang Feng, Jiaming Ma, Simple and effective strategies to generate diverse designs for truss structures, Structures, Volume 32, 2021, Pages 268-278, ISSN 2352-0124, DOI: 10.1016/j.istruc.2021.03.010.

[48] Rozvany, G. (1996). Difficulties in truss topology optimization with stress, local buckling and system stability constraints. Structural Optimization 11, pp. 213-217.

[49] Schmit, L. A. (1960). Structural Design by Systematic Synthesis. Proceedings of the Second National Conference on Electronic Computation, ASCE.

[50] Shanbin Lu, Honggang Ma, Li Xin & Wenjie Zuo (2019) Lightweight design of bus frames from multi-material topology optimization to cross-sectional size optimization, Engineering Optimization, 51:6, 961-977, DOI: 10.1080/0305215X.2018.1506770

[51] Sigmund, O. (2011). On the usefulness of non-gradient approaches in topology optimization. Structural and Multidisciplinary Optimization, 43(5), 589-596. DOI 10.1007/s00158-011-0638-7

[52] Stegmann, Jan & Stolpe, Mathias. (2006). Discrete Material Optimization of Laminated Composites - SIMP vs. Global Optimization. https://doi.org/10.1007/1-4020-5370-3_732

[53] Stolpe, M., (2015) Truss optimization with discrete design variable: a critical review. Structural Multidisciplinary Optimization. DOI: 10.1007/s00158-015-1333-x

[54] Stolpe, M., Stegmann, J., (2007) A Newton method for solving continuous multiple material minimum compliance problems. Struct Multidisc Optim (2008) 35:93–106. DOI: 10.1007/s00158-007-0131-5

[55] Svanberg, K. (1987). The Method of Moving Asymptotes - A New Method for Structural Otimization. INTERNATIONAL JOURNAL FOR NUMERICAL METHODS IN ENGINEERING, 24, pp. 359-373.

[56] Svanberg, K. (1998). The Method of Moving Asymptotes - Modeling Aspects and Solution Schemes. Lyngby: Royal Institute of Technology (KTH).

[57] Svanberg, K. (2002) A class of globally convergent optimization methods based on conservative convex separable approximations SIAM Journal on Optimization, 12 (2), pp. 555-573.

[58] Svanberg, K. (2007). MMA and GCMMA, versions September 2007

[59] Taylor, J.E., & Rossow, M. (1977). OPTIMAL TRUSS DESIGN BASED ON AN ALGORITHM USING OPTIMALITY CRITERIA. International Journal of Solids and Structures, 13, 913-923. https://doi.org/10.1016/0020-7683(77)90004-X

[60] Tenek, L.H., Hagiwara, I. (1993) Static and vibrational shape and topology optimization using homogenization and mathematical programming. Computer Methods in Applied Mechanics and Engineering, 109 (1-2), pp. 143-154. DOI: 10.1016/0045-7825(93)90229-Q

[61] Tyler E. Bruns, Daniel A. Tortorelli, Topology optimization of non-linear elastic structures and compliant mechanisms, Computer Methods in Applied Mechanics and Engineering, Volume 190, Issues 26–27,2001, Pages 3443-3459, https://doi.org/10.1016/S0045-7825(00)00278-4

[62] Weldeyesus, A.G., Gondzio, J., He, L. et al. Adaptive solution of truss layout optimization problems with global stability constraints. Struct Multidisc Optim 60, 2093–2111 (2019). DOI: 10.1007/s00158-019-02312-9

[63] Xu, G., Gengdong, C. Epsilon-continuation approach for truss topology optimization. Acta Mech Sinica 20, 526–533 (2004). https://doi.org/10.1007/BF02484275

[64] Zhou, M. Difficulties in truss topology optimization with stress and local buckling constraints. Structural Optimization 11, 134–136 (1996). https://doi.org/10.1007/BF01376857

[65] Zuo, W., Saitou, K. Multi-material topology optimization using ordered SIMP interpolation. Struct Multidisc Optim 55, 477–491 (2017). https://doi.org/10.1007/s00158-016-1513-3